A thesis submitted for the degree of
Philosophiæ Doctor (Ph.D.)

Mechanotransduction and information coding in the human peripheral tactile system

Ph.D. candidate: **Giulia Corniani**
Supervisor: **Hannes P. Saal, Ph.D.**

October 2022

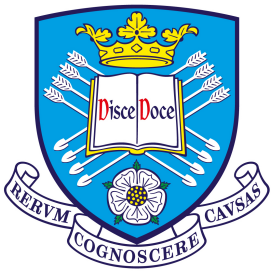

The University Of Sheffield.

Department of Psychology

A thesis submitted for the degree of
Philosophiæ Doctor (Ph.D.)

Mechanotransduction and information coding in the human peripheral tactile system

Ph.D. candidate: **Giulia Corniani**
Supervisor: **Hannes P. Saal, Ph.D.**

October 2022

Department of Psychology

Acknowledgements

I want to express my deepest gratitude to my supervisor Dr. Hannes P. Saal, for his wise guidance and constant and invaluable support during my Ph.D. journey. I also want to acknowledge my colleagues at the Active Touch Laboratory for sharing the lab life over the past three years with countless inspiring discussions and helpful feedback. I am thankful to the University of Sheffield for hosting me during my stay as a Marie Skłodowska–Curie fellow.

This work was supported by the EU Horizon 2020 research and innovation programme under grant agreement 813713 (NeuTouch). I want to acknowledge NeuTouch for providing me with the opportunity to conduct my research in a vibrant international and interdisciplinary environment. Thank you to Dr. Chiara Bartolozzi, the project coordinator, and all the PIs for building such an exciting and stimulating network, and thank you to all the fellow ESRs for being amazing colleagues and friends.

Abstract

The human peripheral tactile system is responsible for the initial processing of tactile stimuli and is composed of the skin and various embedded mechanoreceptors innervated by afferents. Spiking models are widely used to characterize this system and infer how populations of afferents shape tactile perception. Leveraging existing models of tactile afferents and moved by their limitations, we present three studies designed to advance these essential tools in the investigation of the human peripheral tactile system.

Firstly, reconciling existing evidence, we quantitatively characterize the population of peripheral tactile afferents. We estimate that approximately 230,000 afferents cover the human body, provide innervation densities in different skin areas, and show the relation of these numbers with tactile acuity, hair follicle density, and somatosensory cortical representation.

Secondly, we ask how tactile afferents work together to encode information in complex ways. We find that information is spread across classes, and combining information from multiple classes improves transmission. We test the importance of temporal and spatial resolution in the population code, probing that destroying temporal information is more destructive than removing spatial information.

Finally, we use Optical Coherence Tomography to image the skin subsurface in vivo and dynamically and quantify the deformation of individual fingerprint ridges down to the type-1 mechanoreceptors' location. When scanning the skin with a flat surface, the ridge deforms as a single unit. Higher strains emerge from the stick-to-slip transition compared to plate movement reversal. When scanning the skin with small features, different ridge sub-units experience different strain patterns. Higher strains occur in the deepest layer imaged.

Overall, this research provides a better understanding of coding strategies of tactile afferents on a population level and of the link between skin mechanics and transduction mechanisms underlying tactile perception. Our findings will have implications for developing novel spiking models of the human peripheral tactile system.

Contents

List of Figures

List of Tables

List of Acronyms

ITN	Innovative Training Network
FA	Fast adapting afferent (alternative for RA)
FAI	Fast adapting type-1 afferent
ESR	Early Stage Researcher
GLM	Generalized Linear Model
MI	Mutual Information
NMF	Non-negative Matrix Factorization
OCT	Optical Coherence Tomography
PC	Pacinian afferent
RA	Rapidly adapting afferent (alternative for FA)
RQ	Research question
SA	Slowly adapting afferent
SAI	Slowly adapting type-1 afferent
SAII	Slowly adapting type-2 afferent
V1	Ophthalmic branch of the trigeminal nerve
V2	Maxillary branch of the trigeminal nerve
V3	Mandibular branch of the trigeminal nerve

Introduction

1 Preface

Touch is one of the sensory modalities that provide humans with information about their surroundings. It is considered "*the first sense*", given that a 6-week-old fetus can already react to tactile stimuli, although completely blind and deaf [1]. Touch was first classified in the literature as one of the five senses by Aristotele in *De Anima*, who noted the complexity of this sensory modality which is not always biologically, psychophysically, and behaviourally sharply delineated. The complexity of the sense of touch lies in the diversity of the feature it provides awareness of. While for other sensory modalities, a single feature can be identified, as, for example, the sound for hearing, touch can exclusively perceive texture, hardness, weight, mass pressure, shape, temperature, vibrations, ticklishness, wetness, and so forth [2]. The primary sensory organ associated with the touch sensation is the skin which contains heterogeneous populations of receptors with different physiological and functional properties [3]. In addition, touch involves many essential receptors that are located in the muscles, joints, tendons, and on the surface of internal organs [4]. Given these facts, touch cannot be associated solely with the skin in any simplistic way.

Touch has both a passive and active nature. Gibson [5] famously made the distinction as follows: *"active touch refers to what is ordinarily called touching. This ought to be distinguished from passive touch or being touched"*. In the passive form, touch involves solely the activation of cutaneous receptors across the body's surface. This form of touch has played an essential role in the empirical study of touch, especially in characterizing the nature and acuity of the receptors' populations. Active touch implies voluntary, self-generated actions and often involves specialized

movements and grips, such as prehensile manipulation. It combines action planning and execution, proprioception, and tactile sensing. Active sensing is perhaps the most common modality of touch in humans. However, it is much more challenging to measure due to the unconstrained movements and the concurrent activation of several neural pathways.

Despite (or due to, this remains to be disclosed) the complexity and richness of the sense of touch, the number of studies conducted in this field is small compared to other sensory modalities, in particular vision and audition [6], and for this reason, much remains to be explained and discovered about the mechanisms underlying tactile sensations. However, the last two decades have witnessed a growing wave of academic interest in the study of the sense of touch [1], which opened up a variety of exciting new possibilities for further research in several different contexts such as medicine, telemedicine, neuroscience, psychology, prosthetics, robotics, virtual and augmented reality and so forth.

In this manuscript, we tackle research on the sense of touch from a neuroscientific perspective, focusing on a small yet fundamental aspect of the topic. We investigate the peripheral tactile system in humans, narrowing the attention to the early stages of the encoding mechanisms transforming passive tactile stimuli into spike trains. Therefore, skin mechanics, mechanoreceptors and peripheral tactile afferents are the main targets of this research work.

2 Motivation

The skin is the largest human sensory organ [7], and besides protecting our body from the external world, it informs us about what occurs on its surface. Any tactile interaction, be it a caress, lifting a glass, or placing a foot on the ground, results in a complex spatiotemporal mechanical deformation of the outer layer of the skin. The deformation propagates within the skin's inner layers and reaches different types of corpuscles responsible for transducing the mechanical forces into spike trains. The corpuscles responding to innocuous tactile stimulation are low-threshold mechanoreceptors innervated by Aβ myelinated afferent fibers. These fibers enter the spinal cord through the dorsal root and project onto the dorsal brainstem nuclei. Second-order neurons in these nuclei forward light touch information to the thalamus, and third-order thalamocortical neurons project to the somatosensory cortex [3]. Slow, unmyelinated

C fibers, such as C-tactile fibers, which are considered to be primarily in charge of affective touch, also carry some tactile information [8]. However, we will exclusively concentrate on myelinated Aβ fibers and discriminative touch for the remainder of this manuscript.

The collection of all the elements shaping human tactile perception, from the skin to the somatosensory cortex, is referred to as the human tactile system. Generally speaking, a system is a group of interrelated objects that, under a specific external stimulus (spatiotemporal deformation of the skin), produces a response (neural activation of the somatosensory cortex and tactile perception). Complex systems can be modeled to describe their constituent elements, and the relationships between them [9]. Specifically looking at the human tactile system, its principal constituent elements (the skin, the mechanoreceptors, and neurons of different types and order) have been widely studied and modeled in the literature on very different scales, either individually or combined. Models of the human tactile system address, for example, the advanced understanding of all the system components (e.g., the skin [10], mechanoreceptors [11], and tactile neurons [12]), or the characterization and prediction of the neural responses generated by specific tactile stimuli both at the peripheral [13] and cortical level [14].

The focus of this manuscript lies, in particular, on models of human peripheral tactile afferents and has as a starting point the two main hurdles that the investigation of the early stages of tactile sensory processing usually faces.

The first one regards the encoding strategies of tactile stimuli in the population of afferents. Recording the activity of tactile nerve fibers in humans is technically tricky, is slow, and generally yields responses from a single unit at a time [15]. Although such recordings have offered powerful insights into the neural basis of touch, they provide limited insight into the information that the hand conveys to the brain, which is distributed over thousands of afferents.

The second regards the relation between the mechanical properties of the skin and the activation of the receptive organs. The receptors are embedded in the skin and are separated from the surface by several layers of skin tissue that have different mechanical properties and complex morphology. Understanding how a tactile stimulus applied to the skin surface is translated into neural responses presupposes understanding how the stimulus affects the local strain patterns at the receptor location. However, due to technical difficulties, measuring these aspects in-vivo is

particularly challenging, especially in dynamic conditions. The core of our current understanding of the topic comes from ex-vivo studies or finite-element modeling, but still, little is known about the biomechanics of the skin beneath its immediate surface and how it affects stimulus encoding.

Models can fill this gap by simulating the responses of very large populations of mechanoreceptive afferents that innervate the palmar surface of the hand to arbitrary spatiotemporal patterns of skin stimulation, taking into account skin biomechanics and receptor biophysics. Having quantitative functional models that can reproduce the behavior of the skin and the response of tactile neurons can help to overcome the limitations of classical recording techniques. In particular, models allow computer simulations that can be a viable way to study the relation between skin properties and neuron population response and to assess differences in tactile neural coding. Spiking models of human peripheral tactile afferents are an essential tool in somatosensory research to characterize the peripheral representation of tactile stimuli. Additionally, in neuroprosthetic applications, they can help provide somatosensory feedback through interfaces with the peripheral nerve by converting the output of touch sensors on the prosthesis into biomimetic afferent responses, which can then be implemented through electrical stimulation.

In the literature, some computational models that simulate the response of tactile afferents in the skin to tactile stimulation have been proposed [13, 16, 17]. However, they all come with limitations typical of the modeling approach, such as, firstly, the required validation with real data.

Here, leveraging on the existing spiking models of human tactile afferents and inspired by their main limitations, we present three studies designed with the purpose of advancing the state of the art of such essential tools in the study of the human tactile system.

3 Research goals

With the purpose of advancing the modeling of the human peripheral tactile system, we designed the three research studies presented in this manuscript. In particular, we consider two general open questions related to the early stages of tactile processing [18]. The first is what are the significant features of the signal sent to the central nervous system by the many tactile afferents that work together to give rise to the tactile sensation. The second is how the skin's mechanical properties

affect the mechanoreceptors' activation. Starting from these broad questions, we identified the following research questions (RQ).

We first looked at the distribution of peripheral human tactile afferents within the skin. The ensemble responsible for the peripheral encoding of innocuous tactile stimulation comprises Aβ myelinated tactile afferents and their end organs, low-threshold mechanoreceptors [3]. After a pioneer study by Johansson and Valbo (1979) [19], the structural and functional properties of these elements have been extensively studied. However, a large part of the literature in this field just looks at the characterization of single units. Yet even a skin area as small as a fingertip is innervated by several hundred afferents [19]. Therefore, to gain a complete understanding of the encoding process of tactile stimuli, it is necessary to broaden the knowledge of tactile afferents at the population level.

We sought to quantitatively characterize the tactile afferent population, as understanding the makeup of sensory inputs is necessary for studying sensory processing. Aβ myelinated tactile afferents can be classified by their electrophysiological response properties into rapidly adapting (RA) -or, alternatively, fast-adapting (FA)- and slowly adapting (SA) fibers. Six further subdivisions exist based on the termination depth, receptive field size, and skin type (hairy/glabrous) [3]. The presence and prevalence of different afferent classes vary greatly from one part of the body to another. However, precise estimates of innervation density were available for some body parts, such as the hands, but estimates of the total number of tactile afferent fibers were inconsistent and incomplete. Thus, we identified the first research question:

RQ1: *What is a plausible range for the innervation density of each class of Aβ myelinated tactile afferent fibers in every skin region of the human body?*

Keeping the focus on the population of tactile afferents, we then investigated the encoding process of tactile stimuli. One way to explore afferent activity is via neurophysiological acquisitions, but these are subjected to technical limitations, and notably, only individuals or a handful of afferents can be recorded at once. Hence, most existing literature describes the activation of a few afferents at a time, selected for having the receptive field precisely where the tactile stimulus is applied. In this context, afferent activity on a population level has scarcely been investigated, and consequently, the understanding of how information is represented in the

population is limited. At the same time, biased notions may have emerged due to the only partial grasp of the complexity of the encoding process of tactile stimulus into spike trains. In this regard, most literature describes each afferent class as carrying information about different and complementary stimulus features. Indeed, shape, texture, motion, and stretch perceptions are ascribed to be encoded by a single population of afferents. This theory finds ground in a series of reviews by K. Johnson [20–22] who based his claims on decades of psychophysical and neurophysiological research. Lately, various works have challenged the notion of sub-modality segregation in the tactile afferents and approached the study of afferent activity from a population perspective [23–26]. Still, our understanding of tactile information encoding on a population level was primitive. In this context, with the second study, we addressed the second research question:

RQ2: *What is the contribution of a large peripheral neural population in tactile stimulus encoding and the interplay of submodalities in this process?*

Finally, we moved the focus to the skin and its biomechanics for the third study. The skin represents the first component of the human tactile system, and consequently, its biomechanical properties directly affect tactile system processing. The epidermis, dermis, and hypodermis are the three main layers that make up the skin [27]. Each layer has a unique tissue composition, which likely impacts tactile stimulus propagation and mechanoreceptor activation. Skin morphology has been investigated in ex-vivo studies, such as biopsies. However, this type of investigation does not enable complete characterization of the mechanical properties of the tissues because the natural state of pre-tension and elasticity of the skin in vivo conditions is lost. On the other hand, in vivo and dynamic studies of skin mechanics are mostly limited to the skin's outer layer due to the limitations of acquisition techniques. Over the years, computational models of the skin attempted to address the mechanical characteristic of every skin layer (for reviews, see Jor et al. (2013) [28] and Joodaki and Panzer (2018) [10]). Still, these models are critically dependent on the availability of experimental data to identify a large number of unknown parameters reliably. Leveraging a state-of-the-art technique, we imaged the skin subsurface layers and built an experimental setup for acquisitions during dynamic tactile stimulation of the human fingertip. Thus, in the third study, we address the last research question:

RQ3: *How does a tactile stimulus, applied to the skin surface, propagate and reach the location of the receptors in the subcutaneous skin layers?*

4 Contributions

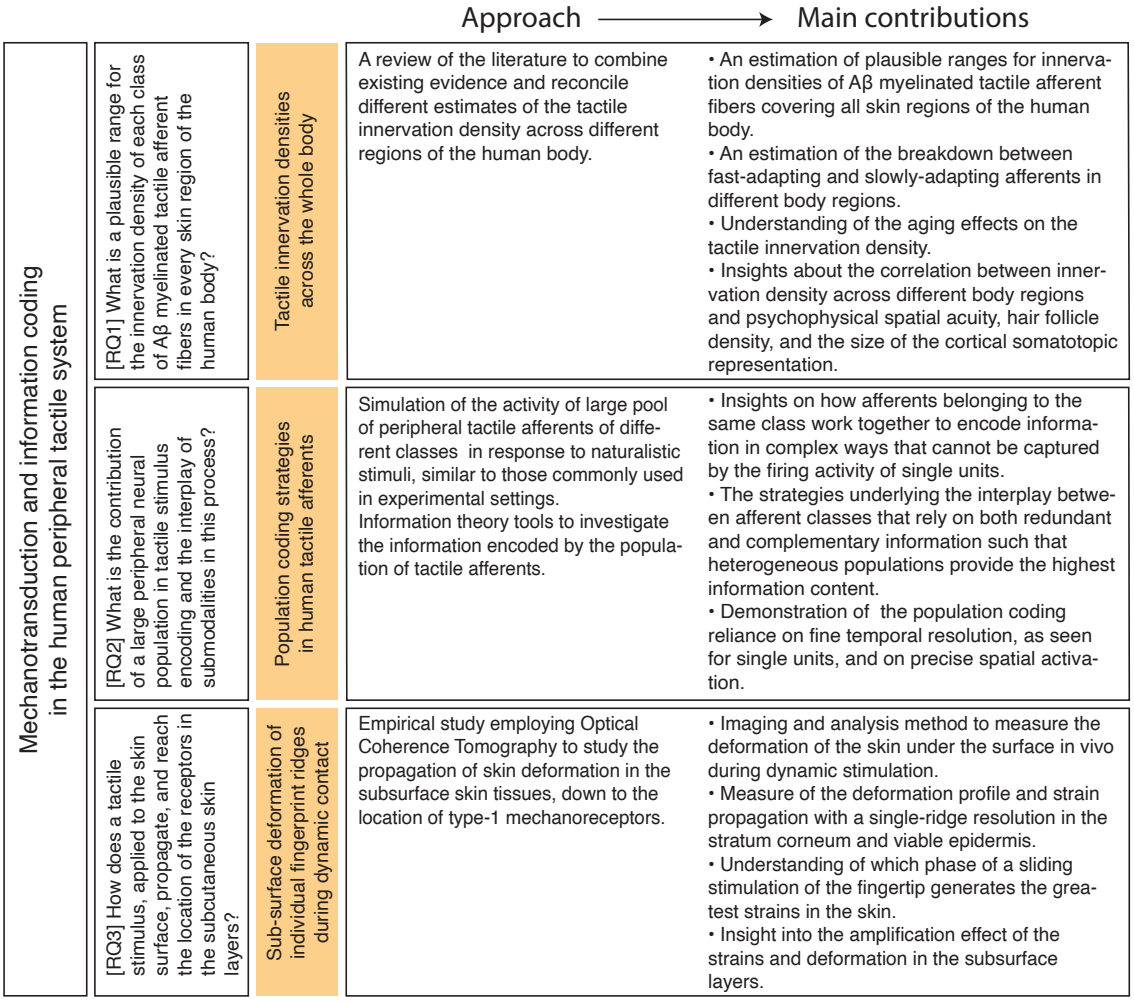

Fig. 1: Overview of the research questions, approaches, and contributions of the manuscript. The diagram organizes the goals of the thesis into three questions (RQ1, RQ2, RQ3), and provides an overview of the experimental approaches and the resulting contributions.

This manuscript is the collection of three complete and self-standing studies, and the contributions and implications of each of them are broadly discussed in the related chapters.

The three studies as a whole advance the characterization of the early stages of tactile processing. In particular, the contributions from the first two studies feed into the exploration of the peripheral

tactile afferents and the significant feature they send to the central nervous system to give rise to tactile sensation. We investigated human tactile afferents from a population perspective: the first study characterizes the population composition quantitatively, while the second analyzes the interplay strategies among afferents when encoding tactile stimuli. The third study contributes to addressing the open issue of early stages of tactile processing related to skin mechanics properties in two ways. On the one hand, we pioneered a methodology that paves the way to investigate the deformation of the skin at the receptors' location, in vivo, and during dynamic stimulation. On the other hand, the study offers a characterization of the strain propagation under the skin surface during sliding interactions of the fingerpad.

In Figure 1, we offer an overview of the research questions, the studies' approach, and the main contributions.

5 Background

In the following, we outline a brief introduction to some key concepts and terms considered fundamental to grasp the studies proposed in the subsequent chapters thoroughly.

5.1 Low-threshold mechanoreceptors

Mechanoreceptors are specialized nerve endings that detect mechanical forces, such as touch, pressure, vibrations, and proprioception. They are found in various body parts, including the skin, muscles, joints, and tendons. They play an essential role in our sense of touch, proprioception, and movement. The mechanoreceptor responding to innocuous tactile interactions are low-threshold mechanoreceptors. They are called "low-threshold" because they have a lower threshold for activation, meaning they are sensitive to weak mechanical forces.

There are several different types of low-threshold mechanoreceptors, each with a unique function and sensitivity to different mechanical stimuli. For example, Merkel cells and Meissner's corpuscles are sensitive to light touch and vibrations, Pacinian corpuscles respond to vibrations, and Ruffini endings respond to stretch.

The sensitivity of mechanoreceptors to different types of mechanical stimuli is determined by

the structure and composition of their membrane, which contains ion channels that respond to mechanical deformation. When a mechanical force is applied, the ion channels open or close, resulting in a change in the membrane potential and generating an action potential, which travels to the spinal cord and brain, where it is interpreted as a tactile sensation. The action potentials travel toward the spinal cord through A-beta myelinated fibers, which innervate low-threshold mechanoreceptors. [29]

5.2 Peripheral tactile afferents

Peripheral tactile afferents are A-beta myelinated afferent fibers, a type of nerve fiber that transmits sensory information from the peripheral nervous system to the central nervous system. These fibers are called "A-beta" because they are classified as "group A" fibers and are more prominent in diameter than other types of sensory fibers. They are also myelinated, which means they are surrounded by a fatty insulating layer called myelin. This myelin coating allows them to conduct action potentials faster than unmyelinated fibers. A-beta myelinated afferent fibers are responsible for conveying information about touch, pressure, and vibration, as well as pain and temperature in some cases. They are found throughout the body and are particularly abundant in the skin and muscles, where they play an important role in the sense of touch and proprioception. One branch of these nerve fibers travels to the spinal cord or brainstem, while the other branch extends to the periphery and terminates as a nerve ending or associates with cutaneous mechanosensory organs, such as the low-threshold mechanoreceptors.

Human peripheral tactile afferents are specialized nerve fibers that transmit information about touch from the skin to the brain. They are part of the human peripheral tactile system, which is responsible for the initial processing of any tactile stimulus.

Peripheral tactile afferents can be divided into two main categories: slowly adapting and rapidly adapting fibers. The slowly adapting fibers are activated by sustained or prolonged stimuli and are responsible for maintaining the perception of a sustained touch. Rapidly adapting fibers, on the other hand, are activated by brief or transient stimuli and are responsible for the perception of a momentary touch. Both types of afferents can be further divided into two categories: type I afferents, which are more numerous and terminate close to the surface of the skin, and type

II afferents, which end in deeper skin layers. In hairy skin, there are two additional types of fast-adapting afferents called hair units and field units, which have similar response properties to classical fast-adapting type-I units but have larger receptive fields and may be more sensitive to higher frequencies. The types and distribution of different afferents vary between glabrous (non-hairy) skin, such as on the palms, soles, and lips, and hairy skin, which covers the rest of the body. [3, 29]

5.3 Skin and its mechanical properties

The skin is the largest organ of the human body, covering an area of about 2 square meters. It serves as a barrier between the body and the external environment, protecting the body from harmful elements such as bacteria, UV radiation, and physical impacts. The skin is composed of three main layers, the epidermis, the dermis, and the subcutaneous tissue, which can be further classified into several sublayers. For the scope of this manuscript, we will just focus on the epidermis, which is composed of stratum corneum and viable epidermis.

The stratum corneum is the outermost layer of the skin and is composed of dead skin cells that have been filled with keratin. It is relatively stiff and non-elastic, and its primary function is to provide a barrier to protect the skin from external environmental factors. The viable epidermis is the layer of the skin beneath the stratum corneum and is composed of living cells. It is relatively elastic and is responsible for the production of new skin cells. The dermis-epidermis junction is the interface between the dermis and epidermis, and it plays a crucial role in the mechanical properties of the skin. The mechanical properties of this junction are influenced by the mechanical properties of the epidermis and the dermis and by the mechanical properties of the adhesion molecules that connect the two layers.

Skin mechanical properties refer to the way in which the skin responds to external mechanical forces, such as touch and pressure. These properties include stiffness, elasticity, and viscoelasticity, and they play an important role in the perception of touch. The skin's mechanical properties are linked to the process of mechanotransduction, which is the conversion of mechanical forces into electrical signals that can be detected by the nervous system.

The skin's mechanical properties are determined by the organization and composition of the

extracellular matrix, which includes collagen, elastin, and other proteins. The stiffness and elasticity of the skin are determined by the density and alignment of collagen fibers, while viscoelasticity is determined by the presence of elastin and other proteins. Changes in the mechanical properties of the skin can affect the way in which it responds to mechanical forces and can lead to changes in the mechanotransduction process.

For example, skin that is stiffer and less elastic will have a lower threshold for the activation of mechanoreceptors, leading to more sensitive touch perception. Conversely, skin that is more elastic and less stiff will have a higher threshold for the activation of mechanoreceptors, leading to less sensitive touch perception. [10, 30]

6 Research in context

The research presented in this manuscript was carried out in the framework of NeuTouch, a project supported by the European Union's Horizon 2020 Marie Skłodowska-Curie Actions (grant agreement 813713). NeuTouch is an Innovative Training Network (ITN) composed of 15 Ph.D. students and 16 principal investigators scattered in 9 partner institutions (universities, research centers, and industrial partners) across Europe. The mission of NeuTouch is to study how tactile perception works in humans and animals to then develop artificial touch perception systems for robots and hand prostheses.

This multidisciplinary research community is built around three main areas: Technologies for Touch, Touch for Robotics, and Touch for Prosthetics (see Figure 2). The development of embedded neuromorphic tactile sensors and their application is at the core of the Technologies for Touch area of research. The objective is twofold. On the one hand, the study of nanowires and materials for smart transduction mimicking human and animal tactile afferents properties. On the other, the design of low-power neuromorphic devices for encoding tactile sensors output and on-chip spiking neural networks inspired by the neural coding strategies of peripheral afferents. Understanding the neural encoding of tactile features, their central representation, and their link to behavior is also fundamental to implementing effective strategies in robots for dexterous manipulation and operation, which is the main objective of the Touch for Robotics area. Autonomous grasping and manipulation with robotic hands predominantly build on vision and

Fig. 2: Visual representation of the contributions of each ESR in NeuTouch to the global research project

feed-forward approaches, with several heavy limitations, such as occlusions. The aim of NeuTouch is to develop algorithms for active object grasping and manipulation by integrating information derived from touch sensors. Finally, in the Touch for Prosthetics area, NeuTouch joins a growing field of research that aims at the functional replacement of missing upper limbs in humans. Initial very promising demonstrations showed that tactile information could be restored by surgically implanting neural interfaces into the peripheral nerves of the residuum of prosthetics device users for restoring the sensory information flow between the hand prosthesis and the nervous system, opening new and exciting possibilities. In this framework, NeuTouch aims to address two important open issues, i.e., the development of more biocompatible neural interfaces and the identification of more natural encoding (stimulation) strategies.

NeuTouch is based on the principle that these three research areas are closely intermingled, and therefore multidisciplinary approach and constant exchange of knowledge hugely facilitate and promote field advancement. Indeed, the research presented here is firmly grounded in the three areas of competence of the network. Over the three years of work and numerous project meetings, it has served as a source for the work of other fellows and received innumerable inputs.

As a matter of fact, the work presented in the paper "Population coding strategies in human tactile afferents" is the result of the collaboration with Miguel Casal (NeuTouch fellow) and his supervisor Stefano Panzeri. In the NeuTouch framework, M. Casal dealt with computational techniques to extract the information contained in neural signals. These methods were used to study the coding strategies of tactile afferents on a population level. The result of this work, together with the human tactile innervation characterization proposed in chapter 2, served as input for the fellows working on neuromorphic tactile sensors. A careful design of these technologies, in fact, starts with a deep understanding of how the biological counterpart works.

Finally, the work presented in the paper "Sub-surface deformation of individual fingerprint ridges during dynamic contact" about human skin subsurface properties, in the context of NeuTouch, provides valuable insight to the fellows developing neural nanowire-based tactile skin in order to embed the sensing component mimicking the setting of the mechanoreceptors in the skin sublayers.

In addition to being a very important networking and collaboration space, NeuTouch offered the

author of this manuscript numerous training opportunities. In the three years of the project, three international summer schools were organized with the participation of distinguished researchers in the three thematic areas on the network, as well as several courses and seminars for scientific training.

7 Manuscript structure

This manuscript is a thesis in a publication format. Therefore, the following chapters consist of papers in a form suitable for publication in a peer-reviewed journal. The current chapter connects the three works and discusses their coherence and significance. Each of the following chapters is a complete and self-standing piece of work.

Paper 1 addresses the RQ1 and consists of the journal paper "Tactile innervation densities across the whole body." which was published in the peer-reviewed Journal of Neurophysiology on the 19th of October 2020 (the first submission in the same journal was on the 28th of May 2020). The paper was published with GOLD open access policy and had a major impact. It was listed on the Journal website home page under the category "Trending research" for over four weeks after publication. At the moment of writing, it counts 72 citations and over 13k downloads.

Paper 2 addresses RQ2 and consists of the journal paper "Population coding strategies in human tactile afferents" which is under review in the journal PLOS Computational Biology (the first submission in the same journal was on the 15th of June 2022). The authors received the decision on the acceptance of the manuscript on the 24th of August 2022, stating that the manuscript was *"likely to be accepted"* pending minor revision. The submission of the revision is due shortly. This work is the result of a close collaboration with Miguel A. Casal (ESR of the NeuTouch ITN) and Prof. Stefano Panzeri. The study started in November 2020 during a two months secondment of the author of this manuscript at the Laboratory of Neural Computation of the Istituto Italiano di Tecnologia (Genova, Italy) led by Prof. Stefano Panzeri. Partial or preliminary results of this work were presented at several international conferences (IEEE NER2021, 50th annual meeting of the Society of Neuroscience, Neuromatch 2021 conference).

Paper 3 addresses RQ3 and consists of the paper "Sub-surface deformation of individual fingerprint ridges during dynamic contact". The works underwent a round of internal revision

offered by the co-authors of the work, Dr. Ben Delhaye, Prof. Roger Lewis, and Prof. Matt Carrè. It is planned to submit this work for publication within 2 months after the submission of this manuscript aiming at a high-impact peer-reviewed generalist journal. Partial or preliminary results of this work were presented at international conferences (BioMedEng21 UK Conference, 50th and 51st annual meeting of the Society of Neuroscience, IEEE Eurohaptics 2022 where the author received the best poster award in the category "Work in Progress").

8 Covid-19 statement

The Ph.D. journey that led to the present manuscript started on November 2019. Less than six months after the start of this project, the Covid-19 pandemic outbroke with a dramatic impact that also affected the project management, schedule, and timing. A contingency plan was put in place to limit the effect of restrictions on the successful implementation of the research plan. We took advantage of the NeuTouch ITN to establish strong collaborations with researchers in the network and overcome the impossibility of traveling to visit laboratories and participate in international conferences and scientific events, which usually represent the primary venue for interacting with the scientific community. The NeuTouch ITN organized several online meetings and training events to ensure Ph.D. students could make the most of their research journey and, at the same time, had a safety net guaranteeing mentorship and support despite the pandemic situation.

From a more practical point of view, the first two studies leveraged existing or simulated datasets to overcome the impossibility of planning face-to-face experiments and empirical acquisitions.

The third study was most severely affected by the restrictions imposed to limit the spread of the virus since it included, as a very first stage, an empirical face-to-face experiment with participants. Access to the laboratory facilities was strictly limited until spring 2021, when the OCT study's first round of pilot acquisition started with more than six months of delay from what was initially planned. Consequently, the actual acquisition stage took place in May 2022, and, considering the limited time in the project left, we had to reduce the number of participants by 2/3 from an initially designed pool of 30.

As soon as most travel restrictions were lifted and in-person events started to be organized again, we also embraced all the opportunities to engage with the scientific community and disseminate

the work. This included the participation in the European Researcher night (September 2021, Genova, Italy), UK BioMedEng Conference (September 2021, Sheffield, UK), IEEE Eurohaptics 2022 conference (May 2022, Hamburg, Germany), International School on Technologies for Touch (September 2022, Arenzano, Italy), 51st meeting of the Society of Neuroscience (expected for November 2022, San Diego, USA), and other NeuTouch training and local events.

References

[1] A. Gallace and C. Spence, *In touch with the future: The sense of touch from cognitive neuroscience*. Oxford University Press, Jan. 2014.

[2] F. de Vignemont and O. Massin, "Touch," in *Oxford Handbook of Philosophy of Perception*. Oxford University Press, Jan. 2015, pp. 294–313.

[3] V. E. Abraira and D. D. Ginty, "The sensory neurons of touch," *Neuron*, vol. 79, no. 4, pp. 618–639, Aug. 2013.

[4] M. L. Zimny, "Mechanoreceptors in articular tissues," *Am. J. Anat.*, vol. 182, no. 1, pp. 16–32, May 1988.

[5] J. J. Gibson, "Observations on active touch," *Psychol. Rev.*, vol. 69, no. 6, pp. 477–491, Nov. 1962.

[6] F. Hutmacher, "Why is there so much more research on vision than on any other sensory modality?" *Front. Psychol.*, vol. 10, p. 2246, Oct. 2019.

[7] Y. Gilaberte, L. Prieto-Torres, I. Pastushenko, and Á. Juarranz, "Chapter 1 - anatomy and function of the skin," in *Nanoscience in Dermatology*. Academic Press, Jan. 2016, pp. 1–14.

[8] J. Cole, M. C. Bushnell, F. McGlone, M. Elam, Y. Lamarre, A. Vallbo, and H. Olausson, "Unmyelinated tactile afferents underpin detection of low-force monofilaments," *Muscle Nerve*, vol. 34, no. 1, pp. 105–107, Jul. 2006.

[9] S. Motta and F. Pappalardo, "Mathematical modeling of biological systems," *Brief. Bioinform.*, vol. 14, no. 4, pp. 411–422, Jul. 2013.

[10] H. Joodaki and M. B. Panzer, "Skin mechanical properties and modeling: A review," *Proc. Inst. Mech. Eng. H*, vol. 232, no. 4, pp. 323–343, Apr. 2018.

[11] M. K. Vasudevan, V. Sadanand, M. Muniyandi, and M. A. Srinivasan, "Coding source localization through inter-spike delay: modelling a cluster of pacinian corpuscles using time-division multiplexing approach," *Somatosens. Mot. Res.*, vol. 37, no. 2, pp. 63–73, Jun. 2020.

[12] C. W. Zhao, M. J. Daley, and J. A. Pruszynski, "Neural network models of the tactile system develop first-order units with spatially complex receptive fields," *PLoS One*, vol. 13, no. 6, p. e0199196, Jun. 2018.

[13] H. P. Saal, B. P. Delhaye, B. C. Rayhaun, and S. J. Bensmaia, "Simulating tactile signals from the whole hand with millisecond precision," *Proc. Natl. Acad. Sci. U. S. A.*, vol. 114, no. 28, pp. E5693–E5702, Jul. 2017.

[14] A. Lucas, T. Tomlinson, N. Rohani, R. Chowdhury, S. A. Solla, A. K. Katsaggelos, and L. E. Miller, "Neural networks for modeling neural spiking in S1 cortex," *Front. Syst. Neurosci.*, vol. 13, p. 13, Mar. 2019.

[15] Å. B. Vallbo, "Microneurography: how it started and how it works," *J. Neurophysiol.*, vol. 120, no. 3, pp. 1415–1427, Sep. 2018.

[16] G. J. Gerling, I. I. Rivest, D. R. Lesniak, J. R. Scanlon, and L. Wan, "Validating a population model of tactile mechanotransduction of slowly adapting type I afferents at levels of skin mechanics, single-unit response and psychophysics," *IEEE Trans. Haptics*, vol. 7, no. 2, pp. 216–228, Apr. 2014.

[17] Q. Ouyang, J. Wu, Z. Shao, D. Chen, and J. W. Bisley, "A simplified model for simulating population responses of tactile afferents and receptors in the skin," *IEEE Trans. Biomed. Eng.*, vol. 68, no. 2, pp. 556–567, Feb. 2021.

[18] D. Deflorio, M. Di Luca, and A. M. Wing, "Skin and mechanoreceptor contribution to tactile input for perception: A review of simulation models," *Front. Hum. Neurosci.*, vol. 16, p. 862344, Jun. 2022.

[19] R. S. Johansson and A. B. Vallbo, "Tactile sensibility in the human hand: relative and absolute densities of four types of mechanoreceptive units in glabrous skin," *J Physiol (Lond)*, vol. 286, pp. 283–300, Dec. 1979.

[20] K. O. Johnson and S. S. Hsiao, "Neural mechanisms of tactual form and texture perception," *Annu. Rev. Neurosci.*, vol. 15, pp. 227–250, 1992.

[21] K. O. Johnson, T. Yoshioka, and F. Vega-Bermudez, "Tactile functions of mechanoreceptive afferents innervating the hand," *J. Clin. Neurophysiol.*, vol. 17, no. 6, pp. 539–558, Nov. 2000.

[22] K. O. Johnson, "The roles and functions of cutaneous mechanoreceptors," *Curr. Opin. Neurobiol.*, vol. 11, no. 4, pp. 455–461, Aug. 2001.

[23] A. I. Weber, H. P. Saal, J. D. Lieber, J.-W. Cheng, L. R. Manfredi, J. F. Dammann, 3rd, and S. J. Bensmaia, "Spatial and temporal codes mediate the tactile perception of natural textures," *Proc. Natl. Acad. Sci. U. S. A.*, vol. 110, no. 42, pp. 17 107–17 112, Oct. 2013.

[24] I. Birznieks, S. McIntyre, H. M. Nilsson, S. S. Nagi, V. G. Macefield, D. A. Mahns, and R. M. Vickery, "Tactile sensory channels over-ruled by frequency decoding system that utilizes spike pattern regardless of receptor type," *Elife*, vol. 8, Aug. 2019.

[25] H. P. Saal and S. J. Bensmaia, "Touch is a team effort: interplay of submodalities in cutaneous sensibility," *Trends Neurosci.*, vol. 37, no. 12, pp. 689–697, Sep. 2014.

[26] A. J. Emanuel, B. P. Lehnert, S. Panzeri, C. D. Harvey, and D. D. Ginty, "Cortical responses to touch reflect subcortical integration of ltmr signals," *Nature*, vol. 600, no. 7890, pp. 680–685, Oct. 2021.

[27] J. Kanitakis, "Anatomy, histology and immunohistochemistry of normal human skin," *Eur. J. Dermatol.*, vol. 12, no. 4, pp. 390–9, Jul. 2002.

[28] J. W. Y. Jor, M. D. Parker, A. J. Taberner, M. P. Nash, and P. M. F. Nielsen, "Computational and experimental characterization of skin mechanics: identifying current challenges and future directions," *Wiley Interdiscip. Rev. Syst. Biol. Med.*, vol. 5, no. 5, pp. 539–556, Sep. 2013.

[29] M. S. Fleming and W. Luo, "The anatomy, function, and development of mammalian Aβ low-threshold mechanoreceptors," *Front. Biol.*, vol. 8, no. 4, Aug. 2013.

[30] J. A. McGrath, R. A. J. Eady, and F. M. Pope, "Anatomy and organization of human skin," *Rook's textbook of dermatology*, vol. 1, pp. 3–2, 2004.

Tactile innervation densities across the whole body

G. Corniani and H. P. Saal, "Tactile innervation densities across the whole body," *Journal of Neurophysiology*, vol. 124, no. 4, pp. 1229–1240, 2020.

DOI: https://doi.org/10.1152/jn.00313.2020

Keywords: *cutaneous afferent* | *mechanoreceptor* | *glabrous skin* | *hairy skin*

Candidate's contribution to the paper

G.C. and H.P.S. conceived and designed research; G.C. and H.P.S. analyzed data; G.C. prepared figures; G.C. drafted manuscript; G.C. and H.P.S. edited and revised manuscript; G.C. and H.P.S. approved final version of manuscript.

Theoretical implementation	**Coding**	**Experiment design**	**Experiment execution**	**Data analysis**	**Paper writing**	**Academic authorship**
Yes	Yes	N/A	N/A	Yes	Yes	First author

Abstract

The skin is our largest sensory organ and innervated by afferent fibers carrying tactile information to the spinal cord and onto the brain. The density with which different classes of tactile afferents innervate the skin is not constant but varies considerably across different body regions. However, precise estimates of innervation density are only available for some body parts, such as the hands, and estimates of the total number of tactile afferent fibers are inconsistent and incomplete. Here we reconcile different estimates and provide plausible ranges and best estimates for the number of different tactile fiber types innervating different regions of the skin, using evidence from dorsal root fiber counts, microneurography, histology, and psychophysics. We estimate that the skin across the whole body of young adults is innervated by approximately 230,000 tactile afferent fibers (plausible range: 200,000-270,000), with a subsequent decrement of 5-8% every decade due to aging. 15% of fibers innervate the palmar skin of both hands and 19% the region surrounding the face and lips. Slowly and fast-adapting fibers are split roughly evenly, but this breakdown varies with skin region. Innervation density correlates well with psychophysical spatial acuity across different body regions, and additionally, on hairy skin, with hair follicle density. Innervation density is also weakly correlated with the size of the cortical somatotopic representation, but cannot fully account for the magnification of the hands and the face.

1 Introduction

Sensory processing cannot be studied without understanding the nature of sensory inputs. Careful study of the visual system has revealed that about 100 million photoreceptors in a single retina convert light into electrical impulses, which are relayed through roughly 1 million retinal ganglion cells in the optic nerve [31]. In audition, about 12,000 hair cells in each cochlea transmit auditory information to the brain [32]. The sense of touch puts to use our largest sensory organ, the skin, which is innervated throughout by cutaneous fibers signaling light touch, temperature, and pain. Despite the importance of touch for manipulation [33], movement [34], our sense of body ownership [35], and affection [36], we know little about the number and distribution of cutaneous fibers innervating different skin regions across the body. Estimates of tactile fiber innervation in the current literature are few, often incomplete and inconsistent, and range from a total innervation of around 45,000 fibers [37] into the millions [38]. Most textbooks do not even venture a guess [39–42]. Reliable estimates exist only for a few regions of glabrous skin. The gold standard is a study by [43] that estimated that around 17,000 myelinated tactile fibers innervate the palmar surface of each hand.

Various techniques can be employed for counting fibers, but individually they all suffer from problems, which explains the discrepancy in estimates. Histological examination can provide estimates for the number of fibers in the peripheral nerves, but cannot distinguish between afferent and efferent fibers. Furthermore, peripheral nerves carry many types of sensory fibers other than tactile ones, for example, proprioceptive fibers or those innervating internal organs, such as the bladder. Immunohistochemistry of samples taken by skin biopsies allow receptor and fiber counts, but the regions covered are necessarily very small, and innervation of the skin is not uniform. Individual tactile fibers often branch and innervate tens of receptors, and estimates of branching and convergence factors differ widely. Another approach estimates innervation density from psychophysically determined two-point discrimination thresholds. Here, the idea is that higher innervation density enables improved spatial localization, so finer spatial discrimination should be associated with higher fiber count. However, such estimates are limited because discrimination thresholds likely rely predominantly on only one of the multiple different afferent classes that innervate the skin [44]. A general problem is that none of the methods described

above can be used to extrapolate between glabrous and hairy skin without taking into account the different composition in the types of tactile afferent fibers. Much valuable insight into the prevalence of different fiber types also comes from microneurography, a technique for obtaining electrophysiological recordings from individual fibers in human nerves. However, this technique has mostly been applied to fibers terminating in the hand, the foot, or the face. A handful of studies has investigated the hairy skin of the arms and legs, but data from the body trunk is sorely lacking, due to the technical challenges of applying the microneurography technique in these areas. Finally, data from animal models, specifically primates, can also provide valuable input, however stark differences in innervation density have been observed across different primate species [45], so such data can only be used with caution.

Here, we combine published evidence from multiple measures—fiber counts in the dorsal root ganglia, histology of the nerves and the skin, microneurography, and psychophysics—to estimate plausible ranges for innervation densities of Aβ myelinated tactile afferent fibers covering all skin regions of the body. We estimate that the skin of young adults in the third decade is innervated by approximately 230,000 tactile afferent fibers (plausible range: 200,000-270,000) in total, with a subsequent decrement due to aging of 5-8% every decade. The hands and the face are the most highly innervated skin regions, as might be expected from the exaggerated cortical representation of these body parts [46]. While we believe our estimates to be robust, more fundamental work remains to be done, especially concerning the innervation of hairy skin.

2 Tactile innervation of the skin

The tactile innervation of the skin has been extensively covered in reviews [36, 47–49] and textbooks [40, 50], so we will only provide a brief overview. Here, as well as in the rest of the paper, we will focus on data from humans. The main tactile fibers underlying discriminative touch are myelinated Aβ fibers. Some tactile information is also carried by slow, unmyelinated C fibers (e.g., C-tactile fibers), which are thought to be mainly responsible for affective touch [51]. However, recent evidence has shown that C-tactile fibers are likely to contribute to tactile sensibility [52] and that the spinal pathways carrying signals from both types of fibers are more intertwined than had previously been thought [53]. For the purposes of this review, we will focus

on myelinated Aβ fibers and discriminative touch exclusively. However, a similar approach to the one pursued here should allow estimation of innervation densities for C-tactile fibers in future work, completing the picture of tactile innervation.

Focusing on Aβ fibers, two major afferent classes exist, which are distinguished by their electrophysiological response properties: fast-adapting (FA) fibers (also called RA: rapidly-adapting or QA: quickly adapting in the literature) that respond exclusively to dynamic stimuli, that is when the skin is in motion; and slowly-adapting (SA) fibers, which, in addition to dynamic responsiveness, also respond to sustained static skin deformation or stretch. Both classes can be further subdivided into type I afferents, which are more numerous and terminate close to the surface of the skin, and type II afferents, which end in deeper skin layers. In the hairy skin, two further classes of fast-adapting afferents can be found, namely hair units and field units; both of these exhibit response properties similar to those of classical FAI units, but their receptive fields are much bigger, and they might be more sensitive to higher frequencies (see sections on the face and hairy skin below for further detail). The presence and prevalence of different afferent classes vary in glabrous (non-hairy) skin as found on the palm, sole, and the lips, as compared to hairy skin, which covers the rest of the body.

Tactile afferents are somatosensory neurons whose cell bodies reside within the dorsal root ganglia (DRG) and the cranial sensory ganglia, respectively. One branch of these sensory neurons penetrates the spinal cord (for DRG neurons) or targets the trigeminal nuclei of the brainstem (for trigeminal neurons). The other branch extends to the periphery and either terminates as a nerve ending or associates with cutaneous mechanosensory end organs. Some of these associations are still debated and might not apply to all skin types. In the following, we will note links between afferent classes and mechanoreceptive end organs that have been made in the literature, but our estimates will be based on electrophysiologically characterized afferent types, and we make no claim regarding their associated mechanoreceptors. We will report innervation densities as units/cm^2, where we take a unit as the structure composed of an afferent fiber and all the mechanoreceptors (if any) innervated by it. The following estimates apply to young adults; for a discussion of the decrease of innervation with age, please see *Tactile innervation over the lifespan*.

2.1 Glabrous skin of the hand

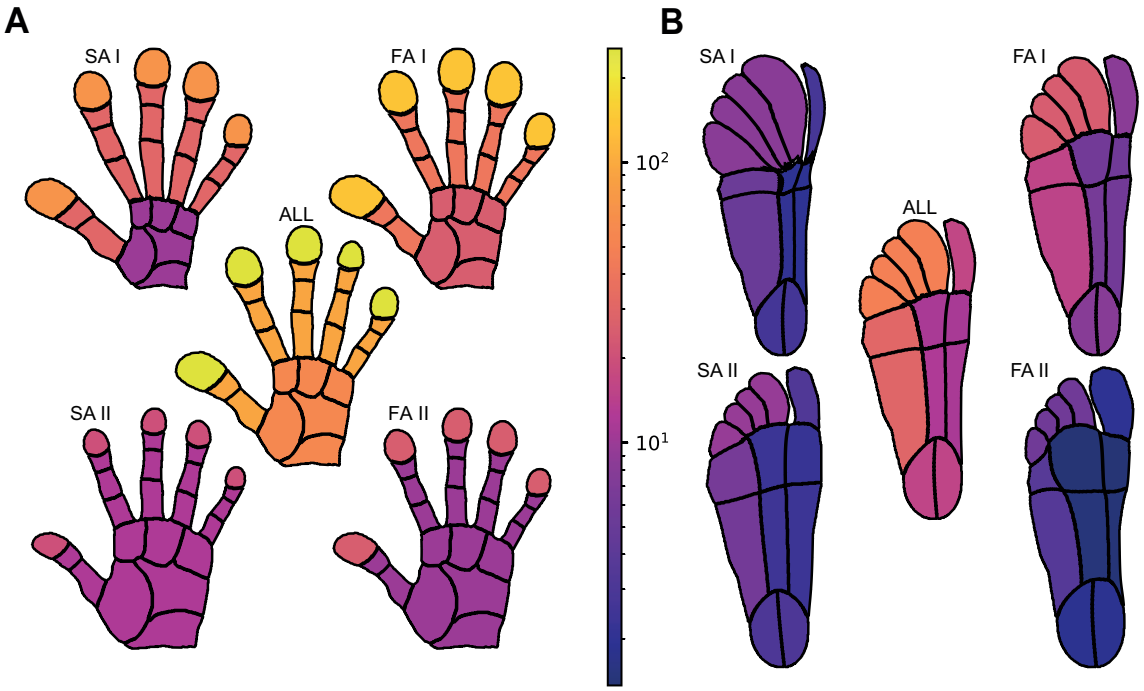

Fig. 3: Innervation densities for (A) the palmar surface of the human hand, and (B) the plantar surface of the human foot. Each area is scaled and colored by its innervation density (units/cm^2) to reveal the hand and foot 'homunculi'. In the hand, both SAI and FAI fibers are densely packed in the distal ends of the fingertips and much less so in the palm, while the two other afferent classes are more evenly spread throughout the hand and exhibit much lower innervation density overall. Compared to the hand, the foot sole is less densely innervated but displays a similar proximal-distal gradient for type I afferents. Additionally, in the foot, a lateral gradient is evident with denser innervation of the lateral than the medial arch for all afferent classes. All illustrations were generated from 2D region outlines using a flow-based algorithm that scales each region according to a target value while preserving border relationships between regions [54]

Unlike other body regions, the glabrous skin of the hand and its tactile afferent innervation have been extensively studied, owing to its importance in grasping and manipulation. The number of tactile afferent fibers in the glabrous skin of the hand of young adults is estimated to be around 17,000 [43]. There are slightly more fast-adapting fibers (56%) than slowly-adapting ones (44%), a common feature of glabrous skin (see section on the foot sole).

Four major afferent types have been identified in the palmar skin of the hand: fast-adapting type I (FAI) fibers that innervate Meissner corpuscles; slowly-adapting type I (SAI) fibers that innervate Merkel cells; slowly-adapting type II (SAII) fibers that innervate Ruffini corpuscles; and fast-adapting type II (FAII) fibers that innervate Pacinian corpuscles.

43% of tactile afferent fibers or around 7,310 fibers are fast adapting type I fibers (FAI). FAI

afferents are densely packed in the human fingertip with 141 units/cm^2 at its distal end. The density decreases in the proximal direction and only 25 units/cm^2 are present in the palm (see Figure 3A). The end organs of FAI fibers are Meissner corpuscles (MCs). Each Meissner corpuscle is innervated by one or two FAI fibers [55], and a single FAI fiber typically branches several times, with each branch innervating a small number of MCs [56, 57]. In the human fingertip, 3-5,000 MCs/cm^2 can be found [45, 58]. Meissner corpuscle density in the palm is considerably lower with 500 MCs/cm^2 at the thenar eminence [59]. These numbers suggest that there are at least twenty times more MCs than FAI fibers in the glabrous skin of the hand (> 155,000) and that each FAI fiber innervates around 40 MCs.

25% of tactile afferent fibers or around 4,250 fibers in the palmar region of a single hand are classed as slowly adapting type I fibers (SAI). SAI fibers are densely concentrated in the fingertips at around 70 units/cm^2 at its distal end, and less so in the more proximal area of the hand with 46 units/cm^2 in the middle phalanx and 10 units/cm^2 in the palm (see Figure 3A). SAI fibers repeatedly branch and innervate Merkel cell neurite complexes, which form clusters within the skin. In the fingerpad of normal adults, up to 10,000 Merkel cells/cm^2 can be found, but not all of them appear to serve mechanoreceptive functions or are connected to nerve fibers [60].

19% of tactile afferent fibers or around 3,230 fibers are classed as slowly adapting type II fibers (SAII). These are uniformly distributed across the glabrous skin area of the hand at an innervation density of approximately 12 units/cm^2. However, there is some evidence for increased density at the skin/nail border on the fingertips [43, 61]. SAII fibers innervate Ruffini corpuscles [62], but it is unclear whether all SAII-like responses originate from Ruffini corpuscles. Where they do, a one-to-one mapping between fibers and corpuscles is assumed [63].

Finally, up to 13% of tactile afferent fibers or around 2,200 fibers are estimated to be fast-adapting type II (FAII). The innervation density of this fiber type is low and relatively uniform across the hand surface at around 10 units/cm^2, but appears more numerous in distal finger segments with around 25 units/cm^2 These numbers yield an estimated total of around 800 FAII fibers terminating in the palm and 350 in each finger. FAII fibers target Pacinian corpuscles, and each corpuscle is innervated by a single fiber. It is possible for a single fiber to innervate multiple corpuscles [64], which often appear in clusters [65, 66] close to the digital nerves and their branches, and thus a

count of corpuscles can serve to establish an upper limit on the number of FAII fibers. Histological counts of Pacinian corpuscles show a steep decline between the fetal stage and old age. However, data from other age ranges is lacking, and the numbers presented here might be an over-estimation (see *Calculations and prior results* for further details).

Receptive fields of the type I fibers on the glabrous skin of the hand are small, circular, and well-defined with a mean area of 13 mm^2 for the FAI and 11 mm^2 for the SAI fibers. Receptive fields of type II fibers are larger with diffuse borders and a mean area of 101 mm^2 for FAII and 59 mm^2 for SAII fibers [67].

2.2 Glabrous skin of the foot sole

Somatosensory feedback from the lower limb, and in particular from the foot sole, plays an important role in controlling balance, posture, and gait [68, 69]. The foot sole is covered with glabrous skin and innervated by the same four classes of tactile afferents as the hand (SAI, SAII, FAI, FAII).

We estimate the total number of plantar cutaneous tactile afferent fibers innervating a single foot sole to be around 4,000, divided as follows: 17% (~680) SAI fibers, 20% (~800) SAII fibers, 51% (~2,040) FAI fibers, and 12% (~480) FAII fibers. These numbers are higher than an earlier estimate provided by [70] (see *Calculations and prior results* for details regarding our estimation methodology). Like the hand, the foot sole contains more fast-adapting (63%) than slowly-adapting fibers (37%). The distribution of cutaneous afferents is not uniform across the foot sole for type I afferents (Figure 3B). The overall highest innervation density is found in the toes (48 units/cm^2), followed by the lateral metatarsals (31 units/cm^2), the lateral arch (29.7 units/cm^2) and the heel (15.7 units/cm^2). Innervation density is lowest in the medial metatarsals (11.3 units/cm^2). FAI afferents are considerably more dense in the toes (24.5 units/cm^2) than in the metatarsal/arch (9.1 units/cm^2) and in the heel (8 units/cm^2). A similar distribution is observed for SAI afferents. Similar to the hand, SAII and FAII fibers are more uniformly distributed across the different areas of the foot sole (Figure 3B). In electrophysiological recordings, fewer tactile afferents have been found terminating in the great toe as would be expected given its size, and its innervation thus appears lower than that of the neighboring toes;

whether this discrepancy reflects a statistical artefact or a genuine difference remains to be seen.

The size of the receptive fields varies considerably for the different tactile fibers and across different foot areas with a mean value of 76 mm^2 for the SAI fibers, 248 mm^2 for SAII fibers, 81 mm^2 for FAI fibers, and 873 mm^2 for FAII fibers. In general, larger receptive fields are reported in the middle metatarsal and heel, and smaller receptive fields are located in the toes [70]. Receptive fields on the foot sole are thus several times larger than those measured in the hand, perhaps owing to the less dense innervation of this skin region and the different mechanical properties of the skin of the foot sole.

2.3 Face

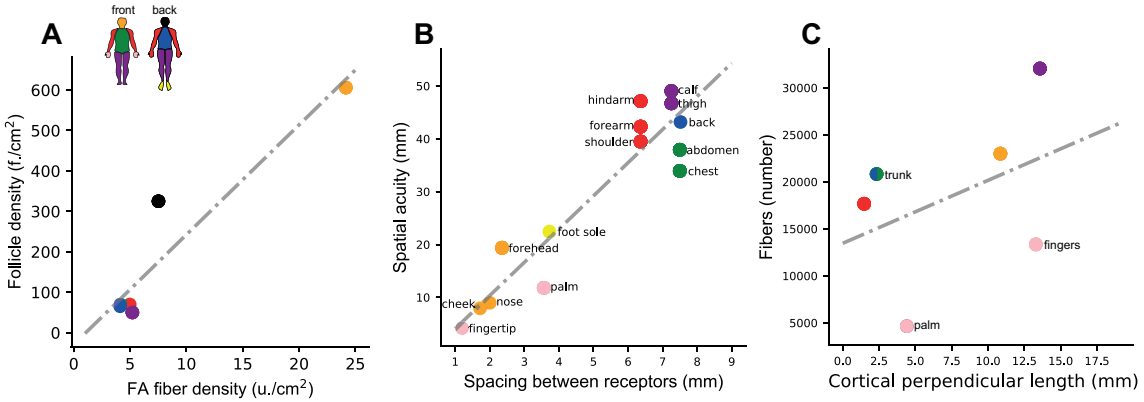

Fig. 4: (A) Estimated fiber density for FA hair cells on different skin regions versus average hair follicle density for the same skin regions. Colours denote different body parts, as indicated in the inset. The grey line shows the line of best fit. (B) Estimated spacing between SAI termination sites versus perceptual tactile acuity as assessed by two-point discrimination tasks for different body regions [71]. There is a strong relationship between a body region's tactile innervation and our ability to spatially discriminate tactile stimuli. (C) Size of cortical somatosensory representation for different body parts versus estimates for the total number of tactile fibers innervating that region. Innervation alone cannot explain cortical representation. Numbers refer to a single brain hemisphere.

The face is densely innervated by cutaneous fibers, especially the region around the mouth and lips, and also the inside of the oral cavity and the tongue, highlighting the essential sensory contribution to mastication and other eating-related behaviors. We estimate that around 43,000-46,000 tactile afferents innervate the hairy facial skin and the lips, excluding the oral cavity, which is likely to be innervated by around 16,000-19,000 fibers (see *Calculations and prior results* for details). For the purposes of this manuscript, we focus on the traditional notion of skin as the outer tissue of the body, which differs considerably in anatomy and physiology from the tissues within the oral cavity. Consequently we will not discuss the innervation of the oral mucosa further and instead refer the

interested reader to reviews by Trulsson (2006) [72] and Haggard and de Boer (2014) [73].

Four different classes of tactile afferents have been found in the hairy skin of the face and the red zone of the lip: slowly-adapting type I and type II, fast adapting type I and fast adapting hair follicle afferents [74]. Slowly adapting afferents are suggested to have two types of end-organs: Merkel cell-neurite complexes for SAI afferents and Ruffini endings for SAII afferents [75]. The hair follicle afferents (FA hair units) encountered in the facial skin are likely similar to hair units described in other hairy skin, but appear in some cases associated with a single hair only [74]. The nature of the end organs of FAI units in the facial skin is uncertain, as no Meissner corpuscles have been reported in this area [75]; possibly they are related to field units as in other hairy skin, though their receptive fields appear smaller. Notably, no FAII afferents have been reported in the literature, and vibrotactile thresholds on the face show no characteristic Pacinian sensitivity around 200 Hz [76], so this afferent class might be absent on the face, while present in other body regions.

Slowly adapting afferents appear more abundant than fast adapting ones in the facial skin [77, 78], with around 65% SA, resulting in 29,000 fibers, and 35% FA, resulting in 15,500 fibers. However, this breakdown is extrapolated from relatively small samples, so should be treated with caution.

Innervation density is not uniform across the face: we estimate an innervation density of 48 units/cm^2 for the forehead, eyes, and nose (V1), 67 units/cm^2 for the central part of the face (V2) and 84 units/cm^2 for the lower lip, the chin, the jaw and an area around the ears (V3). Locally, some regions such as the area immediately surrounding the mouth and the lips are likely to exhibit much higher innervation densities.

The size of the receptive fields varies for the different tactile afferent fibers with a mean value of 4 mm^2 for the SAI fibers, 6 mm^2 for SAII fibers and 6 mm^2 for FA fibers [77]. Most receptive fields have a circular or oval well-demarcated area of high and relatively uniform sensitivity [78]. The highest concentration and smallest size of the receptive fields are measured around the corner of the mouth and in the upper lip. The psychophysical and receptive field properties observed in these areas, including the tactile acuity, are similar to those found in the human fingertip [75], suggesting a similarly high innervation density.

2.4 Hairy skin

Studies investigating the sensory innervation of human hairy skin (other than facial) have often focused on C afferents or proprioceptive fibers, with relatively few targeting Aβ tactile afferents. Data exists for the hand dorsum [79–85], the arm [51, 86, 87], the leg [88–90], and the foot dorsum [85, 91–93], but not for the body core, back, or chest, where microneurography is technically challenging, due to the small size of the nerves involved and continuous movement of skin in this area during breathing.

Hairy skin is innervated by afferent classes with similar response characteristics as found in glabrous skin, though specific end organs might differ. As in all other types of skin, SAI afferents are present and innervate Merkel cells, which in hairy skin are organised into touch domes, as compared to the cell neurite complexes found in glabrous skin. Similarly, SAII afferents have been identified electrophysiologically, though it is unclear whether they always connect to Ruffini-like corpuscles, as is thought to be the case in the hand [94]. Afferents with response properties similar to FAI afferents are frequently observed, but unlike glabrous skin, hairy skin does not contain Meissner corpuscles. Instead, three different types of FA afferents have been identified in the hairy skin: hair units, field units, and FAII units [86]. Hair units branch and terminate in close proximity to hair follicles. Each hair unit is estimated to innervate around 25 individual hair follicles in the forearm [86]. Field units show remarkable similarities with hair units, having numerous high-sensitivity spots distributed over a fairly large area. The nature of the end-organs of field units is unclear. The presence of FAII afferents has been demonstrated both in electrophysiological recordings [86] and psychophysically [95], though Pacinian corpuscles appear to be extremely rare in hairy skin. Innervation patterns vary for different body regions, with a prevalence of SA afferents in the arms at 61% of all fibers, while they only make up 47% in the legs (see *Calculations and prior results* for further details).

Based on fiber counts and estimates of axon diameter distribution in the dorsal roots of the spinal cord (see *Calculations and prior results*), we estimate that around 140,000 Aβ fibers (range: 110,000-180,000) innervate the hairy skin of humans (excluding the face). Innervation is most dense in the back of the head and neck area with around 17 units/cm^2 and in the arms with 12 units/cm^2, while is almost uniform in the rest of the body, with 8.9 units/cm^2 covering the skin of

the chest and abdomen, 9 units/cm^2 on the back, and 9.8 units/cm^2 for the legs.

Hair units terminate on hair follicles in hairy skin, suggesting a relationship between hair follicle density and FA afferent innervation. Hair follicle density is not uniform across the adult body but instead varies by more than an order of magnitude across different body regions [96]. If the number of hair follicles innervated by a single afferent was relatively constant across different areas, one would, therefore, expect a strong correlation between our estimates of FA innervation density and hair follicle density. Indeed, we found a strong correlation ($r = 0.94$, $p < 0.01$) between both quantities (Figure 4A). Our estimates imply that each FA hair fiber innervates, on average, 25 hair follicles (range: 15-52), in strong agreement with earlier estimates for the forearm [86]. Hair follicles include both vellus and terminal hairs, both of which have been found to be innervated by nerve fibers [97].

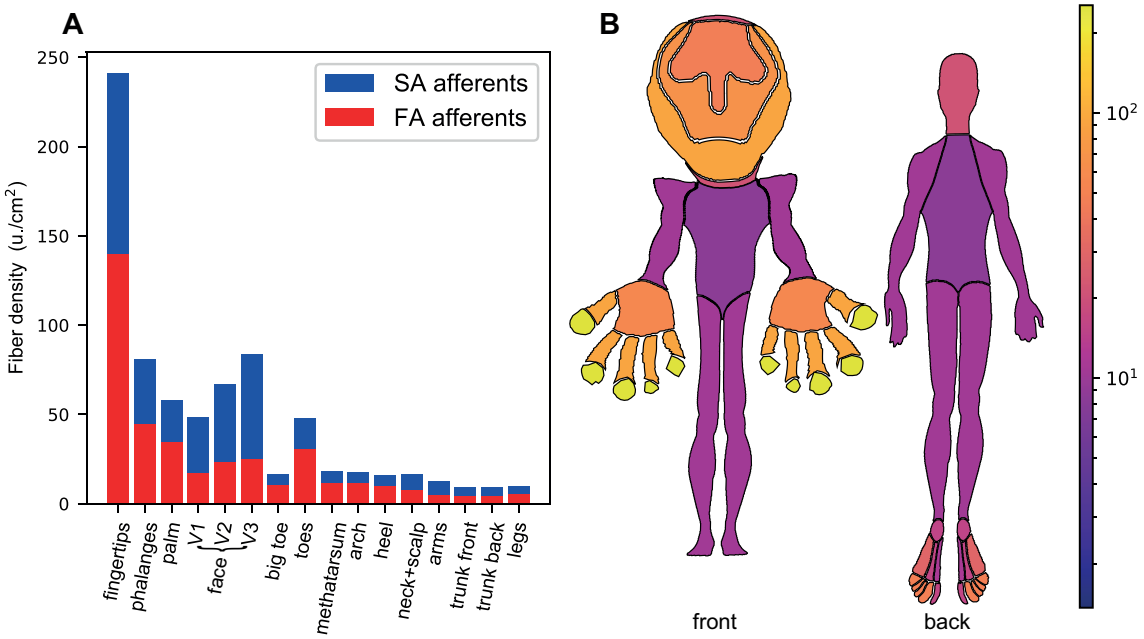

Fig. 5: Whole-body tactile innervation densities. The hand and face are the most densely innervated regions. (A) Total tactile innervation density for fast-adapting (red) and slowly-adapting (blue) afferents (including both type I and type II afferents), for different skin regions across the whole body. The ratio of fast and slowly adapting fibers is not constant but varies with skin region. (B) Illustration of the whole-body peripheral innervation homunculus using the same method as detailed in Figure 3. The color and scaling of each body area denotes its innervation density (units/cm^2), combining both SA and FA fibers.

	# of afferents	Innerv. dens. $u./cm^2$	Skin area cm^2	SA afferents %
Hand	16,500	90	184	43
Fingertips	5,061	241	21	42
Fingers	6,156	81	76	45
Palm	5,046	58	87	41
Foot Sole	3,958	21	200	37
Big Toe	261	16	16	37
Toes	913	48	19	37
Metatarsal	912	18	51	37
Arch	1,362	18	76	37
Heel	597	16	38	37
Face	46,000	69	675	65
Face V1	12,307	48	255	65
Face V2	14,676	67	219	65
Face V3	16,820	84	200	70
Neck+Scalp	8,625	17	516	55
Front trunk	20,886	9	2,272	55
Back trunk	20,775	9	2,272	55
Arms	35,335	13	2,769	61
Legs	56,186	10	5,722	47
Total	~230,000	15	~15,000	53

Table 1: Estimated number of afferents, innervation density, skin area, and proportion of slowly-adapting afferents (of both types) for different body regions. Shaded rows indicate sub-regions of larger body parts. Entries for the hand and foot sole refer to a single body part, while all other estimates are bilateral.

2.5 Whole body

Summarizing all information above, across the whole body the palmar skin of the hands and the perioral region of the face are the most densely innervated regions. Relatively high innervation can also be found in some sections of the foot, such as the toes, while the hairy skin of the arms and legs are the least densely innervated, closely followed by the trunk (see Figures 5, and Table 1).

3 Innervation density in context

3.1 Innervation density and tactile acuity

Innervation density limits the spatial resolution with which tactile features can be resolved on the skin: lower innervation results in a larger spacing between receptors and implies that two

tactile stimuli need to be further apart to be discriminated. One might, therefore, expect a strong correlation between receptor spacing and perceptual tactile acuity as determined in psychophysical experiments. Previous work suggests that spatial acuity is largely driven by SAI afferents [44], which possess the smallest receptive fields and, therefore, the highest spatial resolution. Indeed, a close relationship between SAI receptor spacing and tactile acuity has been established across the different regions of the hand [98, 99]. Following this line of research, we used psychophysical two-point discrimination thresholds obtained from different regions across the whole body [71, 100] and correlated these values with estimated SAI receptor spacing. We found a strong relationship between these two variables ($r = 0.93$, $p < 0.001$, see Fig. 4B). As prior research has shown, tactile acuity is not fixed but improves with training; while the eventual plateau performance is likely determined by innervation density, typical performance might not [44]. Additionally, more reliable measures of spatial acuity than the classical two-point threshold do exist [101], and these suggest that, for example, the lips in fact exhibit higher acuity than the fingertips [102, 103]. Nevertheless, differences in innervation density across the whole body appear large enough to yield a reliable correlation with two-point psychophysical thresholds.

The reasoning above ignores the fact that receptive fields of type I afferents are not uniform, but contain several individual subfields or hot spots, as demonstrated in both glabrous [104, 105] and hairy skin [86]. The number of such hot spots might ultimately determine perceptual limits on the spatial resolution of the skin. Indeed, one of the first studies aiming to relate the accuracy of tactile perception with afferent fiber counts [106] based their analysis on perceptual threshold mapping of the skin on a spatial scale similar to individual subfields [107]. Based on the average estimated number of subfields per fiber (FAI: 15, SAI: 6 for glabrous skin; hair units: 25, field: 10, SAI: 3 for hairy skin) one might therefore expect around 1.5 million hot spots across the whole body, with around 150,000 on the palmar surface of each hand, mostly supported by FA fibers.

3.2 Innervation density and the cortical homunculus

As demonstrated by pioneering work in humans [46, 108] and non-human primates [109, 110], body regions are mapped somatotopically onto the primary somatosensory cortex (S1), with nearby regions on the body generally represented by nearby patches in cortex. However, the size of individual body region representations in cortex is not proportional to that anatomical region's

skin surface area. For example, the area devoted to the thumb in S1 is as large as the area devoted to the entire forearm [40]. These findings have led to the famous homunculus, in which body parts are scaled by the size of their cortical representation, and which displays enlarged hands, face, and tongue. In how far cortical magnification is driven purely by innervation density, or whether usage effects such as increased contact with some body parts over others also play a part, has been debated. Many studies and textbooks argue for a close correlation between innervation density and cortical magnification [41, 111], though quantitative evidence is lacking. To test this idea directly, we took estimates of cortical magnification from the literature [108, 112], and compared these with the innervation density estimates described above. We found a positive, but non-significant, correlation between a region's peripheral tactile fiber count and the size of its representation in cortex ($r = 0.40$, $p = 0.42$, Figure 4C), when assessed as the length of the coronal section onto which that body part is mapped. Crucially, some regions exhibited much larger cortical magnification than would be expected from their peripheral innervation alone. This included the heavily enlarged cortical areas containing the hand and face representations. Thus, it appears that these body parts are further magnified cortically, perhaps reflecting the fact that they are more likely to receive tactile stimulation [113, 114] or that they are especially behaviourally relevant. Interestingly, the apparent cortical magnification of regions with already high innervation mirrors the visual system, where the fovea is further magnified cortically beyond its already higher density of cone photoreceptors [115].

3.3 Tactile innervation over the lifespan

Our estimates of innervation density are based on data from a range of ages, but we have tried, as much as possible, to focus on young adults. It has been widely demonstrated that tactile sensibility declines with age, as evidenced by increased sensory thresholds [116–119] and decreased spatial acuity [120–124]. This decline might be partially explained by age-related mechanical changes of the skin itself, such as in stiffness or moisture levels, but neural degeneration through changes in myelination, and receptor and fiber loss are likely to play a major part.

Focusing on the loss of tactile afferents specifically, a substantial decrease in the number of myelinated fibers in the spinal cord dorsal root from early middle age onwards has been well documented (see [125]). After a considerable increase in the number of myelinated fibers in the

first life decade, a gradual loss of fibers occurs throughout the lifespan from the third decade onwards, with an approximate loss rate of 5-8% per decade [126–128]. Therefore, the proposed estimate of 230,000 tactile afferents in the whole body of a young adult might be reduced to about 160,000 tactile afferents for people over 80 years old. There is evidence that the decrease in the number of fibers due to aging is more pronounced in some body regions than others, and that the skin of the face, arms, legs, hands, and feet are most affected, while the number of fibers innervating the abdomen remains almost unchanged [129].

The mechanoreceptive end organs themselves are also affected by aging and might change their morphology or disappear completely over time. This effect has been best documented for type I afferents. For example, the density of Meissner corpuscles at the fingertip decreases more than three-fold from young adulthood to old age, and that of Merkel cells declines more than five-fold [130].

4 Calculations and prior results

In the following, we provide an overview of measurements from the literature and detail the calculations that led to the estimates of innervation density described in the previous sections. Our approach relies on fiber counts from the dorsal root ganglia and the trigeminal nerve, estimates of the proportion of tactile Aβ fibers within each segment, and finally measurements for the surface area of skin innervated by each. The same basic idea has been pursued before [131], but advances in histology and immunohistochemistry, along with a much advanced understanding of the different classes of fibers involved in tactile sensibility prompted us to provide a modern re-assessment.

4.1 Hand

For the palmar surface of the hand we follow the original estimates by [43], which agree well with later histological analyses: a count of myelinated fibers at both the metacarpophalangeal (MCP) joint, covering all fibers innervating a given finger, and at the terminal trifurcation, covering innervation of the fingertips only, yielded 2,100-4,800 fibers per finger and roughly 1,900-2,600 per fingertip [132]. Assuming that around 45% of these fibers are tactile afferents in

the Aβ range, similar to the proportion that has been estimated at the wrist [133], yields 1,000-2,200 tactile afferents per finger and roughly 800-1,200 per fingertip. These numbers agree remarkably well with Johansson and Vallbo's original estimates of 2,500 for the whole finger and 1,000 for the fingertip of the index finger [43]. Psychophysical measurements also suggest that innervation density decreases dramatically between the fingertip and the palm, and SAI receptor spacing as calculated from Johansson and Vallbo (1979)'s estimates correlates highly with spatial acuity across different regions of the hand [98, 99].

Pacinian corpuscles are relatively large and can, therefore, easily be identified in dissections, at least in principle. No dissection data has been reported from young adults and the few existing studies focus on either fetal tissue or cadavers of elderly individuals. These present a mixed picture. On the one hand, fetal studies are in good agreement with the estimates made by Johansson and Vallbo (1979). [43]. Cauna and Mannan (1958) [134] counted Pacinian corpuscles in the radial half of a fetal index finger and found 178 in total, in almost perfect agreement with Johansson's estimates of afferent numbers (see also [135] for further analysis). In support of these findings, recent counts from the distal segment of several fetal fingers also yielded numbers in close agreement and confirmed that PC innervation is higher in the distal than in other finger segments [136]. On the other hand, studies in elderly individuals report much lower numbers. Dissection of the whole hand of several old-age human cadavers has found around 300 corpuscles per hand [66]. A more recent count in several distal finger segments yielded proportionally higher numbers (around 40 corpuscles per segment), but these counts were still much lower than those in fetal tissue [137]. Taken together, these results suggest a dramatic decrease in the number of Pacinian corpuscles with age, but it is unclear whether this decrease takes place early during development, later in life, or whether it is spread out across the lifetime. As the original estimates by Johansson and Vallbo (1979) [43] are in good agreement with the fetal data, we used them in our report. However, it is possible that the true number of FAII fibers is lower than reported here, perhaps by half or more. More recently, it has been shown that Pacinian corpuscles can be resolved using high-field MRI [138, 139], opening the possibility to establish in-vivo counts across a range of age groups in the future.

4.2 Foot sole

A recent study estimated that around 1,700 tactile afferents innervate the plantar surface of a single foot [70]. Our estimates suggest that the actual innervation is likely higher, by a factor of approximately two, based on several observations. First, the original estimate was based on a study demonstrating a ratio of roughly 10:1 in myelinated fibers between the hand and the foot [132]. However, fiber counts were only taken at the metacarpophalangeal and metatarsophalangeal joints, respectively, and because innervation density gradients are steeper on the hand than on the foot, this does not imply a ratio of 10:1 in the total fiber count. Instead, a ratio of 4-5:1 appears more realistic. Second, tactile acuity is higher on the foot sole compared to the foot dorsum or other regions on the leg [100], suggesting a higher innervation density in this region, in line with our estimates for hairy skin (see below). Taken together, a total tactile innervation of 4,000 afferents per foot sole appears likely. To arrive at updated estimates for different regions of the foot sole, we took the total number of tactile afferents as estimated above and distributed them across the foot sole according to the relative densities established in [70].

As has been done in the hand, Pacinian corpuscles can be identified and counted in human fetal samples. Comparing the results of a recent study that focused on the toes [140] with our estimates yielded 2-3 times more corpuscles in the experimental sample, a reasonably close match given the low numbers involved. The discrepancy might be explained by the fact that the number of corpuscles might decrease after the fetal stage, that several corpuscles might be innervated by a single fiber, or that we have underestimated the overall number of fibers innervating the foot sole. Finally, in the toes Pacinian corpuscles appear much more numerous at the proximal rather than the distal end, in contrast to the fingers, and given the difficulty of pinpointing FAII termination sites in microneurographic experiments, it is possible that some have been attributed to the forefoot region instead.

4.3 Face

The sensory innervation of the face is supplied by the sensory root of the trigeminal nerve or fifth cranial nerve. In this root, the total number of fibers is estimated at 170,000, and approximately 62,000 of these are myelinated and fall within the diameter range of Aβ fibers [141]. The

trigeminal nerve branches into three major divisions which supply different areas of the face; the ophthalmic branch, or V1, innervates the upper part of the face, covering approximately 38% of the facial skin; the maxillary branch, or V2, innervates the mid-third of the face, including part of the nose and down to the upper lip, corresponding to approximately 32% of the total facial area; finally, the mandibular branch, or V3, innervates the lower part of the face and the area around the ears, and covers around 30% of facial skin.

The maxillary division V2 gives rise to six sensory branches, of which two are responsible for the sensory innervation of the hard palate inside the oral cavity (greater palatine and nasopalatine nerves). The mandibular division V3 includes five sensory branches, of which the lingual nerve and the buccal nerve innervate the floor of the oral cavity and the inside of the cheeks. Thus, four out of 11 branches of the V2 and V3 divisions innervate the inside of the mouth. Combining this fact with recent histological analyses, which found that skin within the V3 innervation area contains almost twice the number of fibers than skin innervated by V1 [142], suggests by rough approximation that around 25-30% of the 62,000 myelinated fibers of the trigeminal nerve are responsible for the sensory innervation of the oral mucosa, leaving around 43,000 to innervate the facial skin and lips.

The pattern of the sensory innervation changes across the three divisions and the density of myelinated fibers was estimated by Nolano et al. (2013) [142] as 8.0, 15.9, and 16.4 mm^2 in V1, V2, and V3, respectively. These estimates include multiple branches originating from the same afferent and also count any fibers merely traversing a given skin area rather than terminating there, and thus cannot be used directly to estimate the number of individual afferents. Nevertheless, in relative terms, these histological counts can be expected to scale proportionally to the actual afferent counts. To arrive at estimated innervation densities for V1, V2, and V3, we therefore divided the total number of fibers estimated above across V1, V2, and V3 in the proportions estimated by [142]. A total facial skin area of 675 cm^2 was assumed [143]. See Supplemental Table 2 for precise calculations (or DOI:10.15131/shef.data.12753650).

4.4 Hairy skin on arms, trunk, and legs

The dorsal roots of the spinal cord contain 1-1.2 million fibers in total, ranging from large, medium, and small myelinated to unmyelinated nerve fibers [144, 145]. The region of skin innervated by all tactile afferents passing through a given dorsal root is known as a dermatome. While the specific territory innervated by each dermatome varies between people, and dermatomes also generally overlap within individuals, they nevertheless follow a systematic pattern. Fiber counts in individual dorsal roots can, therefore, be used to estimate the innervation of their associated dermatomes. The estimates presented here are based on recent fiber counts published by Liu et al. (2015) [144]. The territory of each dermatome is derived from an evidence-based map that assessed and combined multiple existing data sets [146]; we traced the published dermatome outlines and then calculated the area of skin innervated by each dermatome as the sum of the areas covering the front and back of the body, respectively, assuming a total area of skin of 1.5 m^2 [147]. This analysis also takes into account that dermatomes generally overlap. We also compared the estimated peripheral fiber innervation densities derived from these maps with ones based on an older dermatome representation in a popular textbook [148]. We found only minor differences, suggesting that our results do not hinge on a particular dermatome map.

Only a subset of dorsal root fibers will be myelinated fibers in the Aβ range and underlie tactile innervation of the skin, rather than internal organs. The fraction of myelinated fibers varies across the spinal tract, being higher in the cervical and lumbar tract [149, 150] and, on average, around 40% of axons have been classified as unmyelinated [151]. Assuming a 50:50 split between Aδ and Aβ myelinated fibers, and considering around 10% of Aβ fibers innervating deep structures [133], an average fraction of 17% (range: 10%-25%) of the fibers in the dorsal roots are estimated to represent Aβ fibers involved in the transmission of tactile sensations. In the dermatomes C6-C8, for example, we estimate that about 53,500 of the 210,000 fibers are tactile afferents. Considering that approximately 36,000 of these are in the ulnar and median nerve and innervate the glabrous skin of the hand, the remaining tactile afferents in the C6-C8 dermatomes cover the hairy skin of the hand dorsum and forearm. This calculation leads to an estimated density of 12.7 units/cm^2 in these areas, which is consistent with the overall hairy skin estimations here proposed. Our estimates also agree well with a recent count in the L4 and L5 dorsal roots that found around 30%

of axons had a diameter bigger than 5 µm, not all of which contribute to the tactile innervation of the skin [152]. Similarly, [150] estimated around 6,000 fibers/mm^2 in the sural nerve. 40% of these have a diameter in the range of 6-12 μm, which led to a total of 13,000 Aβ myelinated afferents in the sural nerve. Considering not all of these fibers are cutaneous afferents, and considering that the sural nerve contributes with other sacral nerves to the innervation of a skin area of around 4,500 cm^2 in the leg and foot, these measures result in good accordance with our estimates. Please see Supplemental Table 3 (or DOI: 10.15131/shef.data.12753650) for full calculations split by dermatomes.

The main source of uncertainty in our estimates is the total number of fibers in the dorsal root and, most importantly, the proportion of myelinated Aβ fibers for each dermatome [149, 152]. This question has only been investigated experimentally in a subset of dorsal roots, and different studies report conflicting results. For this reason, we repeated our calculations assuming a possible positive or negative variation of 20% on the number of tactile afferents for each dermatome. When doing so, we noticed that we fell short of or exceeded the physiologically plausible range in several instances, lending credibility to our original estimates. For example, in dermatomes C6, C7, and C8 considering that 18,000 of the total number of afferents can be expected to innervate the palmar surface of the hand, a reduction of more than 20% of the dorsal root fiber portion considered as tactile afferents, would result in a number close to zero (or even negative) for tactile afferents innervating the hairy skin of the back of the hand and part of the forearm. Similarly, an increase of more than 20% in the portion of dorsal root fibers considered to be tactile afferents would, in some dermatomes such as L1, result in areas of hairy skin having a density of afferents improbably close to that of the hairless skin of the foot and some areas of the palm of the hand. Taking these limits into account, the overall number of tactile afferents innervating the hairy skin is likely to fall in the range 110,000-180,000, leading to a total number of 200,000-270,00 afferents across the whole body.

To determine the proportion of SA and FA fibers, we tallied afferent numbers reported in different microneurography studies. For the hand dorsum and arm, we found a total of 267 reported afferents in the literature, 61% of which were slowly-adapting [51, 82–87]. For the foot dorsum and leg, our sample included 315 afferents, 47% of which were slowly adapting [85, 88–90, 92, 93]. Thus, a higher proportion of slowly-adapting afferents innervates

the arms than the legs. No data exists for the trunk. We assumed that the proportion of SA fibers for this region would fall in between those for the arms and the legs, as does overall innervation density, and settled on an estimate of 55% slowly-adapting fibers for the trunk. See Supplemental Table 4 (or DOI:10.15131/shef.data.12753650) for a detailed breakdown of afferent types reported in the literature on hairy skin.

Supporting information

	fibers total	density in Nolano (2013)	innervation pattern	branches innervating inner mouth/mucosa	sensory branches	fiber innervating skin	% area	skin area	Innervation density	%
		u./mm2	*%*					*cm2*	*u./cm2*	
V1	12307.69231	8	0.198511166			12307.6923	0.38	255.272973	48.21384787	0.28096465
V2	24461.53846	15.9	0.394540943	2	5	14676.9231	0.32	219.399013	66.89603046	0.33505034
V3	25230.76923	16.4	0.406947891	2	6	16820.5128	0.3	200.328013	83.96485618	0.38398502
Face	62000					43805.1282		675	64.91744879	1

Table 2: Calculations for total number and density of A-beta tactile fibers innervating the face.

Dermatom	N° fiber in Dorsal root	% myellinated %	A beta / A delta %	deep structure propio %	estimated% %	skin area total cm^2	glabrous skin cm^2	hairy skin cm^2	# fiber innervating skin total	glabrous	units estimated	density estimated u/cm^2	# of fiber ranges % min	# min	% max	# max
C2	23894.00	0.50	0.50	0.10	0.15	205.066807		205.07	3584.10		3584.10	17.48	0.12	2867.28	0.18	4300.92
C3	43752.00	0.50	0.50	0.10	0.15	315.349428		315.35	6562.80		6562.80	20.81	0.12	5250.24	0.18	7875.36
C4	21294.00	0.50	0.50	0.10	0.15	527.774541		527.77	3194.10		3194.10	6.05	0.12	2555.28	0.18	3832.92
C5	46600.00	0.50	0.50	0.10	0.15	220.013388		220.01	6990.00		6990.00	31.77	0.12	5592.00	0.18	8388.00
C6	72706.00	0.70	0.50	0.10	0.25	1030.53084	200.00	830.53	18176.50	7200.00	10976.50	13.22	0.2	7341.20	0.3	14611.80
C7	79306.00	0.70	0.50	0.10	0.25	1961.81652	200.00	1761.82	19826.50	14400.00	5426.50	3.08	0.2	1461.20	0.3	9391.80
C8	62312.00	0.70	0.50	0.10	0.25	624.306326	200.00	424.31	15578.00	14400.00	1178.00	2.78	0.25	1178.00	0.3	4293.60
T1	53014.00	0.50	0.50	0.10	0.15	1941.07529		1941.08	7952.10		7952.10	4.10	0.12	6361.68	0.18	9542.52
T2	20468.00	0.50	0.50	0.10	0.15	643.483913		643.48	3070.20		3070.20	4.77	0.12	2456.16	0.18	3684.24
T3	29776.00	0.50	0.50	0.10	0.15	488.959474		488.96	4466.40		4466.40	9.13	0.12	3573.12	0.18	5359.68
T4	21698.00	0.50	0.50	0.10	0.15	344.092813		344.09	3254.70		3254.70	9.46	0.12	2603.76	0.18	3905.64
T5	16710.00	0.50	0.50	0.10	0.15	310.014655		310.01	2506.50		2506.50	8.09	0.12	2005.20	0.18	3007.80
T6	20030.00	0.50	0.50	0.10	0.15	346.68822		346.67	3004.50		3004.50	8.67	0.12	2403.60	0.18	3605.40
T7	18246.00	0.50	0.50	0.10	0.15	438.144169		438.14	2736.90		2736.90	6.25	0.12	2189.52	0.18	3284.28
T8	15238.00	0.50	0.50	0.10	0.15	502.480363		502.48	2285.70		2285.70	4.55	0.12	1828.56	0.18	2742.84
T9	16738.00	0.50	0.50	0.10	0.15	472.357295		472.36	2510.70		2510.70	5.32	0.12	2008.56	0.18	3012.84
T10	22668.00	0.50	0.50	0.10	0.15	516.415156		516.42	3398.70		3398.70	6.58	0.12	2718.96	0.18	4078.44
T11	19426.00	0.50	0.50	0.10	0.15	430.139011		430.14	2913.90		2913.90	6.77	0.12	2331.12	0.18	3496.68
T12	20840.00	0.50	0.50	0.10	0.15	709.11081		709.11	3126.00		3126.00	4.41	0.12	2500.80	0.18	3751.20
L1	33640.00	0.60	0.50	0.10	0.20	549.297588		549.30	6728.00		6728.00	12.25	0.16	5382.40	0.24	8073.60
L2	37230.00	0.60	0.50	0.10	0.20	1199.67991		1199.68	7446.00		7446.00	6.21	0.16	5956.80	0.24	8935.20
L3	52382.00	0.60	0.50	0.10	0.20	1441.12435	10.47	1430.65	10476.40	121.7246512	10354.68	7.24	0.16	8259.40	0.24	12449.96
L4	62350.00	0.60	0.50	0.10	0.20	272.993175	173.39	99.61	12470.00	3072.580698	9397.42	94.35	0.16	6903.42	0.24	11891.42
L5	68910.00	0.60	0.50	0.10	0.20	704.143953	173.39	530.76	13782.00	3072.580698	10709.42	20.18	0.16	7953.02	0.24	13465.82
S1	83086.00	0.50	0.50	0.10	0.15	2246.67497	21.38	2225.30	12462.90	825.4296698	11637.47	5.23	0.12	9144.89	0.18	14130.05
S2	37284.00	0.50	0.50	0.10	0.15	1961.08069	21.38	1939.70	5592.60	825.4296698	4767.17	2.46	0.12	3648.65	0.18	5885.69
S3	23942.00		0.00	0.00	0.00	0.00		0.00	0.00		0.00	0.00	0	0.00	0	0.00
S4	6804.00	0.00	0.00	0.00	0.00	0.00		0.00	0.00		0.00	0.00	0	0.00	0	0.00
S5	4412.00	0.00	0.00	0.00	0.00	0.00		0.00	0.00		0.00	0.00	0	0.00	0	0.00
total	999588.00				0.17	20402.79			43917.74		140178.46		0.14	106474.82	0.21	176997.70

division	Cervical	Thoracic	Lumbar	Sacral
neck+scalp	C2+0.7 C3+0.14 C4			
arms + hand	0.3 C4 + C5 + C6,C7 + C8	T1+0.5 T2 +0.14 T3+0.4 T3 + 0.5 T4 + 0.6 T5 + 0.65 T6 + 0.54 T7 + 0.52 T8 + 0.6 T9 + 0.46 T10		
chest/abdomen	0.5 C3 + 0.4 C4	+ 0.52 T11 + 0.36 T12	0.1 L1	
back	0.16 C4	0.32 T2 + 0.5 T2:12	0.4 L1 + 0.2 L2	
legs			0.5 L1 + 0.8 L2 +L3, L4, L5	S1+S2

differents	total area	Thoracic	Lumbar	Sacral	total
	516.1350879				7969
	2769.765252	9487.20			35336
	2272.314614	15654.636	672.8		20230
	2272.314614	16084.464	4180.4		20776
	5722.073081		39782.31595	16404.64	56187

	Density
	15.440
	12.758
	8.903
	9.143
	9.819

overall total number of fibers	230096
max	266915
min	196393

Table 3: Calculations for total number and density of A-beta tactile fibers innervating the hairy skin, excluding the face based on fiber counts in dorsal root ganglia and estimates of the skin territory innervated by dermatomes.

REF	body area	SA%	SAI	SAII	FAI	FAII	Hair Units	Field Units	tot. units considered
Edin, B. B., and J. H. Abbs. 1991. "Finger Movement Responses of Cutaneous Mechanoreceptors in the Dorsal Skin of the Human Hand." Journal of Neurophysiology 65 (3): 657–70.	hand dorsum	0.64	32%	32%	28%	8%			107
Vallbo, A. B., H. Olausson, J. Wessberg, and N. Kakuda. 1995. "Receptive Field Characteristics of Tactile Units with Myelinated Afferents in Hairy Skin of Human Subjects." The Journal of Physiology 483 (Pt 3) (March): 783–95.	forearm	0.65	21	15		2	12	5	55
Edin, B. B., G. K. Essick, M. Trulsson, and K. A. Olsson. 1995. "Receptor Encoding of Moving Tactile Stimuli in Humans. I. Temporal Pattern of Discharge of Individual Low-Threshold Mechanoreceptors." The Journal of Neuroscience: The Official Journal of the Society for Neuroscience 15 (1 Pt 2): 830–47.	hand dorsum	0.46	5	9	12	1	1		28
Löken, Line S., Johan Wessberg, India Morrison, Francis McGlone, and Håkan Olausson. 2009. "Coding of Pleasant Touch by Unmyelinated Afferents in Humans." Nature Neuroscience 12 (5): 547–48.	arm	0.65	8	3			4	2	17
Ackerley, Rochelle, Helena Backlund Wasling, Jaquette Liljencrantz, Håkan Olausson, Richard D. Johnson, and Johan Wessberg. 2014. "Human C-Tactile Afferents Are Tuned to the Temperature of a Skin-Stroking Caress." The Journal of Neuroscience: The Official Journal of the Society for Neuroscience 34 (8): 2879–83.	arm	0.38	2	1			4	1	8
Kakuda, N. 1992. "Conduction Velocity of Low-Threshold Mechanoreceptive Afferent Fibers in the Glabrous and Hairy Skin of Human Hands Measured with Microneurography and Spike-Triggered Averaging." Neuroscience Research 15 (3): 179–88.	hand dorsum	0.65	21	7	15				43
Nagi, Saad S., Andrew G. Marshall, Adarsh Makdani, Ewa Jarocka, Jaquette Liljencrantz, Mikael Ridderström, Sumaiya Shaikh, et al. 2019. "An Ultrafast System for Signaling Mechanical Pain in Human Skin." Science Advances 5 (7): eaaw1297.	hand dorsum	0.44	1	3	3			2	9
	foot dorsum	0.37	10	4	6			18	38
Ribot-Ciscar, E., J. P. Vedel, and J. P. Roll. 1989. "Vibration Sensitivity of Slowly and Rapidly Adapting Cutaneous Mechanoreceptors in the Human Foot and Leg." Neuroscience Letters 104 (1-2): 130–35.	frontal leg/foot dorsum	0.43	23		30				53
Ribot-Ciscar, E., J. P. Roll, M. F. Tardy-Gervet, and F. Harlay. 1996. "Alteration of Human Cutaneous Afferent Discharges as the Result of Long-Lasting Vibration." Journal of Applied Physiology 80 (5): 1708–15.	anterior leg/foot dorsum	0.56	15		12				27
Edin, B. 2001. "Cutaneous Afferents Provide Information about Knee Joint Movements in Humans." The Journal of Physiology 531 (Pt 1): 289–97.	thigh	0.43	23		6		24	1	54
Aimonetti, Jean-Marc, Valérie Hospod, Jean-Pierre Roll, and Edith Ribot-Ciscar. 2007. "Cutaneous Afferents Provide a Neuronal Population Vector That Encodes the Orientation of Human Ankle Movements." The Journal of Physiology 580 (Pt. 2): 649–58.	leg	0.54	21	27	24	17			89
Trulsson, M. 2001. "Mechanoreceptive Afferents in the Human Sural Nerve." Experimental Brain Research. Experimentelle Hirnforschung. Experimentation Cerebrale 137 (1): 111–16.	foot dorsum	0.44	35%	9%	48%	7%			54

arm/hand dorsum	0.61	267
leg/foot dorsum	0.47	315

Table 4: A tally of slowly and fast-adapting fibers reported in the microneurography literature of the hairy skin. Fiber proportions are calculated for two skin regions: the hand dorsum and arms, as well as the foot dorsum and legs.

References

[31] C. A. Curcio, K. R. Sloan, R. E. Kalina, and A. E. Hendrickson, "Human photoreceptor topography," *J. Comp. Neurol.*, vol. 292, no. 4, pp. 497–523, Feb. 1990.

[32] L. Ulehlová, L. Voldrich, and R. Janisch, "Correlative study of sensory cell density and cochlear length in humans," *Hear. Res.*, vol. 28, no. 2-3, pp. 149–151, 1987.

[33] A. G. Witney, A. Wing, J.-L. Thonnard, and A. M. Smith, "The cutaneous contribution to adaptive precision grip," *Trends Neurosci.*, vol. 27, no. 10, pp. 637–643, Sep. 2004.

[34] I. Panek, T. Bui, A. T. B. Wright, and R. M. Brownstone, "Cutaneous afferent regulation of motor function," *Acta Neurobiol. Exp.*, vol. 74, no. 2, pp. 158–171, 2014.

[35] M. Tsakiris, "My body in the brain: a neurocognitive model of body-ownership," *Neuropsychologia*, vol. 48, no. 3, pp. 703–712, Feb. 2010.

[36] F. McGlone, J. Wessberg, and H. Olausson, "Discriminative and affective touch: Sensing and feeling," *Neuron*, vol. 82, no. 4, pp. 737–755, May 2014.

[37] W. Taube Navaraj, C. García Núñez, D. Shakthivel, V. Vinciguerra, F. Labeau, D. H. Gregory, and R. Dahiya, "Nanowire FET based neural element for robotic tactile sensing skin," *Front. Neurosci.*, vol. 11, p. 501, Sep. 2017.

[38] M. Grunwald, *Homo hapticus: Warum wir ohne Tastsinn nicht leben können*. Droemer eBook, Aug. 2017.

[39] M. F. Bear, B. W. Connors, and M. A. Paradiso, *Neuroscience: Exploring the Brain*. Wolters Kluwer, 2016.

[40] E. B. Goldstein, *Sensation and Perception*. Cengage Learning, Feb. 2009.

[41] E. Kandel, J. Schwartz, and T. Jessell, *Principles of Neural Science, Fourth Edition*. McGraw-Hill Companies,Incorporated, Jan. 2000.

[42] D. Purves, G. Augustine, D. Fitzpatrick, W. C. Hall, A. LaMantia, R. Mooney, and L. E. White, *Neuroscience*. Sinauer, Jul. 2018.

[43] R. S. Johansson and A. B. Vallbo, "Tactile sensibility in the human hand: relative and absolute densities of four types of mechanoreceptive units in glabrous skin," *J Physiol (Lond)*, vol. 286, pp. 283–300, Dec. 1979.

[44] R. M. Peters, E. Hackeman, and D. Goldreich, "Diminutive digits discern delicate details: Fingertip size and the sex difference in tactile spatial acuity," *Journal of Neuroscience*, vol. 29, no. 50, pp. 15 756–15 761, Dec. 2009.

[45] A. Verendeev, C. Thomas, S. C. McFarlin, W. D. Hopkins, K. A. Phillips, and C. C. Sherwood, "Comparative analysis of meissner's corpuscles in the fingertips of primates," *J. Anat.*, vol. 227, no. 1, pp. 72–80, Jul. 2015.

[46] W. Penfield and E. Boldrey, "Somatic motor and sensory representation in the cerebral cortex of man as studied by electrical stimulation," *Brain*, vol. 60, no. 4, pp. 389–443, 1937.

[47] V. E. Abraira and D. D. Ginty, "The sensory neurons of touch," *Neuron*, vol. 79, no. 4, pp. 618–639, Aug. 2013.

[48] R. S. Johansson and J. R. Flanagan, "Coding and use of tactile signals from the fingertips in object manipulation tasks," *Nat. Rev. Neurosci.*, vol. 10, no. 5, pp. 345–359, Apr. 2009.

[49] H. P. Saal and S. J. Bensmaia, "Touch is a team effort: interplay of submodalities in cutaneous sensibility," *Trends Neurosci.*, vol. 37, no. 12, pp. 689–697, Sep. 2014.

[50] V. B. Mountcastle, *The Sensory Hand: Neural Mechanisms of Somatic Sensation*. Harvard University Press, Nov. 2005.

[51] L. S. Löken, J. Wessberg, I. Morrison, F. McGlone, and H. Olausson, "Coding of pleasant touch by unmyelinated afferents in humans," *Nat. Neurosci.*, vol. 12, no. 5, pp. 547–548, May 2009.

[52] J. Cole, M. C. Bushnell, F. McGlone, M. Elam, Y. Lamarre, Å. Vallbo, and H. Olausson, "Unmyelinated tactile afferents underpin detection of low-force monofilaments," *Muscle Nerve*, vol. 34, no. 1, pp. 105–107, Jul. 2006.

[53] A. G. Marshall, M. L. Sharma, K. Marley, H. Olausson, and F. P. McGlone, "Spinal signalling of c-fiber mediated pleasant touch in humans," *Elife*, vol. 8, Dec. 2019.

[54] M. T. Gastner, V. Seguy, and P. More, "Fast flow-based algorithm for creating density-equalizing map projections," *Proc. Natl. Acad. Sci. U. S. A.*, vol. 115, no. 10, pp. E2156–E2164, Mar. 2018.

[55] S. Matsuoka, H. Suzuki, S. Morioka, Y. Ogawa, and T. Kojima, "Quantitative and qualitative studies of meissner's corpuscles in human skin, with special reference to alterations caused by aging," *J. Dermatol.*, vol. 10, no. 3, pp. 205–216, Jun. 1983.

[56] N. Cauna, "Nerve supply and nerve endings in meissner's corpuscles," *Am. J. Anat.*, vol. 99, no. 2, pp. 315–350, Sep. 1956.

[57] M. Paré, A. M. Smith, and F. L. Rice, "Distribution and terminal arborizations of cutaneous mechanoreceptors in the glabrous finger pads of the monkey," *J. Comp. Neurol.*, vol. 445, no. 4, pp. 347–359, Apr. 2002.

[58] M. Nolano, V. Provitera, C. Crisci, A. Stancanelli, G. Wendelschafer-Crabb, W. R. Kennedy, and L. Santoro, "Quantification of myelinated endings and mechanoreceptors in human digital skin," *Ann. Neurol.*, vol. 54, no. 2, pp. 197–205, 2003.

[59] C. F. Bolton, R. K. Winkelmann, and P. J. Dyck, "A quantitative study of meissner's corpuscles in man," *Neurology*, vol. 16, no. 1, pp. 1–9, 1966.

[60] J. P. Lacour, D. Dubois, A. Pisani, and J. P. Ortonne, "Anatomical mapping of merkel cells in normal human adult epidermis," *Br. J. Dermatol.*, vol. 125, no. 6, pp. 535–542, Dec. 1991.

[61] I. Birznieks, V. G. Macefield, G. Westling, and R. S. Johansson, "Slowly adapting mechanoreceptors in the borders of the human fingernail encode fingertip forces," *J. Neurosci.*, vol. 29, no. 29, pp. 9370–9379, Jul. 2009.

[62] Z. Halata, "Ruffini corpuscle–a stretch receptor in the connective tissue of the skin and locomotion apparatus," *Prog. Brain Res.*, vol. 74, pp. 221–229, 1988.

[63] R. S. Johansson and A. B. Vallbo, "Spatial properties of the population of mechanoreceptive units in the glabrous skin of the human hand," *Brain Res.*, vol. 184, no. 2, pp. 353–366, Feb. 1980.

[64] K. Sathian and M. S. Devanandan, "Receptors of the metacarpophalangeal joints: a histological study in the bonnet monkey and man," *J. Anat.*, vol. 137 (Pt 3), pp. 601–613, Oct. 1983.

[65] M. R. Miller, H. J. Ralston, 3rd, and M. Kasahara, "The pattern of cutaneous innervation of the human hand," *Am. J. Anat.*, vol. 102, no. 2, pp. 183–217, Mar. 1958.

[66] B. Stark, T. Carlstedt, R. G. Hallin, and M. Risling, "Distribution of human pacinian corpuscles in the hand," *J. Hand Surg. Am.*, vol. 23, no. 3, pp. 370–372, Jun. 1998.

[67] A. B. Vallbo and R. S. Johansson, "Properties of cutaneous mechanoreceptors in the human hand related to touch sensation," *Hum. Neurobiol.*, vol. 3, no. 1, pp. 3–14, 1984.

[68] J. T. Inglis, P. M. Kennedy, C. Wells, and R. Chua, "The role of cutaneous receptors in the foot," in *Sensorimotor Control of Movement and Posture*, S. C. Gandevia, U. Proske, and D. G. Stuart, Eds. Boston, MA: Springer US, 2002, pp. 111–117.

[69] G. E. P. Pearcey and E. P. Zehr, "We are Upright-Walking cats: Human limbs as sensory antennae during locomotion," *Physiology*, vol. 34, no. 5, pp. 354–364, Sep. 2019.

[70] N. D. J. Strzalkowski, R. M. Peters, J. T. Inglis, and L. R. Bent, "Cutaneous afferent innervation of the human foot sole: what can we learn from single-unit recordings?" *J. Neurophysiol.*, vol. 120, no. 3, pp. 1233–1246, Sep. 2018.

[71] S. Weinstein, "Intensive and extensive aspects of tactile sensitivity as a function of body part, sex, and laterality," in *The skin senses*, D. R. Kenshalo, Ed. Springfield: Thomas, 1968, pp. 195–222.

[72] M. Trulsson, "Sensory-motor function of human periodontal mechanoreceptors," *J. Oral Rehabil.*, vol. 33, no. 4, pp. 262–273, Apr. 2006.

[73] P. Haggard and L. de Boer, "Oral somatosensory awareness," *Neurosci. Biobehav. Rev.*, vol. 47, pp. 469–484, Nov. 2014.

[74] M. Trulsson and G. K. Essick, "Sensations evoked by microstimulation of single mechanoreceptive afferents innervating the human face and mouth," *J. Neurophysiol.*, vol. 103, no. 4, pp. 1741–1747, Apr. 2010.

[75] M. Nordin and K. E. Hagbarth, "Mechanoreceptive units in the human infra-orbital nerve," *Acta Physiol. Scand.*, vol. 135, no. 2, pp. 149–161, Feb. 1989.

[76] S. M. Barlow, "Mechanical frequency detection thresholds in the human face," *Exp. Neurol.*, vol. 96, no. 2, pp. 253–261, May 1987.

[77] M. Bukowska, G. K. Essick, and M. Trulsson, "Functional properties of low-threshold mechanoreceptive afferents in the human labial mucosa," *Exp. Brain Res.*, vol. 201, no. 1, pp. 59–64, Feb. 2010.

[78] R. S. Johansson, M. Trulsson, K. A. Olsson, and K. G. Westberg, "Mechanoreceptor activity from the human face and oral mucosa," *Exp. Brain Res.*, vol. 72, no. 1, pp. 204–208, 1988.

[79] T. Järvilehto, H. Hämäläinen, and P. Laurinen, "Characteristics of single mechanoreceptive fibres innervating hairy skin of the human hand," *Exp. Brain Res.*, vol. 25, no. 1, pp. 45–61, May 1976.

[80] F. Konietzny and H. Hensel, "Response of rapidly and slowly adapting mechanoreceptors and vibratory sensitivity in human hairy skin," *Pflugers Arch.*, vol. 368, no. 1-2, pp. 39–44, Mar. 1977.

[81] T. Järvilehto, H. Hämäläinen, and K. Soininen, "Peripheral neural basis of tactile sensations in man: II. characteristics of human mechanoreceptors in the hairy skin and correlations of their activity with tactile sensations," *Brain Res.*, vol. 219, no. 1, pp. 13–27, Aug. 1981.

[82] N. Kakuda, "Conduction velocity of low-threshold mechanoreceptive afferent fibers in the glabrous and hairy skin of human hands measured with microneurography and spike-triggered averaging," *Neurosci. Res.*, vol. 15, no. 3, pp. 179–188, Oct. 1992.

[83] B. B. Edin and J. H. Abbs, "Finger movement responses of cutaneous mechanoreceptors in the dorsal skin of the human hand," *J. Neurophysiol.*, vol. 65, no. 3, pp. 657–670, Mar. 1991.

[84] B. B. Edin, G. K. Essick, M. Trulsson, and K. A. Olsson, "Receptor encoding of moving tactile stimuli in humans. i. temporal pattern of discharge of individual low-threshold mechanoreceptors," *J. Neurosci.*, vol. 15, no. 1 Pt 2, pp. 830–847, Jan. 1995.

[85] S. S. Nagi, A. G. Marshall, A. Makdani, E. Jarocka, J. Liljencrantz, M. Ridderström, S. Shaikh, F. O'Neill, D. Saade, S. Donkervoort, A. Reghan Foley, J. Minde, M. Trulsson, J. Cole, C. G. Bönnemann, A. T. Chesler, M. Catherine Bushnell, F. McGlone, and H. Olausson, "An ultrafast system for signaling mechanical pain in human skin," *Science Advances*, vol. 5, no. 7, p. eaaw1297, Jul. 2019.

[86] A. B. Vallbo, H. Olausson, J. Wessberg, and N. Kakuda, "Receptive field characteristics of tactile units with myelinated afferents in hairy skin of human subjects," *J. Physiol.*, vol. 483 (Pt 3), pp. 783–795, Mar. 1995.

[87] R. Ackerley, H. Backlund Wasling, J. Liljencrantz, H. Olausson, R. D. Johnson, and J. Wessberg, "Human c-tactile afferents are tuned to the temperature of a skin-stroking caress," *J. Neurosci.*, vol. 34, no. 8, pp. 2879–2883, Feb. 2014.

[88] E. Ribot-Ciscar, J. P. Roll, M. F. Tardy-Gervet, and F. Harlay, "Alteration of human cutaneous afferent discharges as the result of long-lasting vibration," *J. Appl. Physiol.*, vol. 80, no. 5, pp. 1708–1715, May 1996.

[89] B. Edin, "Cutaneous afferents provide information about knee joint movements in humans," *J. Physiol.*, vol. 531, no. Pt 1, pp. 289–297, Feb. 2001.

[90] J.-M. Aimonetti, V. Hospod, J.-P. Roll, and E. Ribot-Ciscar, "Cutaneous afferents provide a neuronal population vector that encodes the orientation of human ankle movements," *J. Physiol.*, vol. 580, no. Pt. 2, pp. 649–658, apr 2007.

[91] J. P. Vedel and J. P. Roll, "Response to pressure and vibration of slowly adapting cutaneous mechanoreceptors in the human foot," *Neurosci. Lett.*, vol. 34, no. 3, pp. 289–294, Dec. 1982.

[92] E. Ribot-Ciscar, J. P. Vedel, and J. P. Roll, "Vibration sensitivity of slowly and rapidly adapting cutaneous mechanoreceptors in the human foot and leg," *Neurosci. Lett.*, vol. 104, no. 1-2, pp. 130–135, Sep. 1989.

[93] M. Trulsson, "Mechanoreceptive afferents in the human sural nerve," *Exp. Brain Res.*, vol. 137, no. 1, pp. 111–116, Mar. 2001.

[94] M. R. Chambers, K. H. Andres, M. von Duering, and A. Iggo, "The structure and function of the slowly adapting type II mechanoreceptor in hairy skin," *Q. J. Exp. Physiol. Cogn. Med. Sci.*, vol. 57, no. 4, pp. 417–445, Oct. 1972.

[95] R. T. Verrillo, "Vibrotactile thresholds for hairy skin," *J. Exp. Psychol.*, vol. 72, no. 1, pp. 47–50, Jul. 1966.

[96] G. Szabo, "The regional anatomy of the human integument with special reference to the distribution of hair follicles, sweat glands and melanocytes," *Philos. Trans. R. Soc. Lond. B Biol. Sci.*, vol. 252, no. 779, pp. 447–485, Sep. 1967.

[97] K. Hashimoto, M. Ito, and Y. Suzuki, "Innervation and vasculature of the hair follicle," in *Hair and Hair Diseases*, C. E. Orfanos and R. Happle, Eds. Berlin, Heidelberg: Springer Berlin Heidelberg, 1990, pp. 117–147.

[98] J. C. Craig and K. B. Lyle, "A comparison of tactile spatial sensitivity on the palm and fingerpad," *Percept. Psychophys.*, vol. 63, no. 2, pp. 337–347, 2001.

[99] J. C. Craig and K. B. Lyle, "A correction and a comment on Craig and Lyle (2001)," *Percept. Psychophys.*, vol. 64, no. 3, pp. 504–506, Apr. 2002.

[100] F. Mancini, A. Bauleo, J. Cole, F. Lui, C. A. Porro, P. Haggard, and G. D. Iannetti, "Whole-body mapping of spatial acuity for pain and touch," *Ann. Neurol.*, vol. 75, no. 6, pp. 917–924, 2014.

[101] J. C. Craig and K. O. Johnson, "The Two-Point threshold: Not a measure of tactile spatial resolution," *Curr. Dir. Psychol. Sci.*, vol. 9, no. 1, pp. 29–32, Feb. 2000.

[102] R. W. Van Boven and K. O. Johnson, "The limit of tactile spatial resolution in humans: grating orientation discrimination at the lip, tongue, and finger," *Neurology*, vol. 44, no. 12, pp. 2361–2366, Dec. 1994.

[103] K. Sathian and A. Zangaladze, "Tactile spatial acuity at the human fingertip and lip: bilateral symmetry and interdigit variability," *Neurology*, vol. 46, no. 5, pp. 1464–1466, May 1996.

[104] R. S. Johansson, "Tactile sensibility in the human hand: receptive field characteristics of mechanoreceptive units in the glabrous skin area," *J. Physiol.*, vol. 281, pp. 101–125, 1978.

[105] J. A. Pruszynski and R. S. Johansson, "Edge-orientation processing in first-order tactile neurons," *Nat. Neurosci.*, no. August, pp. 1–7, Aug. 2014.

[106] S. W. Ranson, "Cutaneous sensation," *Science*, vol. 78, no. 2027, pp. 395–399, Nov. 1933.

[107] H. Strughold, "Über die dichte und schwellen der schmerzpunkte der epidermis in den verschiedenen körperregionen," *Zeitschrift für Biologie*, vol. 80, pp. 367–380, 1924.

[108] W. Penfield and T. Rasmussen, *The cerebral cortex of man; a clinical study of localization of function*. Oxford, England: Macmillan, 1950, vol. 248.

[109] W. H. Marshall, C. N. Woolsey, and P. Bard, "Cortical representation of tactile sensibility as indicated by cortical potentials," *Science*, vol. 85, no. 2207, pp. 388–390, Apr. 1937.

[110] J. H. Kaas, R. J. Nelson, M. Sur, C. S. Lin, and M. M. Merzenich, "Multiple representations of the body within the primary somatosensory cortex of primates," *Science*, vol. 204, no. May, pp. 521–523, 1979.

[111] M. Catani, "A little man of some importance," *Brain*, vol. 140, no. 11, pp. 3055–3061, 2017.

[112] G. S. Gandhoke, E. Belykh, X. Zhao, R. Leblanc, and M. C. Preul, "Edwin boldrey and wilder penfield's homunculus: A life given by mrs. cantlie (in and out of realism)," *World Neurosurg.*, vol. 132, pp. 377–388, Dec. 2019.

[113] W. M. Jenkins, M. M. Merzenich, M. T. Ochs, T. Allard, and E. Guíc-Robles, "Functional reorganization of primary somatosensory cortex in adult owl monkeys after behaviorally controlled tactile stimulation," *J. Neurophysiol.*, vol. 63, no. 1, pp. 82–104, 1990.

[114] M. Sur, M. M. Merzenich, and J. H. Kaas, "Magnification, receptive-field area, and "hypercolumn" size in areas 3b and 1 of somatosensory cortex in owl monkeys," *J. Neurophysiol.*, vol. 44, no. 2, pp. 295–311, 1980.

[115] Z. Popovic and J. Sjöstrand, "Resolution, separation of retinal ganglion cells, and cortical magnification in humans," *Vision Res.*, vol. 41, no. 10-11, pp. 1313–1319, 2001.

[116] P. J. Dyck, P. W. Schultz, and P. C. O'Brien, "Quantitation of touch-pressure sensation," *Arch. Neurol.*, vol. 26, no. 5, pp. 465–473, May 1972.

[117] J. M. Thornbury and C. M. Mistretta, "Tactile sensitivity as a function of age," *J. Gerontol.*, vol. 36, no. 1, pp. 34–39, Jan. 1981.

[118] R. T. Verrillo, "Age related changes in the sensitivity to vibration," *J. Gerontol.*, vol. 35, no. 2, pp. 185–193, Mar. 1980.

[119] G. A. Gescheider, S. J. Bolanowski, K. L. Hall, K. E. Hoffman, and R. T. Verrillo, "The effects of aging on information-processing channels in the sense of touch: I. absolute sensitivity," *Somatosens. Mot. Res.*, vol. 11, no. 4, pp. 345–357, 1994.

[120] K. L. Woodward, "The relationship between skin compliance, age, gender, and tactile discriminative thresholds in humans," *Somatosens. Mot. Res.*, vol. 10, no. 1, pp. 63–67, 1993.

[121] H. Manning and F. Tremblay, "Age differences in tactile pattern recognition at the fingertip," *Somatosens. Mot. Res.*, vol. 23, no. 3-4, pp. 147–155, Sep. 2006.

[122] F. Tremblay, K. Wong, R. Sanderson, and L. Coté, "Tactile spatial acuity in elderly persons: assessment with grating domes and relationship with manual dexterity," *Somatosens. Mot. Res.*, vol. 20, no. 2, pp. 127–132, 2003.

[123] J. C. Stevens and M. Q. Patterson, "Dimensions of spatial acuity in the touch sense: changes over the life span," *Somatosens. Mot. Res.*, vol. 12, no. 1, pp. 29–47, 1995.

[124] J. C. Stevens and K. K. Choo, "Spatial acuity of the body surface over the life span," *Somatosens. Mot. Res.*, vol. 13, no. 2, pp. 153–166, 1996.

[125] P. S. Spencer and J. Ochoa, "The mammalian peripheral nervous system in old age," in *Aging and Cell Structure*, J. E. Johnson, Ed. Plenum Press, 1981, vol. 1, pp. 35–104.

[126] K. B. Corbin and E. D. Gardner, "Decrease in number of myelinated fibers in human spinal roots with age," *Anat. Rec.*, vol. 68, no. 1, pp. 63–74, Apr. 1937.

[127] P. A. Low and P. J. Dyck, "Splanchnic preganglionic neurons in man: II. morphometry of myelinated fibers of T7 ventral spinal root," *Acta Neuropathol.*, vol. 40, no. 3, pp. 219–225, Nov. 1977.

[128] E. Gardner, "Decrease in human neurones with age," *Anat. Rec.*, vol. 77, no. 4, pp. 529–536, Aug. 1940.

[129] J. Decorps, J. L. Saumet, P. Sommer, D. Sigaudo-Roussel, and B. Fromy, "Effect of ageing on tactile transduction processes," *Ageing Res. Rev.*, vol. 13, pp. 90–99, Jan. 2014.

[130] J. García-Piqueras, Y. García-Mesa, L. Cárcaba, J. Feito, I. Torres-Parejo, B. Martín-Biedma, J. Cobo, O. García-Suárez, and J. A. Vega, "Ageing of the somatosensory system at the periphery: age-related changes in cutaneous mechanoreceptors," *J. Anat.*, vol. 234, no. 6, pp. 839–852, Jun. 2019.

[131] C. E. Ingbert, "On the density of the cutaneous innervation in man," *J. Comp. Neurol.*, vol. 13, no. 3, pp. 209–222, Oct. 1903.

[132] S. Auplish and S. Hall, "An immunohistochemical study of palmar and plantar digital nerves," *J. Hand Surg. Br.*, vol. 23, no. 1, pp. 6–11, Feb. 1998.

[133] A. B. Vallbo and R. S. Johansson, "The tactile sensory innervation of the glabrous skin of the human hand," in *Active Touch, the Mechanism of Recognition of Objects by Manipulation*, G. Gordon, Ed. Pergamon Press Ltd. (Oxford), 1978, pp. 29–54.

[134] N. Cauna and G. Mannan, "The structure of human digital pacinian corpuscles (corpus cula lamellosa) and its functional significance," *J. Anat.*, vol. 92, no. 1, pp. 1–20, Jan. 1958.

[135] A. J. Brisben, S. S. Hsiao, and K. O. Johnson, "Detection of vibration transmitted through an object grasped in the hand," *J. Neurophysiol.*, vol. 81, no. 4, pp. 1548–1558, Apr. 1999.

[136] J. H. Kim, C. Park, X. Yang, G. Murakami, H. Abe, and S. Shibata, "Pacinian corpuscles in the human fetal finger and thumb: A study using 3D reconstruction and immunohistochemistry," *Anat. Rec.*, vol. 301, no. 1, pp. 154–165, Jan. 2018.

[137] K. Kobayashi, K. H. Cho, M. Yamamoto, K. Mitomo, G. Murakami, H. Abe, and S. Abe, "Tree of Vater-Pacinian corpuscles in the human finger and thumb: a comparison between the late fetal stage and old age," *Surg. Radiol. Anat.*, vol. 40, no. 3, pp. 243–257, Mar. 2018.

[138] E. Laistler, B. Dymerska, J. Sieg, S. Goluch, R. Frass-Kriegl, A. Kuehne, and E. Moser, "In vivo MRI of the human finger at 7 T," *Magn. Reson. Med.*, vol. 79, no. 1, pp. 588–592, 2018.

[139] N. G. Rhodes, N. S. Murthy, N. Lachman, and D. A. Rubin, "Normal pacinian corpuscles in the hand: radiology-pathology correlation in a cadaver study," *Skeletal Radiol.*, May 2019.

[140] Z. W. Jin, K. H. Cho, D. Y. Xu, Y. Q. You, J. H. Kim, G. Murakami, and H. Abe, "Pacinian corpuscles in the human fetal foot: A study using 3D reconstruction and immunohistochemistry," *Ann. Anat.*, vol. 227, p. 151421, Jan. 2020.

[141] E. Pennisi, G. Cruccu, M. Manfredi, and G. Palladini, "Histometric study of myelinated fibers in the human trigeminal nerve," *J. Neurol. Sci.*, vol. 105, no. 1, pp. 22–28, Sep. 1991.

[142] M. Nolano, V. Provitera, G. Caporaso, A. Stancanelli, M. Leandri, A. Biasiotta, G. Cruccu, L. Santoro, and A. Truini, "Cutaneous innervation of the human face as assessed by skin biopsy," *J. Anat.*, vol. 222, no. 2, pp. 161–169, Feb. 2013.

[143] M. Siemionow and E. Sonmez, "Face as an organ," *Ann. Plast. Surg.*, vol. 61, no. 3, pp. 345–352, Sep. 2008.

[144] Y. Liu, X. Zhou, J. Ma, Y. Ge, and X. Cao, "The diameters and number of nerve fibers in spinal nerve roots," *J. Spinal Cord Med.*, vol. 38, no. 4, pp. 532–537, Jul. 2015.

[145] C. Ingbert, "An enumeration of the medullated nerve fibers in the dorsal roots of the spinal nerves of man," *J. Comp. Neurol.*, vol. 13, no. 2, pp. 53–120, Jun. 1903.

[146] M. W. L. Lee, R. W. McPhee, and M. D. Stringer, "An evidence-based approach to human dermatomes," *Clin. Anat.*, vol. 21, no. 5, pp. 363–373, Jul. 2008.

[147] C.-Y. Yu, C.-H. Lin, and Y.-H. Yang, "Human body surface area database and estimation formula," *Burns*, vol. 36, no. 5, pp. 616–629, Aug. 2010.

[148] J. C. B. Grant and J. E. Anderson, *Grant's Atlas of anatomy*. Williams & Wilkins, 1983.

[149] H. A. Davenport and R. T. Bothe, "Cells and fibers in spinal nerves. II. a study of c2, c6, t4, t9, l3, s2, and S5 in man," *J. Comp. Neurol.*, vol. 59, no. 1, pp. 167–174, Feb. 1934.

[150] D. J. O'Sullivan and M. Swallow, "The fibre size and content of the radial and sural nerves," *J. Neurol. Neurosurg. Psychiatry*, vol. 31, no. 5, pp. 464–470, Oct. 1968.

[151] D. Sheehan, "Some problems relating to the dorsal spinal nerve roots," *Yale J. Biol. Med.*, vol. 7, no. 5, pp. 425–440, May 1935.

[152] Z. J. Sperry, R. D. Graham, N. Peck-Dimit, S. F. Lempka, and T. M. Bruns, "Spatial models of cell distribution in human lumbar dorsal root ganglia," *J. Comp. Neurol.*, Dec. 2019.

Population coding strategies in human tactile afferents

G. Corniani, M. A. Casal, S. Panzeri and H. P. Saal, "Population coding strategies in human tactile afferents," *PLOS Computational Biology*, *under review*.

Keywords: *tactile coding* | *population coding* | *mechanoreceptors* | *mutual information*

Candidate's contribution to the paper

G.C., M.A.C., S.P., and H.P.S. conceived and designed research; G.C. and M.A.C. implemented the study (in particular, G.C. designed and produced the simulated dataset, G.C. implemented the dimensionality reduction pipeline, M.A.C. designed and implemented the GLM classifier, M.A.C. implemented the information theory analysis); G.C., M.A.C., S.P., and H.P.S. analyzed results; G.C. and M.A.C. prepared figures; G.C. and M.A.C. drafted manuscript; G.C., M.A.C., S.P., and H.P.S. edited and revised manuscript; G.C., M.A.C., S.P., and H.P.S. approved final version of manuscript.

Theoretical implementation	**Coding**	**Experiment design**	**Experiment execution**	**Data analysis**	**Paper writing**	**Academic authorship**
Yes	Yes	Yes	Yes	Yes	Yes	Co-first author

Abstract

Sensory information is conveyed by populations of neurons, and coding strategies cannot always be deduced when considering individual neurons. Moreover, information coding depends on the number of neurons available and on the composition of the population when multiple classes with different response properties are available. Here, we study population coding in human tactile afferents by employing a recently developed simulator of mechanoreceptor firing activity. First, we highlight the interplay of afferents within each class. We demonstrate that the optimal afferent density to convey maximal information depends on both the tactile feature under consideration and the afferent class. Second, we find that information is spread across different classes for all tactile features and that each class encodes both redundant and complementary information with respect to the other afferent classes. Specifically, combining information from multiple afferent classes improves information transmission and is often more efficient than increasing the density of afferents from the same class. Finally, we test the importance of timing precision and afferent identity in the population code to probe whether temporal and spatial information can be traded against each other. Destroying temporal information turns out to be more destructive than removing spatial information, and the contribution of either cannot be completely recovered from the other. Overall, our results suggest that both optimal afferent innervation densities and the composition of the population depend in complex ways on the tactile features in question, potentially accounting for the variety in which tactile peripheral populations are assembled in different regions across the body.

Author summary

Touching an object elicits neural responses from hundreds or thousands of individual tactile receptors of different classes embedded within our hand. Information about the extent of contact, the strength of the touch, and its temporal profile are carried jointly in this population response to be processed further by the central nervous system. However, studying the nature of the population code is empirically challenging, as electrophysiological recordings are typically obtained from single or a small number of neurons at most. Here, we make use of a computer simulation to recreate the population activity of large numbers of tactile neurons and examine

how information is spread across different neurons. We find that tactile information increases with afferent density, but the saturation point depends on both the tactile feature and afferent class. Importantly, information is generally spread across multiple afferent classes, such that a combination of afferents from multiple classes yields higher information than the same number of neurons from a single class. These results will be useful to guide future experiments and theoretical work on the processing of tactile information by the central nervous system.

1 Introduction

The brain processes information and makes decisions based on the activity of a large number of neurons [153]. Studying population activity can reveal aspects of the neural code that are obscured when only individual neurons are considered [154]. For example, the well-known population vector technique has shown that the direction of arm movements can be precisely decoded from a population of cortical motor neurons, even though individual neurons are only broadly tuned to direction [155]. Moreover, some coding strategies will become evident only if the responses of multiple neurons are considered. For example, while a neuron that remains silent to a certain stimulus might not appear to convey any information at all, when it is part of a larger population where other neurons are responding, this silence can be meaningful [156]. Response correlations between neurons also affect decoding (see [157] for an example). Furthermore, populations often consist of heterogeneous classes of neurons, especially in sensory systems, such as the diversity of retinal ganglion cells in the visual pathway [158] or the different classes of tactile neurons in the somatosensory periphery [159]. Theoretical studies have shown how response properties and class membership of individual neurons can be optimized to maximize joint information coding in the population [160–162]. However, because this optimization relies on the full population, predicting how or to what extent an individual neuron contributes to population coding becomes impossible without considering the properties of other neurons that make up the population. Given these findings, it is thus paramount to study the population activity of sensory neurons in order to understand what stimulus information is available at subsequent processing stages.

Tactile interactions are mediated by mechanoreceptive afferents and the glabrous skin of the human hand is innervated by approximately 17,000 fibers [163]. These are divided into different classes based on their response properties and receptive fields. Three classes are mainly involved in discriminative touch: slowly adapting type 1 afferents (SAI) exhibit small receptive fields and respond to static or low-frequency indentations, rapidly adapting afferents (RA) possess slightly larger receptive fields and respond to dynamic flutter stimuli, and Pacinian afferents (PC) exhibit extremely large receptive fields and are most responsive to high frequency vibrations. These classes also differ in the density with which they innervate the skin, both compared to each other and at different locations on the skin [163]. A stimulus applied to a specific skin area will

typically activate hundreds if not thousands of afferents of different classes all responding with distinct spiking responses [164]. However, peripheral neurophysiological measurements are subject to technical limitations, and typically only one or a small number of afferents are recorded at once. Moreover, many studies place the stimulus directly above the targeted afferent's receptive field hotspot, in an effort to maximize neural responses within the limited recording window, but such a setup implies that responses from receptors located away from the contact location will be neglected. Given these constraints, afferent activity on a population level has scarcely been investigated, and, consequently, our understanding of how tactile information is represented in the peripheral population is limited (though see [165] for a summary of tactile population codes).

A particular source of debate in the tactile literature has been the role of different afferent classes. Traditionally, each afferent class was thought to carry information about different and complementary stimulus features [166]. However, more recently it has become clear that most natural stimuli elicit responses from multiple afferent classes simultaneously (see summary in [167]), for example in texture perception [168]. Furthermore, both experimental evidence [169] and computational modeling [170] suggest that information from multiple classes of afferents is integrated in cortex, if not before, and psychophysical studies have revealed that the quality of a tactile percept does not necessarily depend on receptor class [171]. However, to what extent peripheral tactile population activity carries complementary information about relevant stimulus features in different afferent classes has not been quantified and it is therefore unclear when and how it would be beneficial to integrate such information.

Here, we investigate the contribution of large neural populations in tactile stimulus coding and examine the interplay of tactile submodalities in this process. Because the lack of population level data currently precludes empirical study, we used a large-scale computational model, Touchsim [172], to simulate the activity of hundreds of peripheral tactile afferents of three classes in response to naturalistic stimuli, similar to those commonly used in experimental settings. First, we parametrically studied the role of afferent density in single-class afferent populations to explore if and how the composition, and particularly the number of afferents, affects the stimulus information encoding. Secondly, we considered the three classes together and asked whether each class encoded complementary or redundant information regarding stimulus features.

Finally, we assessed the importance of temporal and spatial encoding precision when considering afferents on a population level. Overall, our work demonstrates that a population-level view of tactile coding is crucial for a thorough understanding of tactile information processing.

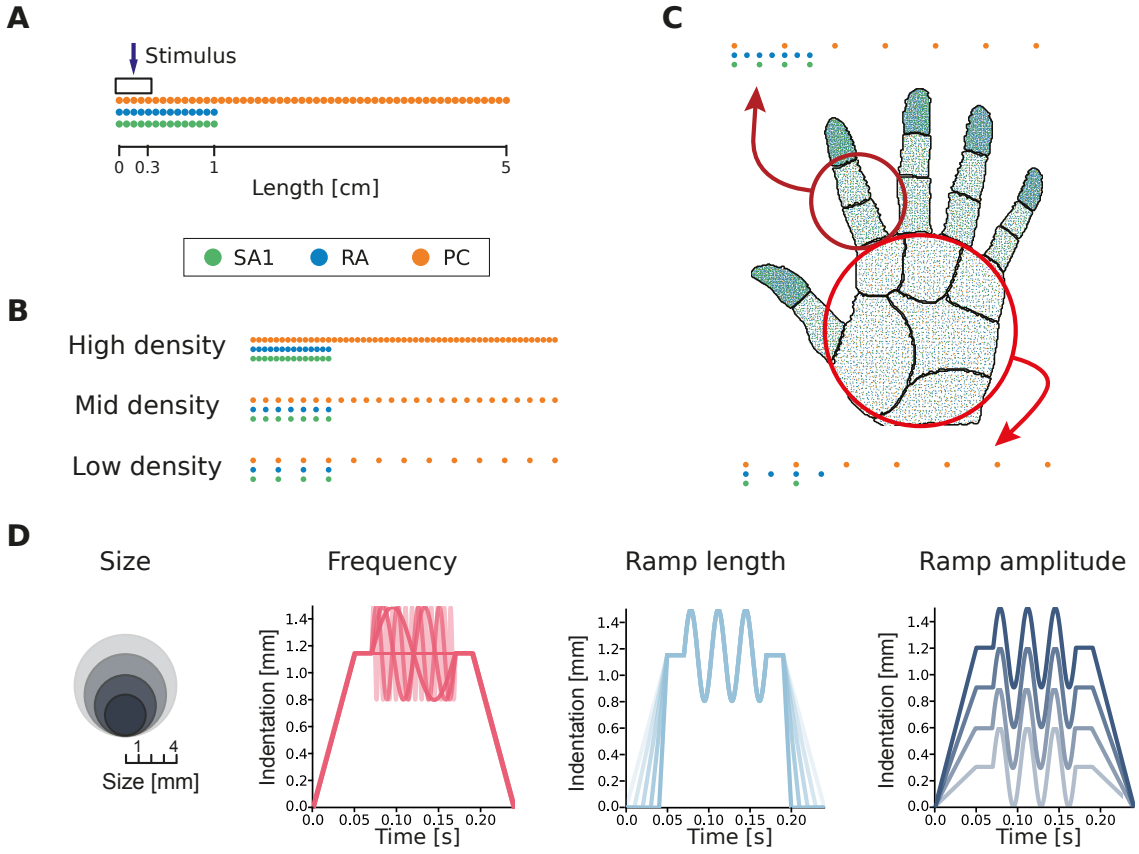

Fig. 6: Simulation setup. (A) Example of afferents terminating along a line, radiating outwards from the probe centre (indicated by the arrow). The probe has circular shape (of varying size) and is centred on the origin of the line. Dots of different colors corresponds to different afferent classes (separated in the illustration to facilitate visualization). **(B)** Example of afferent populations with different densities. **(C)** Representation of afferent densities measured on the human hand and corresponding simulated populations distributed over a line that mimic the densities observed in the palm and finger. **(D)** Illustration of the different stimulus features considered: probe size, vibration frequency, ramp length, and ramp amplitude.

2 Results

We used a large-scale neural simulator [172] to simulate the spiking activity of individual afferents belonging to three afferent classes (SAI, RA, PC) jointly spanning the range of tactile sensitivity. In our setup, we simulated the responses of a population of receptors placed along a line extending outwards from the contact location of the stimulus probe (see Fig 6A). This spatial

arrangement of receptors allowed for systematic manipulation of the receptor density in the simulations. Sixteen different afferent populations with a density ranging between 1 and 140 afferents/cm^2 were considered for each afferent class. Therefore, we could test the effect of low, medium, and high densities (Fig 6B) on information encoding and also directly examine natural innervation densities, such as those encountered on the palm or finger (Fig 6C). The simulated stimulus was a circular probe indented into the skin and then vibrated. We varied four stimulus features systematically across trials: the probe size (1-4 mm), the ramp amplitude (0.3-1.2 mm), the ramp length (10-50 ms), and the vibration frequency (0-200 Hz) (see Fig 6D and Methods). These parameters were chosen to span the range of tactile stimuli that are typically experienced. They are also similar to stimuli commonly employed in neurophysiological experiments, such as those used to fit the initial Touchsim model [172], and simulated responses can therefore be expected to be a close match to what would be recorded in an actual experiment. Finally, varying the stimulus across multiple parameters simultaneously ensures that the complexity of everyday tactile interactions is reproduced in the resulting population responses.

To analyse the simulated responses, we coupled advanced machine learning techniques with information-theoretic analysis to compute how much information about each stimulus feature was encoded in the activity of different populations of afferents (see Methods for details). In short, after simulating the spiking responses (Figure 7A), we first used Non-Negative Matrix Factorization (NMF) [173] to succinctly capture the spatiotemporal patterns of neural responses for each afferent class (Fig 7B). This technique linearly decomposes each single-trial spatiotemporal sequence of spike trains into a sum of non-negative spatiotemporal modules (describing the recurrent spatiotemporal patterns of firing of the population) and non-negative activation coefficients (describing how strongly each pattern is recruited in a given trial). NMF was chosen to reduce the dimensionality of population activity because it is a natural decomposition for spike trains, which are by definition non-negative, because it can give accurate single-trial representations of activity even when neural responses are non-orthogonal and overlapping from trial to trial, and because its coefficients are biologically interpretable [174, 175]. Following previous work [176], we then approximated the probabilities of occurrence of the NMF activation coefficients using a Generalized Linear Model (GLM; see Fig 7C). We then used this probabilistic model to compute the posterior probability of each

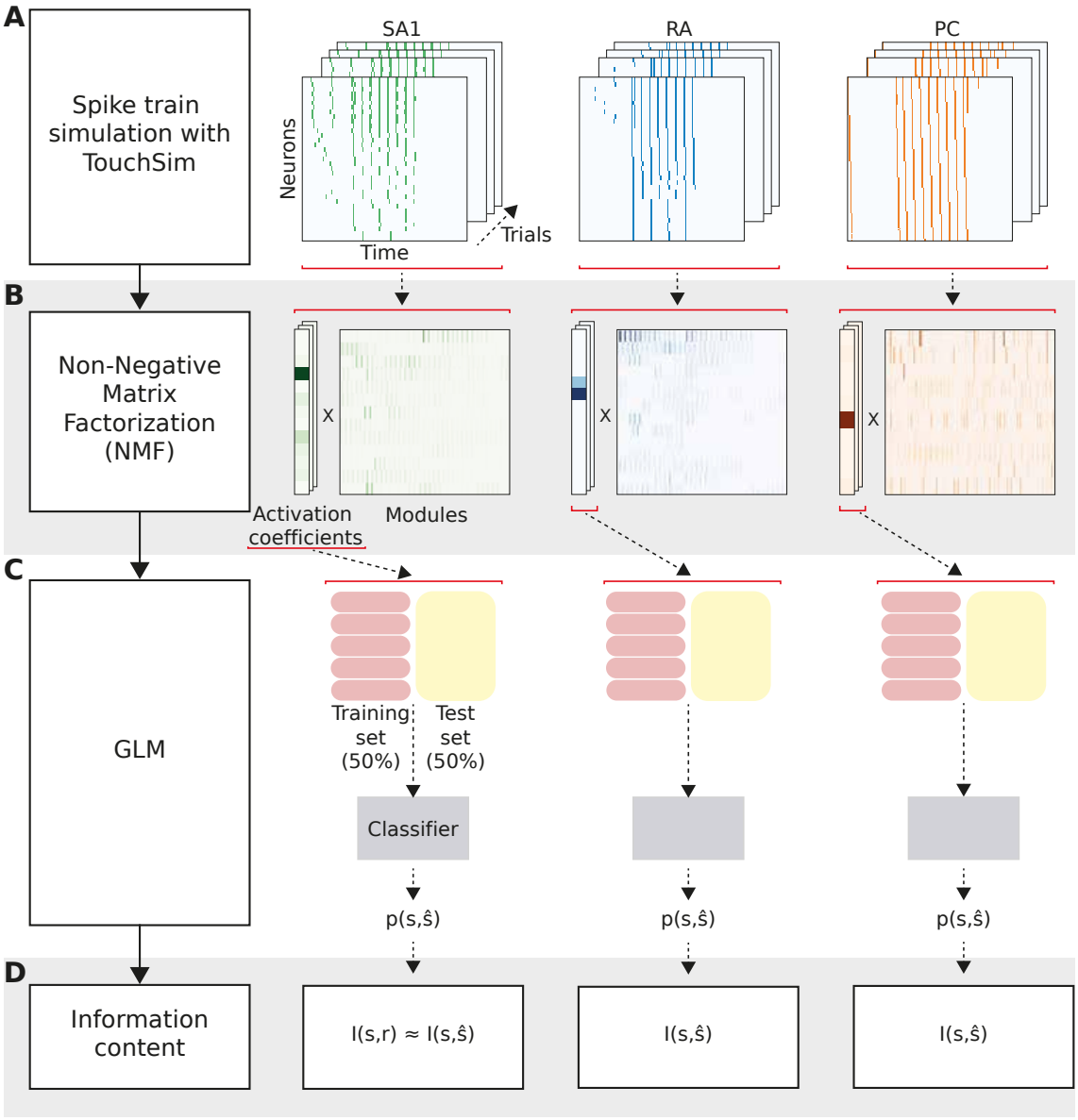

Fig. 7: Analysis pipeline and calculation of information. **(A)** The spike trains are simulated using Touchsim. **(B)** The spike matrices are then decomposed using the Non-Negative Matrix Factorization (NMF) method, obtaining a set of non-negative activation coefficients and modules. **(C)** A Generalized Linear Model (GLM) fed with the neural activity captured in the NMF activation coefficients gives the probability of observing each stimulus feature. **(D)** Probabilities are used to compute mutual information (MI), representing the information that the neural activity carries about the stimulus.

stimulus feature given the observation of the spatiotemporal population spike train in each trial. Finally, we computed the information using the posterior probabilities between the presented and the decoded stimulus (Fig 7D). This procedure provides a data-robust but effective lower bound to the total information carried by population activity [154].

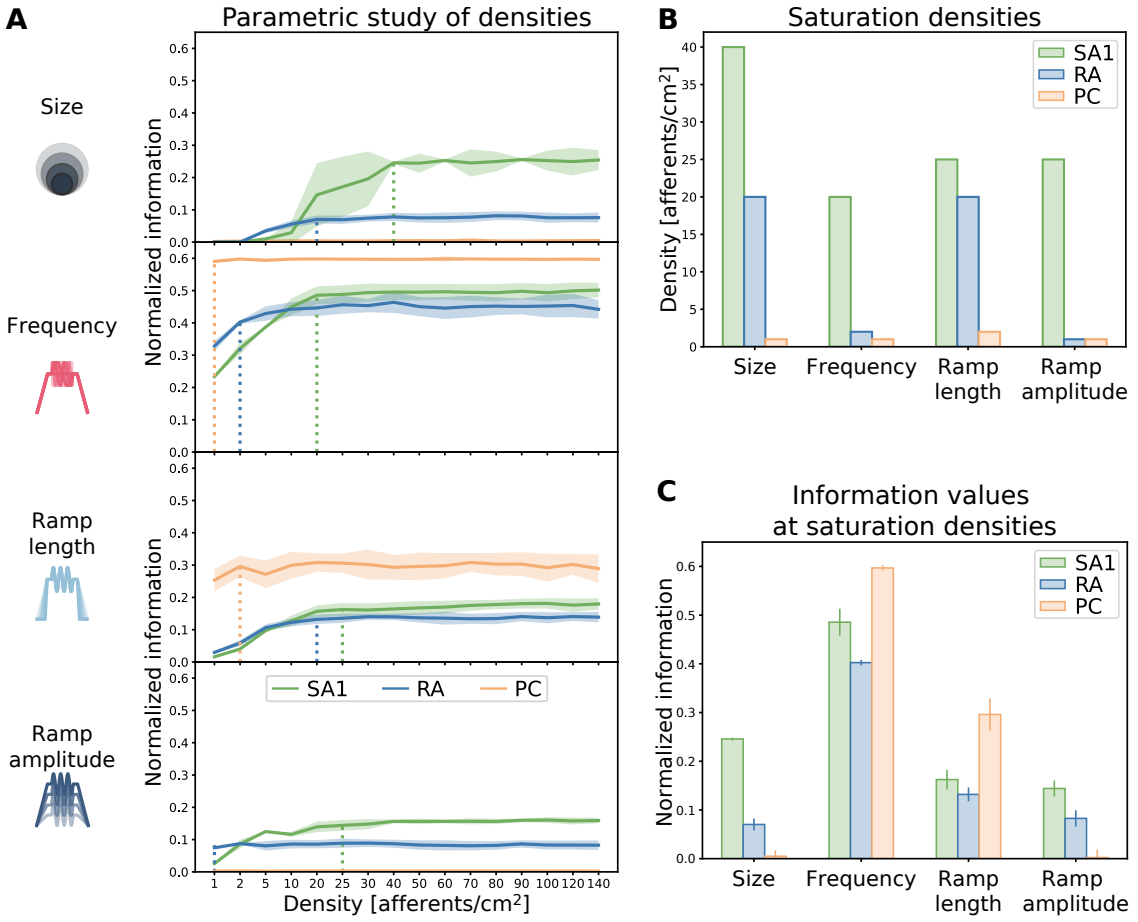

Fig. 8: Effect of afferent density on stimulus feature coding. **(A)** Information content (normalized by the stimulus entropy) for different stimulus features provided by single-class afferent populations of varying density. Solid lines represent the average over 40 trials, shaded regions represent standard deviation. Dotted vertical lines indicate information saturation points. **(B)** Saturation densities for each feature and afferent class. **(C)** Maximum information content provided by each afferent class at the saturation density for each feature.

2.1 Information carried by individual afferent populations

In a first analysis, we investigated the information carried by each of the three afferent populations separately. To understand which afferent population best encoded any given feature and how the information depended on the spatial density of the afferents, we calculated the total information carried by each population (Fig 8A) by simulating responses with different spatial receptor densities.

For encoding stimulus size, we found that SAI afferents were most informative, with information increasing and then saturating at a density of 40 afferents/cm^2. RA afferents provided more

information at very low densities and saturated at a lower level (20 afferents/cm^2). In contrast, PC afferents did not carry any information about stimulus size at any of the densities considered. This result can be explained by the fact that PC afferents exhibit extremely large receptive fields [177], certainly larger than the differences in size between the stimuli we applied.

Next, we considered the encoding of the frequency of stimulation. PC afferents provided the highest frequency information, as predicted by the fact that PC afferents are well known to carry frequency information in vibrotactile stimulation [166]. Given their large receptive field size, frequency information of PC cells already saturated with the lowest density of afferents considered. In agreement with previous studies, RA afferents also carried considerable information about frequency [166]. SAI populations carried low amounts of frequency information at small spatial densities, but slightly exceeded the frequency information of RA afferents at higher spatial densities. This result may appear to contradict earlier empirical studies, where SAI afferents were shown to respond only to the lower extreme of the range examined in our study [178]. However, in our simulations the sinusoidal wave is superimposed on a ramp-and-hold indentation. This sustained indentation causes low spiking activity in the SAI afferents, with spikes aligned to the vibration (see Fig 12B). Our finding suggests that this information emerges when taking into account the activity of SAI afferents on a population level rather than single afferents separately.

PC afferents were also the most informative class about the stimulus ramp length, followed by SAI and RA afferents, which provided similar levels of information, but required higher densities than PCs to reach saturation. Finally, SAI afferents carried the highest amounts of information about ramp amplitude, with PC afferents not encoding any information. RA afferents again provided higher information than SAI ones at the lowest density, but adding more fibers did not increase information for this class.

The information saturation density, which we defined as the smallest value of density at which the population carried the asymptotic value of information reached for the highest simulated density, was the highest across classes for SAI afferent for all considered stimulus features. Conversely, the information saturation density was the smallest for PC afferents in all cases (Fig 8B). Notably, when considering purely spatial features such as the stimulus size, the

population encoding the highest asymptotic information level corresponds to the one with the highest saturation density (Fig 8B and C). Consequently, a high density of afferents is required to extensively innervate a skin area and discriminate between fine differences in the shape of stimulation. On the other hand, when looking at temporal features such as the frequency or the ramp length, sparsely distributed PC afferents overcome the information content encoded by the other more densely packed afferents classes.

Finally, our result shows that the RA class at saturation density always encodes less information than the SAI and PC populations about any feature considered in this study (Fig 8C). However, at low densities (<10 afferents/cm^2), RA afferents were more informative than SAI for all features considered, suggesting that the optimal way to encode a tactile feature might depend on the number of neurons available.

2.2 Information encoded by multiple afferent classes

Next, we investigated how tactile stimulus information was encoded in the joint activity of multiple afferent classes. In particular, we asked whether the information about stimulus features carried by an afferent class adds to and complements the information carried by other classes or whether the information carried by different afferent classes is redundant. To answer this question, we computed the information carried about each stimulus feature by the joint activity of populations of two or three afferent classes and compared the resulting values with the single-class information calculated above. Specifically, we used the concept of complementary information [179]: we defined the complementary information carried by additional afferent classes over that of a reference class as the information carried by all considered classes jointly subtracted by the information carried by the reference class alone. All possible combinations of classes were considered. In these calculations, unless otherwise stated, we set the density of each class to the one measured on the glabrous skin of the human finger (see Methods for details). This allowed us to compare the information contribution of different classes in a realistic and biologically relevant setting.

We first considered whether afferent classes that were not the principal source of information about a stimulus feature added information that was complementary to that of the principally

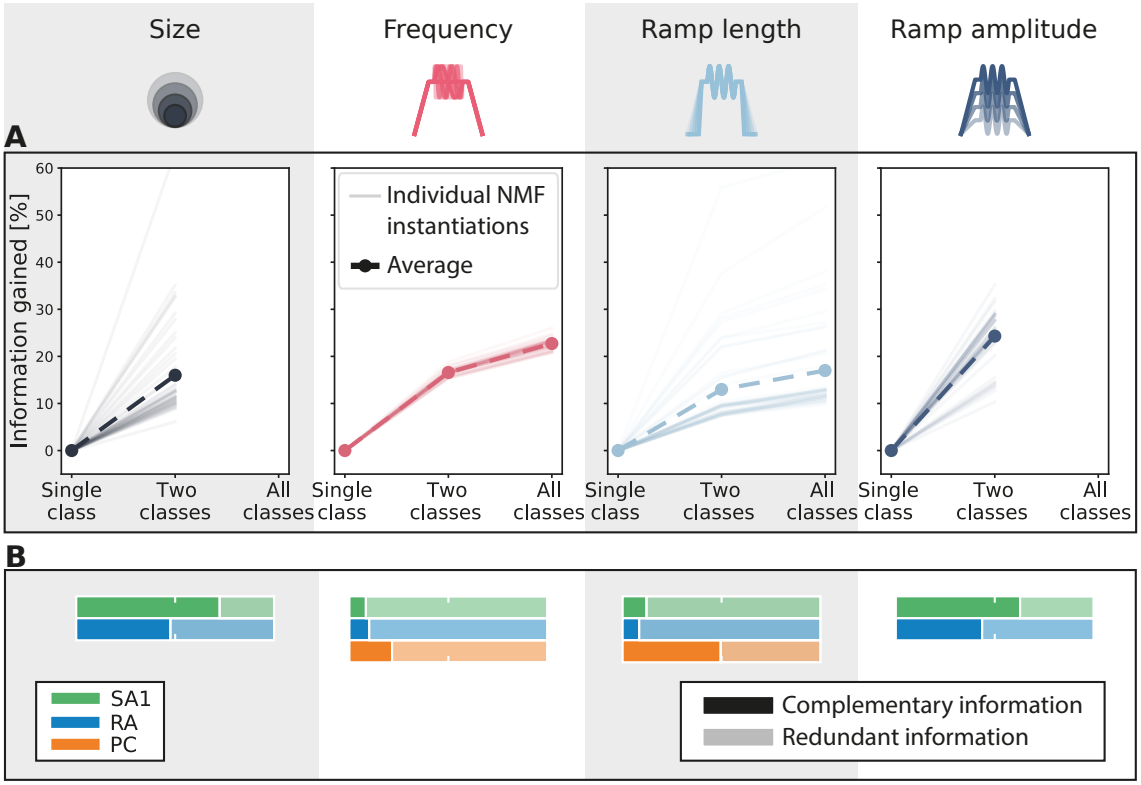

Fig. 9: **(A)** Information gain considering the two and the three most informative classes together with respect to the most informative class alone. The density measured on the human finger was taken for each afferent class. Thin lines correspond to different instantiations of the NMF decomposition, and the thick dashed lines correspond to their averages. **(B)** Decomposition of information into redundant and complementary contributions of each class with respect to the remaining two classes together. Information for each afferent class has been normalized to 100% and was calculated at the density measured on the human finger. Note that in both panels **(A)** and **(B)** only two afferent classes were considered for the analyses regarding stimulus size and ramp amplitude since the third class (PC) was carrying null information (see Fig 8C).

contributing afferent class. To do so, for each feature, we quantified the amount of complementary information that the less informative classes add to the information carried by the most informative class (Fig 9A). The amount of this complementary information was normalized to the amount of stimulus information carried by the most informative class. For all features, we found that the second and third most informative classes added information that complements the information carried by the most informative class alone. On average, the second most informative class added between 12 and 25% complementary information, depending on the feature considered. When considered jointly, the second and third most informative classes added on average between 15 and 30% of complementary information, compared to the most informative class alone. This result indicates that for each tactile stimulus feature, each class encodes some amount of complementary

information about the stimulus that cannot be found in the activity of the other two classes.

Next, we investigated which amount of each afferent class's information contribution was complementary or redundant when considered against the information contribution of the other afferent classes. For each stimulus feature and each individual afferent type, we computed the fraction of the information carried by the considered afferent that is complementary with respect to the information already carried by the other two afferent classes. This fraction is an index of the specific novelty of the information of a given afferent class with respect to all others (Fig 9B). In general, a significant fraction of information carried by each afferent class was complementary to that of other classes. In most cases however, this fraction was not close to 1, meaning that there was also redundancy between the information carried by afferent classes. When examining how this fraction varied across stimulus features, interesting patterns emerged.

For vibration frequency and ramp length, the two stimulus features for which all three afferent classes encoded considerable information, we found mostly redundant coding, with relatively small fractions of complementary information (on average 13% for frequency and 23% for ramp length, Fig 9B). All three classes encode vibratory stimuli by locking their spiking activity to the sinusoidal traces, which explains the redundancy across classes. However, the fact that the frequency ranges encoded by each class do not completely overlap explains the existence of significant fractions of complementary information across all three afferent classes. Given that all three classes encoded large amounts of frequency information, the actual amount of complementary information added by each class was surprisingly large. A similar pattern of complementarity and redundancy of information was observed for ramp length, which like frequency is a dynamic feature that depends on timing.

For stimulus size, the SAI afferent population carried most of the information (Fig 8), and this information had a high value of complementarity (72%), indicating that it could not be found in other afferent types (Fig 9B). The RA afferent population added less information (Fig 8), but also exhibited a relatively large fraction of complementarity (48%) (Fig 9B). The encoding of size for SAI and RA afferents seems to depend on the number of afferents that are activated by the stimulus (Fig 12A), and the observed complementarity between RA and SAI afferents is partly due to differences in spatial sensitivity across the two populations. Information carried by PCs

about probe size was negligible and therefore this class was not considered in the complementarity analysis for this feature.

Finally, for ramp amplitude we found results that resemble those for stimulus size. The SAI population carried most information, which was largely complementary (63%) to that of other classes. RA afferents carried less information than SAI afferents, but part of this information (43%) was complementary to that of SAI afferents. In this case, the encoding appears again to depend on the fraction of afferents that are activated by the stimulus, as was the case for stimulus size. This is a genuine form of population coding that would not be evident from single afferent analyses. PCs again provided negligible information (see Fig 8C), and thus were not taken into account.

2.3 Effect of afferent density on complementary information

Having established that information about individual stimulus features is carried by multiple, rather than single, afferent classes and that different afferent classes often carry complementary stimulus information, we next asked how the complementarity of information depends on the spatial density of afferents. We were especially interested in whether, given the functional properties of afferents in each class, it would be more efficient to allocate all receptors to the most informative class or spread the receptors across different classes to take advantage of the complementarity of different classes. To address these questions, we systematically analyzed the information carried by individual afferent classes and their combination at different densities (Fig 10A). We tested the same upper and lower density limits as used previously. For a more realistic comparison with human biology, we also considered two other cases of spatial density arrangements, in which each population has a density equal to that experimentally found either in the palm or in the finger of the human hand (see Methods for precise numbers).

A substantial increase in the amount of encoded information was found for all features when increasing the density from the lower limit to realistic densities. Conversely, increasing the densities from the finger values further to the upper limit did not lead to additional increases of encoded information, neither when considering individual classes nor their combination, suggesting that the information in multi-class population coding saturates similarly to

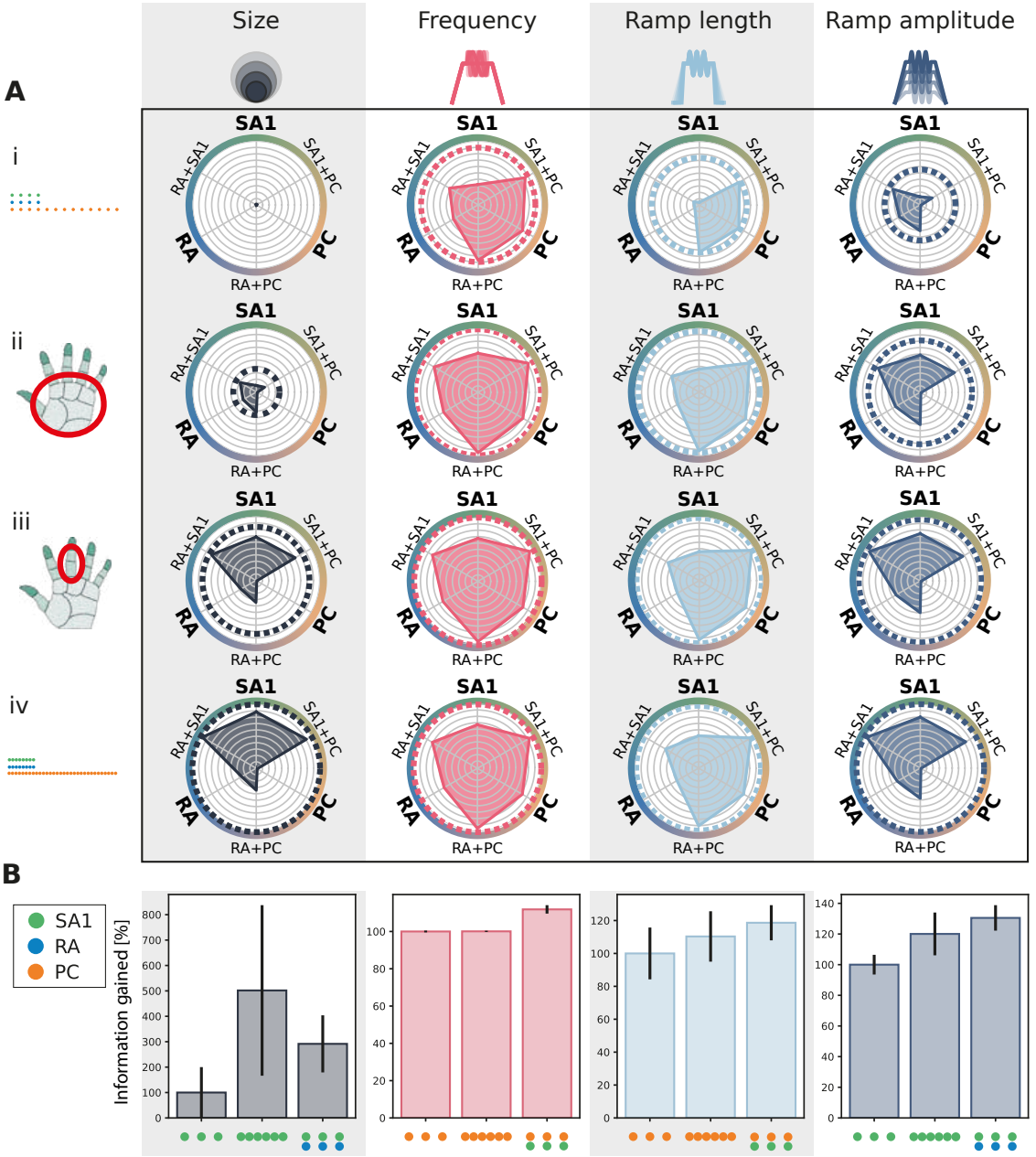

Fig. 10: **(A)** Radar plot of the information content provided by single and combined classes at different densities for individual tactile features. Each radial axis represents the information content of a single afferent class or combination of two classes. Dotted circular lines correspond to the information given by the three afferent classes together. Information is normalized for each stimulus feature with respect to the information provided by the three classes altogether at the upper-limit density (i). Four different density sets were considered: (i) lower limit, (ii) human palm, (iii) human finger, and (iv) upper limit as reported in Table 6 **(B)** Comparison of the information gained when doubling the density of the most informative class (central bar) or when combining with a different population (right bar). The baseline density (left bar) was set at 10 afferents/cm^2. Error bars represent standard deviation.

	Stimulus size	Frequency	Ramp length	Ramp amplitude
Most informative class	SAI	PC	PC	SAI
Optimal encoding strategy	Increase density of SAI population	Add SAI population	Add SAI population	Add RA population
Underlying rationale	Highest gain in information by increasing SAI density, PC provide no information	SAI adds more information than RA, PC information is density independent	SAI adds more information than RA, PC information is density independent	SAI+RA reaches the highest information content, PC provide no information

Table 5: Information maximizing encoding strategies for each stimulus feature trading off increases in innervation density for a single afferent class versus adding fibers from a different class.

single-class coding. The only exception was probe size, for which information content at the upper limit was higher than at the finger density. As shown in Fig 10B and summarized in Table 5, stimulus size is also the only feature for which increasing the density of the most informative class, SAI, improves the information content more than combining different classes. As discussed previously, stimulus size is a purely spatial feature, and a high density of afferents is necessary to discern small differences in the shape of the stimulus. In contrast, for all other features considered, combining the content of the two most informative afferent classes yields more information than doubling the afferent density of the most informative class alone.

Together, these results show the advantages for information encoding at the population level of spreading information across classes of receptors with complementary information rather than simply packing more receptors of a given class into the skin, even if receptors of this class are highly informative about the stimulus.

2.4 Spatial and temporal contributions to information coding

After establishing how much information is encoded in each afferent class and their combination, we investigated the nature of this population coding in more detail. In particular, we asked two questions relevant to understanding the spatial and temporal organization of the population code. First, how important is the precise temporal structure of the population activity for stimulus decoding? Second, how important are differences in spatial neuron-to-neuron response profiles to decode stimulus information?

The importance of the spatial structure of the afferent population code for information coding, that is, the afferent-to-afferent difference in stimulus tuning properties at different spatial locations, is supported by the finding that natural tactile stimuli elicit specific firing patterns in afferents located

in different places [168, 180]. A critical role for the temporal structure of individual afferent activity has been demonstrated in previous studies [180, 181] and is also supported by the fact that thalamic and cortical somatosensory neurons also encode tactile information with millisecond-scale spike timing precision [182–185]. However, it is unknown whether these expectations would hold at the level of afferent population coding. For example, precise spike timing might be less important when considering a full population of afferents rather than a single one. Furthermore, information in the spatial and the temporal structure might be redundant, such that information in the spatial structure could be recovered from the temporal structure or vice versa. Addressing these questions therefore requires a direct test with a large population.

First, we evaluated whether the distribution of afferents in the space, parameterized in the current setup as the distance of the afferent location from the stimulation site, impacts the population coding capabilities. To do so, we repeated the analysis pipeline used to compute the information content in the spiking activity after corrupting the spatial information in the spike matrices by randomly permuting the identity of afferents. We called this "space-coding neglected" information. The difference between the original and the space-coding neglected information quantifies how much of the original information can only be accessed using the spatial structure of the code. Note that this quantification is performed at a fixed spatial density, and it is thus different from the previous analyses of the effect of spatial density. We found that, after destroying the spatial structure, information content dropped by on average 26% (Fig 11). The loss of information was higher for SAIs (39%) compared with RAs (18%) or PCs (16%).

Next, to quantify the specific contribution of temporal structure to the total information in the population code, we computed a "time-coding neglected" information value from the population responses. To do so, we randomly shifted the spikes with a Gaussian distribution of zero mean and standard deviation of 10 ms, before proceeding with the rest of the analysis pipeline. The difference between the original and the time-coding neglected information quantifies how much of the original information can only be accessed using the millisecond-scale temporal structure of the code. We found that, after destroying the temporal structure, information content dropped by on average 54% across all classes (Fig 11). Information loss was highest for PCs (88%) and relatively lower for RAs (51%) and SAIs (39%). Notably, across our set of stimuli we found higher information loss when neglecting the temporal resolution of spike trains rather than the spatial

distribution. This result indicates that even in large afferent populations spike timing with high temporal precision remains an important part of the neural code. In contrast, the ramp amplitude for both SAI and RA classes and the stimulus size for SAI rely more on spatial than temporal activation, which can be explained by the spatial nature of these two features.

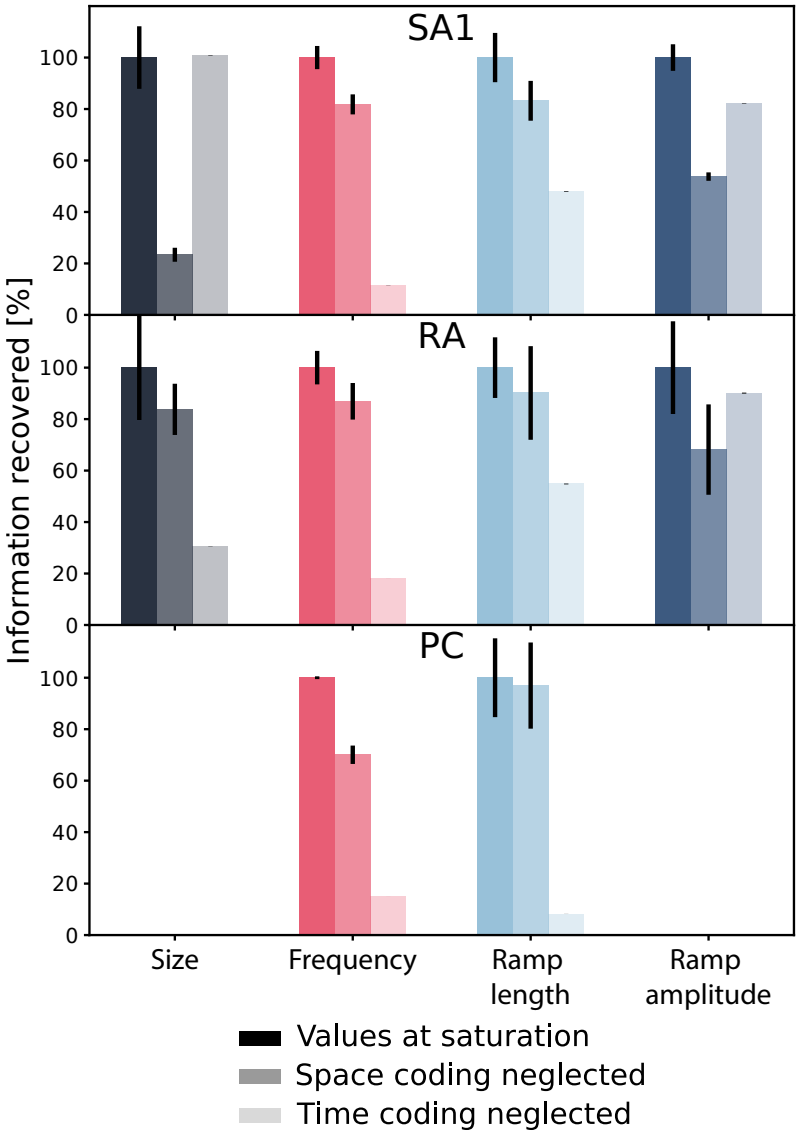

Fig. 11: Information recovered after corrupting spatial or temporal coding. Information recovered for each afferent class after neglecting either spatial organization or precise spike timing, normalized with respect to the maximum information content in the original data at the saturation level (see Figure 8C). Note that for both stimulus size and ramp amplitude, information carried by PC class was null (see Figure 8C) and such class was excluded from this analysis. Error bars represent standard deviation.

3 Discussion

This study is based on a simulation paradigm, which provides novel insights on stimulus coding by tactile afferent populations. Much of our current understanding of encoding mechanisms of tactile stimuli derives from electrophysiological studies. However, these are severely limited in the number of afferents that can be recorded at a time. In addition, many previous studies have focused only on those afferents terminating directly at the stimulus contact location. Thus, a biased picture of tactile coding might have emerged. In fact, to our knowledge, population coding of tactile afferents, taken as the spatiotemporal activation of multiple afferents belonging to one or *more* classes, has scarcely been investigated before. Here, we used a recently developed computational model that allows simulation of tactile neural responses at the population level with high accuracy. Although any putative population-level coding mechanisms derived from modeling would need to be experimentally verified, this approach allows investigating aspects of the neural code that are currently experimentally intractable and can therefore generate ideas for potential downstream decoding mechanisms.

3.1 Single-class coding and receptor density

We first investigated how the density of afferents from a single class plays a role in the encoding process. We showed that the information content of both SAI and RA populations increases asymptotically with afferent density until saturation. This effect was consistent for all features considered, although the specific saturation densities varied between features. This result highlights that tactile information is generally spread across a population of multiple afferents, even for features that are not explicitly spatial. Furthermore, the afferent class most informative about a tactile feature at low innervation densities might be different from the most informative class at high densities. Consequently, judging or predicting the information content of a population from recordings of single afferents only might be misleading and provide a biased picture of how information is represented in full populations.

In contrast to SAI and RA afferents, the information level for PC afferents was essentially constant for all density values considered across all tactile features. While this result might be taken to suggest that the PC population does not contribute information above that of a single afferent,

there is evidence to suggest that PC populations might be important in different tactile contexts than the ones explored here: making contact with surfaces causes mechanical waves to spread throughout the hand, activating PC afferents as far away as the palm and their joint population activity carries information about how contact is made and other aspects of the grasp [186].

It should be noted that for all afferent classes, the minimum density needed to recover the maximum information for any tactile feature is lower than the empirical afferent densities estimated for the human hand [163]. We speculate that the minimum density of afferents required to reach the information saturation might be higher for more complex features. Indeed, as an initial investigation into the power of large-scale neural simulations on a population level, this study considered relatively simple stimulus features compared to the complexity of realistic tactile interaction. Similarly, previous studies showed a strong relationship between SAI density and tactile spatial acuity [163]: afferents, particularly of SAI type, need to be densely packed in the skin to resolve and discriminate extremely fine features. While our setup included one clearly spatial stimulus (probe size), none of the others were purely spatial. Finally, afferent innervation densities across most of the skin of the human body are much lower than those in the hand and indeed within the range identified in the current study, suggesting that our stimulus set was covering a large part of the physiologically relevant range.

Interestingly, we found that the RA class at saturation density tended to encode less information than the SAI and PC populations, but in contrast, was more informative than SAIs at low densities (<10 afferents/cm^2). This result suggests that the way information is spread across afferent classes depends in part on receptor density, and in turn, should affect optimal decoding downstream. Indeed, tactile innervation density changes dramatically across different body areas, both in terms of the absolute number of afferents and relative innervation densities of different classes [163], and it is possible that changes in the class composition at different skin sites partially reflect density-dependent optimal allocation of afferent classes. Our findings also suggest that tactile information need not be linked firmly to a given receptor type, but that information is spread in a dynamic way across different afferent classes (see [171] for a concrete example in frequency coding).

3.2 Complementarity and redundancy across afferent classes

The second step of our analysis was to consider combinations of afferent classes and to evaluate their information content with respect to different stimulus features. Here, we found both redundant and complementary contributions to the information across afferent classes. All afferent classes generally provided at least some complementary information about stimulus features, suggesting that downstream areas should integrate information from different classes to maximize information (see also [167]). Quantifying such complementary information is a necessary first step towards further study of submodality convergence in the stimulus encoding process, especially considering that directly accessing the integration mechanisms in humans is complicated. Convergence has previously been inferred from cortical recordings in primates for multiple individual stimulus attributes [170, 187, 188], but here we quantitatively demonstrate that information is spread across afferent types in most cases, and therefore, submodality integration can be expected to be a general feature of downstream processing.

Not all information was complementary however, and we also found considerable degrees of redundancy between afferent classes. Redundancy in neural coding has been extensively debated (see [189] for a review) and can be a strategy for robust stimulus encoding. Indeed, over-representing stimulus information using large populations of neurons increases the probability of having a relevant impact in downstream neurons, guaranteeing —or, at least, making more plausible— that critical information is processed while negligible information is discarded —or less likely used—. Redundancy can rank information according to relevance, overcoming the associated coding inefficiency in favor of a significant performance increase [190]. Furthermore, redundancy could be interpreted as a strategy to make the neural code resilient in the event of temporary or permanent lack, shortage, or failure of input from an afferent class. This theory is supported by recent findings in an experimental study in mice that showed that the use of genetic ablation strategies to suppress the response of either rapidly or slowly adapting afferents leaves responses in the somatosensory cortex mostly unchanged [169], which implies that the required information can be recovered from the remaining afferent input. This would not have been possible if the two classes had encoded complementary information only. Such a process might be beneficial when several features are processed simultaneously, and

redundancy between classes might help to disambiguate the stimulus.

3.3 Information maximizing receptor selection

We investigated whether increasing the density of afferents of a given class or combining them with afferents of a different class yields higher information gain. We found that adding afferents belonging to a different class was generally more efficient than increasing the density of the most informative class by the same amount, confirming that the information about stimulus features is not segregated in single afferent classes, but is spread across them. Indeed, while absolute tactile innervation densities vary widely across the body, the fraction of slowly adapting afferents at any given site varies only between 40 and 70% and is relatively evenly split for most body regions [163], especially for those with lower innervation. Our results suggest that such a composition increases information transmission, while minimizing fiber count. The number of tactile fibers that can fit into the nerves and spinal cord is naturally constrained, and consequently, extensive skin areas are innervated at low density. Neurons are also energetically expensive, and therefore it is plausible that evolutionary optimization might have maximized the ratio between information and energy consumption by spatially distributing the mechanoreceptors and diversifying response properties across different receptor classes.

In several sensory systems other than touch neural populations are also composed of multiple cell classes with distinct response properties. Indeed, early sensory pathways frequently split into different classes with disparate response properties (e.g. the large number of retinal ganglion cell classes [158]). According to the efficient coding hypothesis, sensory systems have evolved to optimally transmit information about the surrounding world, given constraints on their biophysical components and energy use [191]. This theory also explains splitting a population into two or more cell classes as a strategy to maximize information transmission, as shown in previous studies for different sensory systems [160–162]. Our findings support this hypothesis, showing that, in most cases, a combination of classes was more informative than a single class higher-density population.

3.4 Limitations and future work

Our study focused on the three main classes of tactile afferents that mediate discriminative touch, but other classes, such as SAII afferents that primarily signal skin stretch or unmyelinated

afferents, also contribute to tactile coding. Furthermore, tactile innervation and neural response properties differ somewhat in the hairy skin [163], which covers most of the human body. Thus, our results will most directly reflect tactile coding on the human hand, but future studies should consider how these results might extend to other regions of the body.

As the findings are based on computer simulations, the veracity of the results will depend on the accuracy with which the spiking responses can be replicated in the computational model. The stimuli we used, namely indentations by a single probe orthogonal to the skin surface with a superimposed vibration, are similar to those on which the original model was fit and fall into the range where it has been validated most extensively [172]. Still, by combining multiple tactile features, we believe that our simulated stimuli are sufficiently complex, varied, and natural that the resulting findings can be considered of behavioral importance. One avenue for future research would be to investigate information transfer on tactile inputs arising from natural behaviors such as grasping and manipulating objects, which include multiple contacts, shear forces, and movement between the object and the skin. However, this would require further work on the precise spatiotemporal force patterns on the hand during such behaviors and spiking models that take into account more complex afferent response properties (see [192] for an example).

To study the effects of different innervation densities, we considered a simplified setup, distributing the afferents over a single dimension while neglecting some properties affecting the spatial distribution of afferents, for example the complex shape of the human hand. Future studies should take this aspect into account to reveal how the shape of the hand, the different afferent densities, and the composition of the population in different areas of the hand play a role in stimulus encoding. In the same direction, population coding strategies and afferent distribution might be coupled with natural stimulus statistics in different body areas to deepen the understanding of how the human somatosensory system is optimised to receive and process natural tactile stimuli.

4 Methods

Class	Palm	Finger	Fingertip
SAI	10	30	70
RA	25	40	140
PC	10	10	25

Table 6: Estimated innervation densities of afferent classes (afferents/cm^2) for different regions of the human hand [177].

4.1 Simulation of spiking activity

To generate the spiking activity of tactile afferents, we used a previously published and validated model called Touchsim [172]. We employed the model to simulate populations of SAI, RA, and PC afferents terminating along a line of 1 cm for SAIs and RAs, and 5 cm for PCs radiating outwards from the stimulus location. The density of afferents varied between 1 and 140 afferents/cm^2 for a total of 16 different populations per afferent type. This range includes the physiological innervation densities estimated for the human hand [177]. In some analyses we also directly set individual class densities to those of the human palm or finger (see Table 6 for precise values).

We designed stimuli with circular shapes, which are indented in the skin following a ramp-and-hold function (see Fig 6 B). When the maximum amplitude of the ramp is reached, a sinusoidal wave is superimposed. This setup simulates well-established psychophysical setups in which a probe is brought into contact with the skin and then vibrated at a set frequency. It also includes many aspects of natural tactile stimulation: indentation, retraction, and constant stimulation at different depths and spatial scales, as well as vibrations at different frequencies. Individual stimuli are created by varying 4 different features: 1) the stimulus size (4 conditions: [1:1:4] mm), 2) the maximum ramp amplitude (4 conditions: [0.3:0.3:1.2] mm), 3) the ramp-up time (5 conditions: [0.01:0.01:0.05] s), and 4) the frequency of the superimposed sinusoidal wave (10 conditions: [0, 10, 20, 40, 60, 80, 100, 130, 160, 200] Hz). This setup yielded 800 unique stimuli, and the afferent response to each was simulated for 40 trials. The model included simulated neural noise. Additionally, in order to simulate environmental noise such as motor noise during active touch, we jittered the stimulus location (by $\pm$ 0.3 mm), the amplitude of the sinusoidal wave (by $\pm$ 0.05 mm), and the ramp amplitude (by $\pm$ 0.1 mm) on every trial.

4.2 Dimensionality reduction

Information calculations from high dimensional data require prohibitively large datasets. A common strategy to address this issue is by performing dimensionality reduction on the data. Here, we used Non-Negative Matrix Factorization (NMF) to decompose the spatio-temporal matrix of spiking responses across the population.

Responses were discretized by binning the spike trains into 2 ms long intervals and counting the number of spikes falling into each bin. This resulted in a matrix $R \in \mathbf{R}^{M \times TN}$, where M is the total number of trials, T the number of time bins, and N the number of afferents in the population. NMF decompositions are naturally suited to describe spatio-temporal matrices of spiking responses, because spike trains are non-negative, and because often recurrent spike patterns may be non-orthogonal (as NMF) and partly overlapping (explainable by the same underlying activity pattern). NMF describes a single trial spike train as a sum of trial-independent non-negative spatiotemporal modules (describing the most often recurring spatio-temporal firing patterns) and trial-dependent non-negative activation coefficients representing the strength of recruitment of each module in the considered trial [174, 175]:

$$R = HW + residuals, \tag{1}$$

where $H \in \mathbf{R}^{M \times K}$ contains the non-negative activation coefficients for the K modules in each trial and $W \in \mathbf{R}^{K \times TN}$ contains the non-negative modules. We used the function *NMF* included in the scikit-learn Python library [193] to calculate the NMF decomposition.

We performed the NMF decomposition separately for each of the three afferent classes at each density value considered. Beforehand, we randomly separated the whole set of trials into balanced sets with a 25/75 split. We used the 25-set to determine the number of modules K as the minimum number of modules capable of explaining a selected level of variance of the original data in R, as follows. First, to consistently select the level of variance explained between populations of the same class but with different densities, we calculated the saturation level of the accounted variance for each population considered (tolerance <1%). We averaged the saturation levels across populations of the same class with different densities and used this value as the new threshold for

the explained variance. Finally, we calculated k modules W and activation coefficients H on the same 25-set. Given the W modules from the 25-set, we computed the activation coefficients H on the remaining 75-set.

4.3 Stimulus decoder

After dimensionality reduction, we fed the activation coefficients H computed with the NMF to a stimulus decoder. We used multinomial logistic regression to decode each stimulus feature separately on a trial-by-trial basis based on the neural activity (similarly to [176]). The scikit-learn Python library [193] was used for the implementation. This type of classifier uses a linear function $f(s, i)$ to predict the probability of outcome s for trial i such that:

$$f(s, i) = \beta_s \cdot \mathbf{H}_i \tag{2}$$

where $\mathbf{H}_i$ is a vector containing the NMF activation coefficients for trial i and β_k stores the coefficients associated with outcome s. When generalizing to S_n features, the multinomial logistic regression model consists of $S_n - 1$ independent logistic regression models regressed against the remaining S_n outcomes. Note that outcomes correspond to the possible values that the stimulus features could take and vary for each feature.

The 75-set was divided equally and stratified into training and test sets. We trained the classifier on the activation coefficients of the training set and evaluated performance using the activation coefficients of the test set. The training procedure was performed using a stratified 5-fold cross-validation. This process was repeated for each population of afferents (both for single and combined classes) and all afferent densities. The solver used for the fitting procedure was *lbfgs* in combination with *L2* regularization. We selected the parameter *C* for the regularization by performing grid search. The scoring of the classifier was the negative log-likelihood, also known as the cross-entropy loss.

The final fitted model outputs the posterior probability of observing each stimulus feature given the neural activity captured in the NMF activation coefficients [176]. From this posterior probability, we decoded the stimulus $\hat{s}$ that was most likely given the observed afferent activity.

4.4 Mutual Information

Next, we computed the mutual information [194] from the confusion matrix of the decoder as follows [154]:

$$I(S;\hat{S}) = \sum_{s\in S}\sum_{\hat{s}\in\hat{S}} p(s,\hat{s}) \log_2 \left(\frac{p(s,\hat{s})}{p(s)p(\hat{s})} \right) \tag{3}$$

where S, $\hat{S}$ stand for the set of all possible presented and decoded stimuli, respectively. $p(s,\hat{s})$ denotes joint probability distribution, which is derived from the confusion matrix obtained empirically across all trials, of presenting stimulus s and decoding stimulus $\hat{s}$ in a given trial. $p(s)$ and $p(\hat{s})$ correspond to the marginal probabilities of s and $\hat{s}$, respectively. The information in the confusion matrix is a data-robust lower bound to the total information carried by population activity. This approximation is tight when neural activity can be categorically binned into as many values as the number of distinct stimuli without losing considerable information. The information in the confusion matrix captures aspects of information processing, such as the distribution of decoding errors, which are not captured by simple measures such as the fraction of correctly decoded stimuli [154]. Since the information upper bound is the entropy of the stimulus set (indicating perfect single-trial stimulus discrimination), we normalised information values by dividing them by the entropy of the stimulus set:

$$H(S) = \log_2(S_n) \tag{4}$$

where S_n is the number of values that the stimulus can take.

4.5 Computation of complementary information

To assess the complementarity of stimulus information carried by different classes, we computed the information carried about each stimulus feature by the joint activity of populations of two or three afferent classes and compared it to the information carried by a single-class population. We defined the amount of information carried by the pair of afferent classes that is complementary to that of a reference class as the difference between the information carried by all the classes (including the reference class and the additional ones) and the information carried by the reference class. We repeated this process, taking each class as the reference class in turn. As an example,

for SAI afferents as the reference class, the complementary information is computed as:

$$\begin{aligned} I_{com}(S, SAI) =& I(S, \{SAI, RA, PC\}) \\ & - I(S, \{RA, PC\}) \end{aligned} \tag{5}$$

We defined the redundant information between the additional classes and the reference class as the sum of the information carried individually by the reference class and the additional ones minus the information carried by all the classes together, such that (again, taking SAIs as the reference class):

$$\begin{aligned} I_{red}(S, SAI) =& I(S, SAI) \\ & + I(S, \{RA, PC\}) \\ & - I(S, \{SAI, RA, PC\}) \end{aligned} \tag{6}$$

The sum of redundant (eq. 6) and complementary (eq. 5) information for a class equals the total information carried by that class.

Supporting information

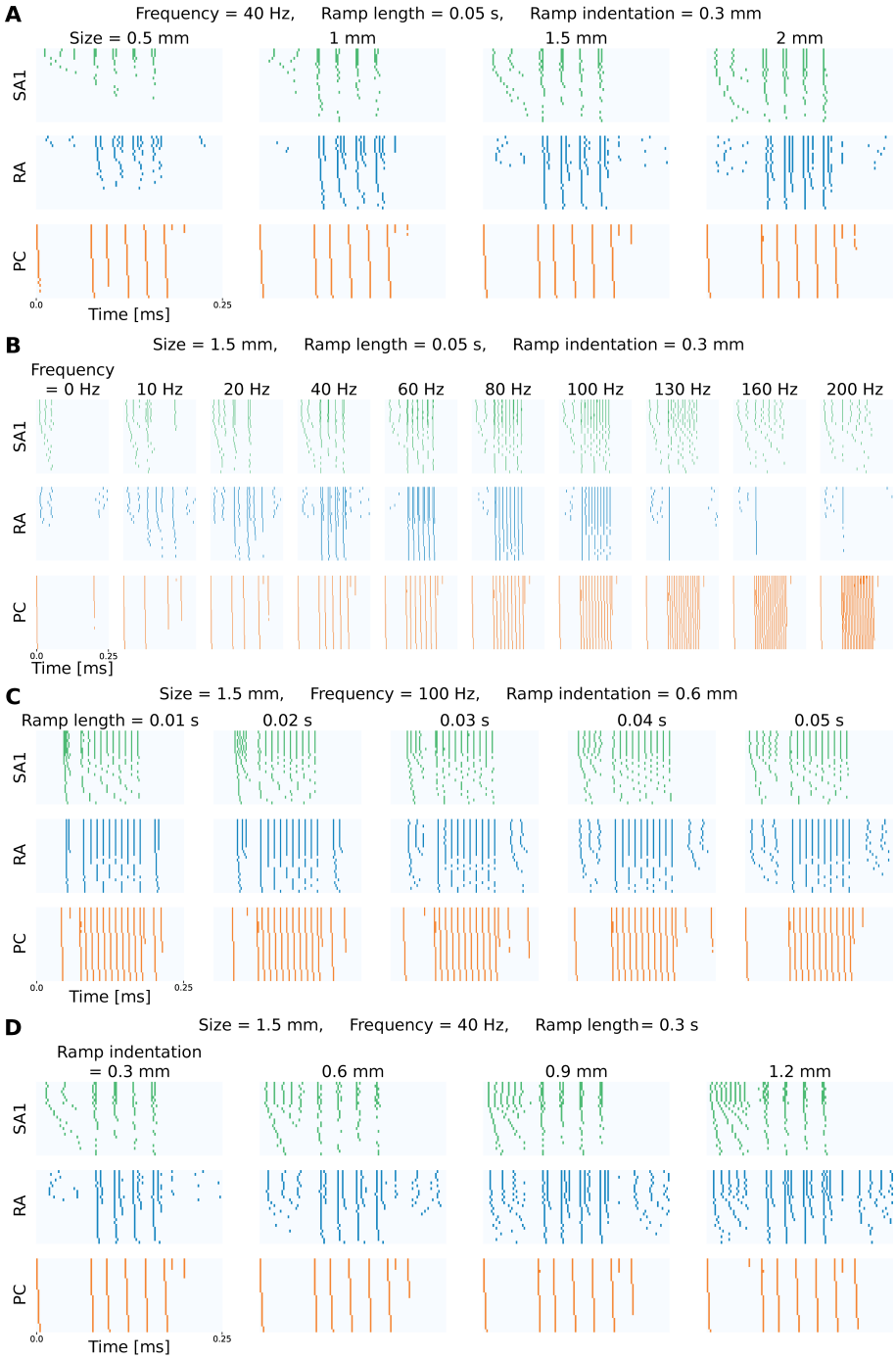

Fig. 12: Illustrative examples of simulated spiking activity. Responses are shown for the three afferent classes as a function of **(A)** stimulus size, **(B)** frequency, **(C)** ramp length, and **(D)** ramp amplitude. Note that we conditioned on the remaining features for each panel and that the afferent densities in this example are the ones in the finger.

References

[153] A. Pouget, P. Dayan, and R. Zemel, "Information processing with population codes," *Nat. Rev. Neurosci.*, vol. 1, no. 2, pp. 125–132, Nov. 2000.

[154] R. Quian Quiroga and S. Panzeri, "Extracting information from neuronal populations: information theory and decoding approaches," *Nat. Rev. Neurosci.*, vol. 10, no. 3, pp. 173–185, Mar. 2009.

[155] A. P. Georgopoulos, A. B. Schwartz, and R. E. Kettner, "Neuronal population coding of movement direction," *Science*, vol. 233, no. 4771, pp. 1416–1419, Sep. 1986.

[156] E. Schneidman, J. L. Puchalla, R. Segev, R. A. Harris, W. Bialek, and M. J. Berry, "Synergy from silence in a combinatorial neural code," *Journal of Neuroscience*, vol. 31, no. 44, pp. 15 732–15 741, Nov. 2011.

[157] M. Adibi, J. S. McDonald, C. W. G. Clifford, and E. Arabzadeh, "Population decoding in rat barrel cortex: Optimizing the linear readout of correlated population responses," *PLoS Comput. Biol.*, vol. 10, no. 1, pp. e1 003 415–e1 003 415, Jan. 2014.

[158] T. Baden, P. Berens, K. Franke, M. Román Rosón, M. Bethge, and T. Euler, "The functional diversity of retinal ganglion cells in the mouse," *Nature*, vol. 529, no. 7586, pp. 345–350, Jan. 2016.

[159] V. E. Abraira and D. D. Ginty, "The sensory neurons of touch," *Neuron*, vol. 79, no. 4, pp. 618–639, Aug. 2013.

[160] J. Gjorgjieva, H. Sompolinsky, and M. Meister, "Benefits of pathway splitting in sensory coding," *J. Neurosci.*, vol. 34, no. 36, pp. 12 127–12 144, 2014.

[161] D. B. Kastner, S. A. Baccus, and T. O. Sharpee, "Critical and maximally informative encoding between neural populations in the retina," *Proceedings of the National Academy of Sciences*, vol. 112, no. 8, pp. 2533–2538, Feb. 2015.

[162] J. Gjorgjieva, M. Meister, and H. Sompolinsky, "Functional diversity among sensory neurons from efficient coding principles," *PLoS Comput. Biol.*, vol. 15, no. 11, p. e1007476, Nov. 2019.

[163] G. Corniani and H. P. Saal, "Tactile innervation densities across the whole body," *J. Neurophysiol.*, vol. 124, no. 4, pp. 1229–1240, Oct. 2020.

[164] R. S. Johansson and A. B. Vallbo, "Tactile sensibility in the human hand: relative and absolute densities of four types of mechanoreceptive units in glabrous skin," *J Physiol (Lond)*, vol. 286, pp. 283–300, Dec. 1979.

[165] A. W. Goodwin and H. E. Wheat, "Sensory signals in neural populations underlying tactile perception and manipulation," *Annu. Rev. Neurosci.*, vol. 27, pp. 53–77, Dec. 2004.

[166] K. O. Johnson, "The roles and functions of cutaneous mechanoreceptors," *Curr. Opin. Neurobiol.*, vol. 11, no. 4, pp. 455–461, Aug. 2001.

[167] H. P. Saal and S. J. Bensmaia, "Touch is a team effort: interplay of submodalities in cutaneous sensibility," *Trends Neurosci.*, vol. 37, no. 12, pp. 689–697, Sep. 2014.

[168] A. I. Weber, H. P. Saal, J. D. Lieber, J.-W. Cheng, L. R. Manfredi, J. F. Dammann, 3rd, and S. J. Bensmaia, "Spatial and temporal codes mediate the tactile perception of natural textures," *Proc. Natl. Acad. Sci. U. S. A.*, vol. 110, no. 42, pp. 17 107–17 112, Oct. 2013.

[169] A. J. Emanuel, B. P. Lehnert, S. Panzeri, C. D. Harvey, and D. D. Ginty, "Cortical responses to touch reflect subcortical integration of ltmr signals," *Nature*, vol. 600, no. 7890, pp. 680–685, Oct. 2021.

[170] H. P. Saal, M. A. Harvey, and S. J. Bensmaia, "Rate and timing of cortical responses driven by separate sensory channels," *Elife*, vol. 4, no. 12, pp. 7250–7257, 2015.

[171] I. Birznieks, S. McIntyre, H. M. Nilsson, S. S. Nagi, V. G. Macefield, D. A. Mahns, and R. M. Vickery, "Tactile sensory channels over-ruled by frequency decoding system that utilizes spike pattern regardless of receptor type," *Elife*, vol. 8, Aug. 2019.

[172] H. P. Saal, B. P. Delhaye, B. C. Rayhaun, and S. J. Bensmaia, "Simulating tactile signals from the whole hand with millisecond precision," *Proceedings of the National Academy of Sciences*, vol. 114, no. 28, pp. 201 704 856–201 704 856, Jun. 2017.

[173] D. D. Lee and H. S. Seung, "Learning the parts of objects by non-negative matrix factorization," *Nature*, vol. 401, no. 6755, pp. 788–791, Oct. 1999.

[174] A. Onken, J. K. Liu, P. P. C. R. Karunasekara, I. Delis, T. Gollisch, and S. Panzeri, "Using matrix and tensor factorizations for the Single-Trial analysis of population spike trains," *PLoS Comput. Biol.*, vol. 12, no. 11, p. e1005189, Nov. 2016.

[175] P. L. Williams and R. D. Beer, "Nonnegative decomposition of multivariate information," *arXiv preprint arXiv:1004.2515*, 2010.

[176] C. A. Runyan, E. Piasini, S. Panzeri, and C. D. Harvey, "Distinct timescales of population coding across cortex," *Nature*, vol. 548, no. 7665, pp. 92–96, 2017.

[177] A. B. Vallbo and R. S. Johansson, "Properties of cutaneous mechanoreceptors in the human hand related to touch sensation," *Hum. Neurobiol.*, vol. 3, pp. 3–14, 1984.

[178] E. Ribot-Ciscar, J. P. Vedel, and J. P. Roll, "Vibration sensitivity of slowly and rapidly adapting cutaneous mechanoreceptors in the human foot and leg," *Neurosci. Lett.*, vol. 104, no. 1-2, pp. 130–135, Sep. 1989.

[179] S. Panzeri, N. Brunel, N. K. Logothetis, and C. Kayser, "Sensory neural codes using multiplexed temporal scales," *Trends Neurosci.*, vol. 33, no. 3, pp. 111–120, Mar. 2010.

[180] E. L. Mackevicius, M. D. Best, H. P. Saal, and S. J. Bensmaia, "Millisecond precision spike timing shapes tactile perception," *J. Neurosci.*, vol. 32, no. 44, pp. 15 309–15 317, Oct. 2012.

[181] R. S. Johansson and I. Birznieks, "First spikes in ensembles of human tactile afferents code complex spatial fingertip events," *Nat. Neurosci.*, vol. 7, no. 2, pp. 170–177, Feb. 2004.

[182] K. H. Long, J. D. Lieber, and S. J. Bensmaia, "Texture is encoded in precise temporal spiking patterns in primate somatosensory cortex," *bioRxiv*, 2021.

[183] S. Panzeri, R. S. Petersen, S. R. Schultz, M. Lebedev, and M. E. Diamond, "The role of spike timing in the coding of stimulus location in rat somatosensory cortex," *Neuron*, vol. 29, no. 3, pp. 769–777, Mar. 2001.

[184] R. S. Petersen, S. Panzeri, and M. E. Diamond, "Population coding of stimulus location in rat somatosensory cortex," *Neuron*, vol. 32, no. 3, pp. 503–514, Nov. 2001.

[185] R. S. Petersen, S. Panzeri, and M. E. Diamond, "The role of individual spikes and spike patterns in population coding of stimulus location in rat somatosensory cortex," *Biosystems.*, vol. 67, no. 1-3, pp. 187–193, Oct. 2002.

[186] Y. Shao, V. Hayward, and Y. Visell, "Compression of dynamic tactile information in the human hand," *Science Advances*, vol. 6, no. 16, p. eaaz1158, Apr. 2020.

[187] Y.-C. Pei, P. V. Denchev, S. S. Hsiao, J. C. Craig, and S. J. Bensmaia, "Convergence of submodality-specific input onto neurons in primary somatosensory cortex," *J. Neurophysiol.*, vol. 102, no. 3, pp. 1843–1853, Sep. 2009.

[188] A. W. Carter, S. C. Chen, N. H. Lovell, R. M. Vickery, and J. W. Morley, "Convergence across tactile afferent types in primary and secondary somatosensory cortices," *PLoS One*, vol. 9, no. 9, pp. e107 617–e107 617, Jan. 2014.

[189] H. Barlow, "Redundancy reduction revisited," *Network*, vol. 12, no. 3, pp. 241–253, Aug. 2001.

[190] J. L. Puchalla, E. Schneidman, R. A. Harris, and M. J. Berry, "Redundancy in the population code of the retina," *Neuron*, vol. 46, no. 3, pp. 493–504, 2005. [Online]. Available: https://www.sciencedirect.com/science/article/pii/S0896627305003119

[191] H. B. Barlow, "Possible principles underlying the transformations of sensory messages," in *Sensory Communication*. The MIT Press, Aug. 2013.

[192] J. A. Pruszynski and R. S. Johansson, "Edge-orientation processing in first-order tactile neurons," *Nat. Neurosci.*, no. August, pp. 1–7, Aug. 2014.

[193] F. Pedregosa, G. Varoquaux, A. Gramfort, V. Michel, B. Thirion, O. Grisel, M. Blondel, P. Prettenhofer, R. Weiss, V. Dubourg, J. Vanderplas, A. Passos, D. Cournapeau, M. Brucher, M. Perrot, and E. Duchesnay, "Scikit-learn: Machine learning in Python," *Journal of Machine Learning Research*, vol. 12, pp. 2825–2830, 2011.

[194] C. E. Shannon, "A mathematical theory of communication," *The Bell system technical journal*, vol. 27, no. 3, pp. 379–423, 1948.

Sub-surface deformation of individual fingerprint ridges during dynamic contact

G. Corniani, Z. Lee, M. J. Carrè, R. Lewis, B. P. Delhaye and H. P. Saal, "Sub-surface deformation of individual fingerprint ridges during dynamic contact"

Keywords: *skin mechanics* | *biotribology* | *haptics* | *Optical Coherence Tomography*

Candidate's contribution to the paper

G.C., Z.L., M.J.C., R.L., B.P.D, and H.P.S. conceived and designed research; G.C. and Z.L. built experimental setup; G.C. performed experimental acquisition; G.C., B.P.D, and H.P.S. designed analysis pipeline; G.C. developed analysis pipeline; G.C., B.P.D, and H.P.S. analyzed results; G.C. prepared figures; G.C. and H.P.S. drafted manuscript; G.C., R.L., B.P.D, and H.P.S. edited and revised manuscript; G.C., Z.L., M.J.C., R.L., B.P.D, and H.P.S. approved final version of manuscript.

Theoretical implementation	**Coding**	**Experiment design**	**Experiment execution**	**Data analysis**	**Paper writing**	**Academic authorship**
Yes	Yes	Yes	Yes	Yes	Yes	First author

Abstract

Human skin is composed of multiple layers with different mechanical properties and complex morphology. How a tactile stimulus propagates through this complex tissue to activate tactile mechanoreceptors is challenging to study in vivo but crucial for understanding mechanotransduction. Here, we imaged the epidermis of the fingertip during contact events with sliding surfaces. We tracked sub-surface deformations of the fingertip on a scale smaller than a single papillary ridge and estimated strain in both the stratum corneum and viable epidermis. When scanning the skin with a flat surface, the whole ridge deformed uniformly as a single unit under the stimulation. In every transit of the plate, the skin adhered to the plate before slipping under it; we measured higher strain in the transition from the adherence to the full slipping phase compared to the reversal of the plate movement. When scanning the skin with small features on the scale of a single ridge, different ridge sub-units experienced different strain patterns, and we measured higher strains in the deepest layer of the skin. Our study paves the way for a better characterization of the skin mechanics beneath the immediate surface and provides valuable information for improving models of tactile afferent responses.

1 Introduction

The human fingertip is a highly effective tactile sensing organ populated by thousands of mechanoreceptors [195] that translate different aspects of skin deformations into neural responses [196], which underlie our capacity for fine tactile discrimination and object manipulation [197, 198].

Before activating the tactile mechanoreceptors, any force applied to the skin surface will propagate through the epidermis, which is itself composed of several different types of cells and layers. The stratum corneum is the relatively stiff outer layer with a thickness of several hundred micrometers on the fingertip [199] and exhibits a ridged structure that gives rise to the fingerprints. This structure is mirrored on the inner border of the epidermis but with a doubled frequency, as each outer fingerprint ridge is associated with an inner primary ridge directly underneath and an inner secondary ridge that phase locks with a fingerprint valley. In between those secondary ridges are the dermal papillae (see illustration in Figure 13E).

Type-1 mechanoreceptors, namely Merkel cells and the Meissner corpuscles, are embedded at the border between the epidermis and the dermis, within the ridged structure of the skin. Merkel cells, innervated by slowly-adapting type 1 tactile afferents (SA1), respond to static or low-frequency indentations and are found at the base of primary ridges. Meissner corpuscles, innervated by rapidly-adapting afferents (RA), respond to dynamic flutter stimuli and are nestled into the dermal papillae projecting upwards on either side of them (see illustration in Figure 13E) [196, 200, 201].

It is widely believed that the morphology and tissue composition of the epidermis of glabrous skin affects transmission of touch stimuli to the level of mechanoreceptors. Several studies investigated the role of the constant ridge structure [201–203] and the mechanical properties of the epidermis tissues [204–206] in stimulus propagation. However, characterizing the biomechanics of the skin beneath its immediate surface, especially in dynamic conditions, is extremely challenging due to the technical difficulties of measuring these aspects. Prior empirical work has focused chiefly on ex-vivo measurements, but it is likely that the mechanical parameters of the skin change outside its natural environment. Simulation work has also made invaluable contributions, though the quality of these results depends on the precision with which mechanical

parameters can be measured (see Jor et al. (2013) [207] and Joodaki and Panzer (2018) [208] for reviews). Because of these difficulties, recent studies on skin deformation under dynamic conditions have focused on surface measurements, mainly by tracking the movements of fingerprint ridges via cameras at high resolution, demonstrating how surface strains arise when making contact [209] or during the onset of slip [210]. Yet the mechanical properties of the skin below its immediate surface during dynamic conditions remain largely unexplored, and it is an open question whether and how a surface stimulus would affect skin deformation at the level of mechanoreceptors.

Here, we employed Optical Coherence Tomography (OCT) to capture the fingertip skin's internal morphology while it dynamically deforms due to contact with external objects. OCT is a non-invasive optical imaging technique that, through an infrared broadband light source, offers a view into the subsurface layers of the skin in vivo in real-time [211]. This technique is commonly used in the field of dermatology for skin analysis and diagnostics. Additionally, in recent years, OCT has been widely used for the in-vivo static characterization of skin sub-surface properties [212–219]. Building on a pilot study that, for the first time, showed the feasibility of employing this technique during dynamic stimulation of the skin [220], we acquired OCT images of a cross-section of the fingertip during sliding interactions with flat plates embossed with tactile features to investigate dynamic strain rates associated with different skin layers.

2 Results

We built a linear stage that slides custom-made transparent thin plates in the distal and proximal directions across a participant's fingertip at a set speed (Fig. 13A). In all trials, the plate made 8 transits traveling 4 mm each at a constant speed of 0.8 mm/s. The fingertip was initially loaded with a 0.2 N normal force. One of the plates was flat, while the two others had an oriented edge embossed or engraved and orientated perpendicular to the scanning direction (Fig. 13B). The OCT scanner acquired images of the skin's surface and sub-surface morphology through the plate, which were 4 mm wide slices along the proximal-distal axis at a 4.5 μm lateral and 5 μm axial resolution with a sampling frequency of 20 Hz. The stratum corneum and viable epidermis were both clearly visible and distinguishable (Fig. 13C and D). After image pre-processing, we semi-

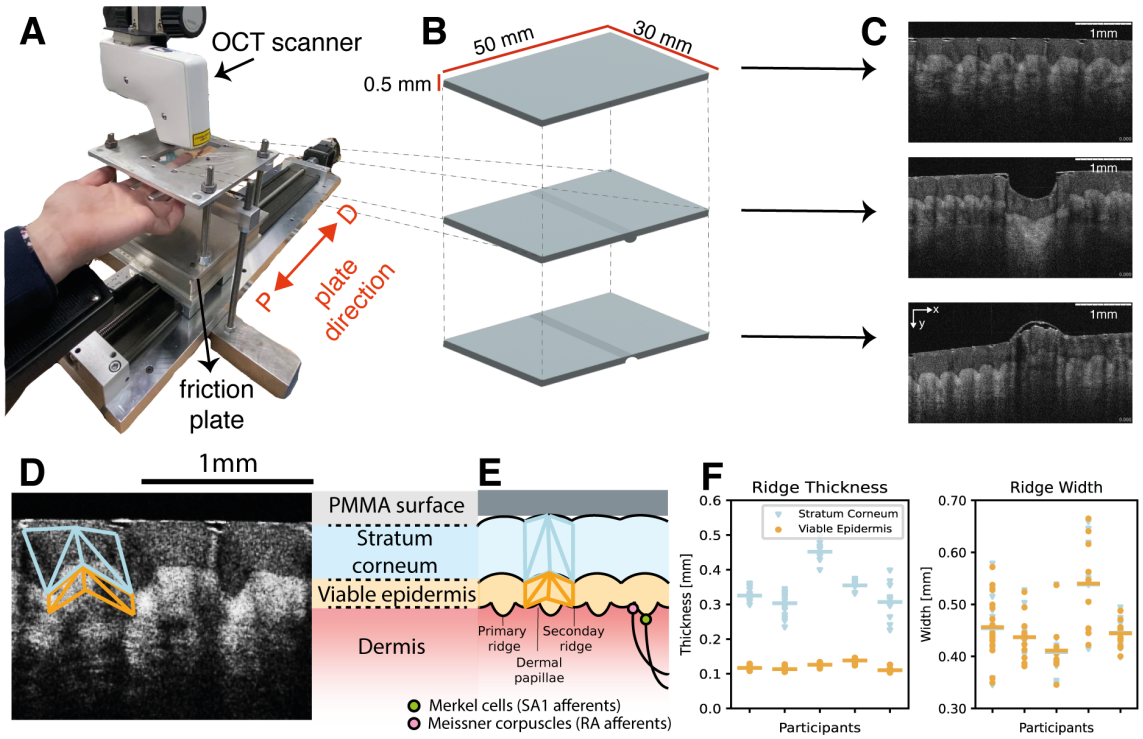

Fig. 13: Experimental set-up and identification of individual fingerprint ridges. A. The experimental apparatus consisted of a finger holder to which the left middle finger of the participant was secured and a linear stage that moved a transparent plate in the distal/proximal direction across the fingertip. An OCT scanner recorded images of the top skin layers through the transparent plate. **B.** Transparent plates were used: a flat one, a plate embossed with an edge, and a grooved one. **C.** Individual images recorded by the OCT scanner display the complex morphology of the skin. **D.** Identification and tracking of landmarks associated with different skin layers on a pre-processed portion of an OCT image. The tracking enables a fine-grained view of the deformation of individual ridges. **E.** Mechanoreceptors are located at the border between the viable epidermis and the dermis, close to or partially overlapping with the extent of tracking. **F.** Left panel: Thickness of stratum corneum (blue) and viable epidermis (yellow) as calculated from the tracked ridges. Each dot corresponds to an individual tracked ridge with the mean indicated by the horizontal line. Right panel: Width of all individual ridges across all participants.

automatically tracked (sub-)surface landmarks associated with individual ridges across different video frames (see Methods for details). The resulting triangular mesh included 8 facets per ridge, which were split between the stratum corneum and viable epidermis, and between the two flanks of the ridge, respectively, therefore allowing fine-grained measurements of individual sub-surface ridge deformation in response to different tactile events (Fig. 13D). Importantly, the depth of the meshes extended to and partly covered the dermis-epidermis border, where type-1 low-threshold mechanoreceptors are located (Fig. 13E). Averaged across participants, we calculated a thickness of 0.3 mm for the stratum corneum and 0.12 mm for the viable epidermis, along with an average ridge width of 0.46 mm, all agreeing with previous measurements [214, 221].

2.1 Tracking ridge deformation during mechanical events

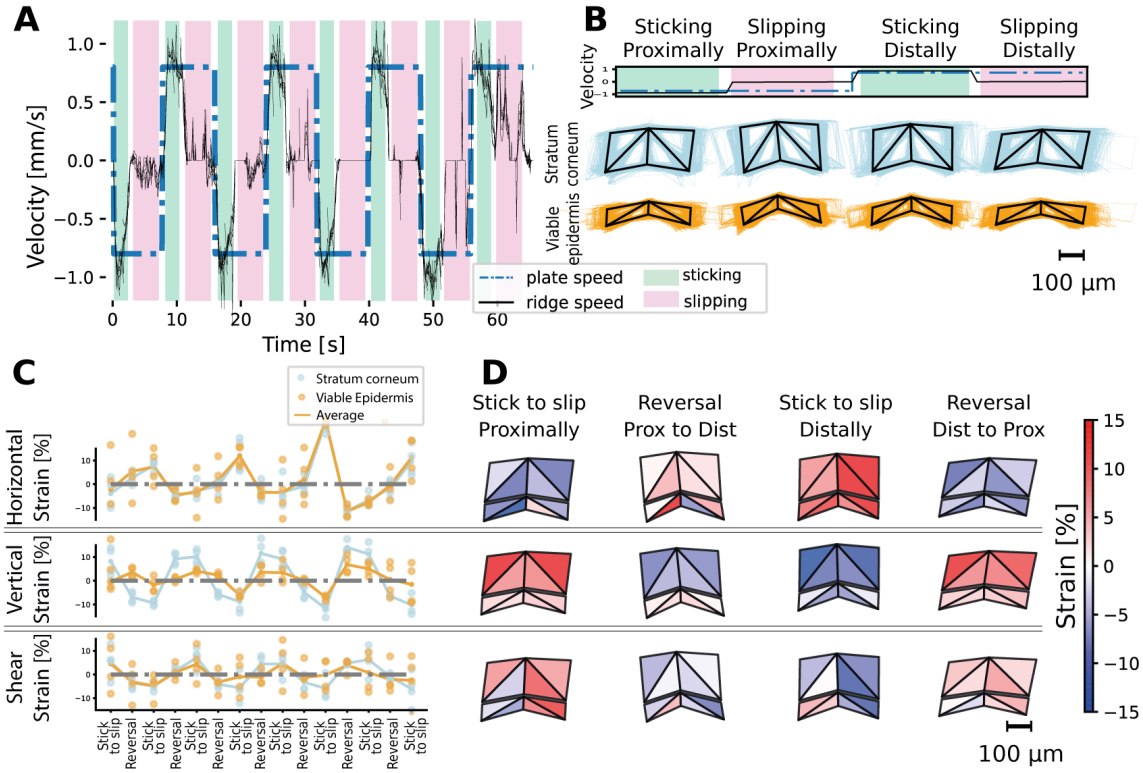

Fig. 14: Determining skin strains linked to different mechanical events. A. Velocity of the plate (dash-dotted blue line) and average velocity of each tracked fingerprint ridge (thin black lines) during all eight transitions of the flat plate for a single participant. Two phases are evident: when the ridge is moving along with the plate (stick, indicated by green shading) and when the ridge is stationary, but the plate is moving (slip: indicated by pink shading). **B.** Average ridge meshes (black lines) during each of the four phases calculated over all tracked ridges and all time points assigned to every phase for a single participant. Colored lines indicate individual sample meshes (blue: stratum corneum, yellow: viable epidermis). **C.** Strains magnitude during each phase transition in the 8 transits of the flat plate. Each dot corresponds to one of the 8 triangles composing the ridge mesh. The full line represents the average strain in the stratum corneum (blue) and viable epidermis (yellow). **D** Strains in each phase transition average across trials with the same movement direction. Red shades represent tensile strains, blue shades represent compressive strains.

We were interested in quantifying the (sub-)surface deformation of individual fingerprint ridges during mechanical events. These events could be related to the movement of the transparent plate itself, such as a reversal in the direction of movement of the plate or the transit of an edge or groove over an individual ridge, or they could be caused by the interaction between the plate and the mechanical properties of the skin itself, such as the transition between the skin sticking to the plate and full slip [222]. Indeed, in every transit of the flat plate, distally to proximally and vice versa, we identified two phases of the relative movement of the skin with respect to the movement of the plate: the ridges initially adhere to the plate and move together with it (stick phase); then the

ridges stop moving, and the plate slips over them (slip phase). The stick-to-slip transition happens near-simultaneously for all ridges observed in the frame (cross-correlation across the horizontal speed of every ridge >0.8 across all participants). This clear distinction between stick and slip phases allowed us to classify each phase from the average horizontal velocity over all tracked ridges (see example for a single participant in Fig. 14A).

For each phase, we then calculated a stereotypical mesh covering a single papillary ridge by averaging the meshes of all tracked ridges across all the central time points within the same phase (Fig. 14B, see Methods for detail). Within a single subject, the variability in the shape of different ridges was much smaller within a given phase (average standard deviation of 9μm in the stratum corneum and 11μm in the viable epidermis per tracked landmark) than across different phases (standard deviation of 22μm in the stratum corneum and 22μm in the viable epidermis), thus suggesting that the averaging process accurately captured systematic deformations between phases. Subsequent analyses were therefore carried out on the stereotypical ridge.

We quantified the deformation of the stereotypical ridge across the different phases by calculating the horizontal, vertical, and shear strain experienced by each facet of the mesh during the transition from each phase to the next (see Methods for details). The resulting strain profile was consistent across different transits of the plate (see example for one participant in Fig. 14C), highlighting that ridges underwent repeatable and systematic deformations. For the participant considered here, the strain profiles were generally uniform within the stereotypical ridge in all three components, indicating that all components of the ridge were either compressed or stretched simultaneously during each transition from one phase to the next (Fig. 14D). Different plate directions (distal or proximal) were associated with different strain profiles (tensile or compressive) of comparable magnitude.

2.2 Large deformations during stick-to-slip transitions

Having established a method for robustly tracking canonical ridge deformations, we next examined the resulting sub-surface skin deformations across different participants, focusing first on trials using the flat plate as stimulus. Every participant exhibited a clear transition between stick and slip phases. However, the time spent in either phase varied markedly across participants (range:11.4-

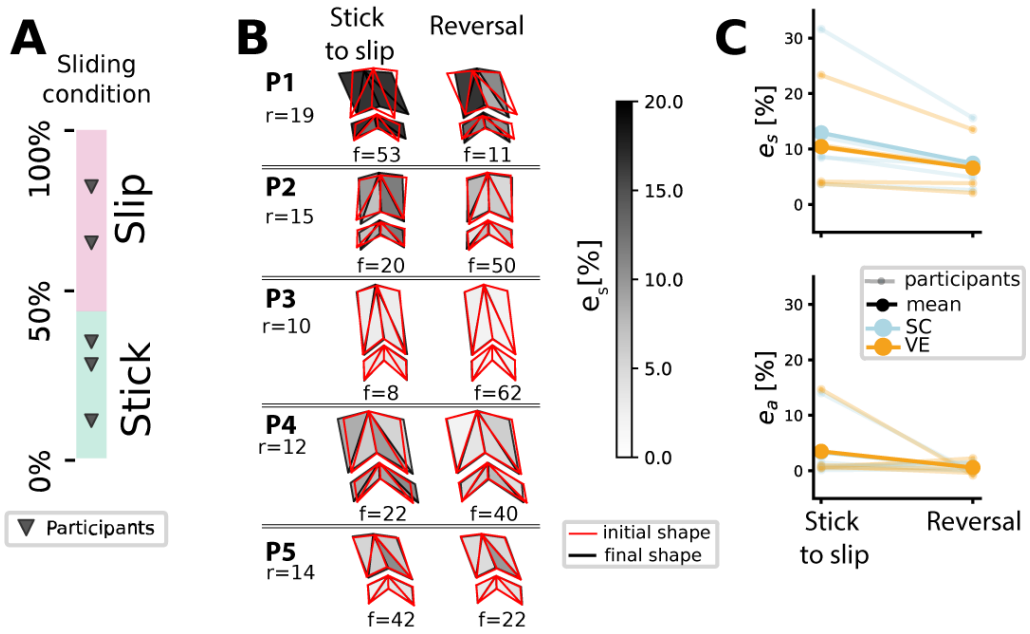

Fig. 15: Stick-slip transitions dominate strain patterns during contact with a flat surface. A. Average percentage of time spent in stick or slip phases during repeated transitions of the flat plate for all participants. Individual marks denote different participants, while the colored bars show the average. There is large variability across participants, but all display the transition between stick and slip. **B.** Deformation of average fingerprint ridges during the transition from stick to slip (left column) and during reversals in movement direction of the plate (right column) for all participants. Red meshes show the initial shape, while black ones denote the final shape, with the darkness of the shading of each facet referring to the corresponding maximum shear strain value e_s. Deformations appear larger during stick-to-slip transitions than during movement reversals. For every participant P, r is the total number of ridges tracked, and f is the number of frames considered in each phase in each one of the eight plate transits. **C.** Average maximum shear strain e_s (top row), and triangle area variation (bottom) in both the stratum corneum (SC, light blue shading) and viable epidermis (VE, yellow shading) averaged over all facets in that layer for all participants. Thick, full lines show the averages across all participants, while faded ones denote individual participants. Both metrics are larger during stick-to-slip transitions than during plate reversals.

82.7%, mean: 44.7%, see Fig. 15A). These differences are partly attributable to differences in skin mechanics across participants (e.g., moisture level) but also depend on the precise location of the imaging site on the fingertip, as previous research has shown that stable contact is lost progressively over time across the whole fingertip during the transition from stick to slip [222].

Next, we compared the deformation of the stereotypical ridge for transitions from stick to slip, and for reversals in the movement direction of the plate. Stick-to-slip events have previously been shown to elicit strain waves on the surface of the fingertip skin, but it is unclear how they affect sub-surface structure. Similarly, a reversal of the movement direction of the plate changes the direction of the tangential force applied to the skin, which might be expected to induce shear deformation in the stratum corneum or the viable epidermis.

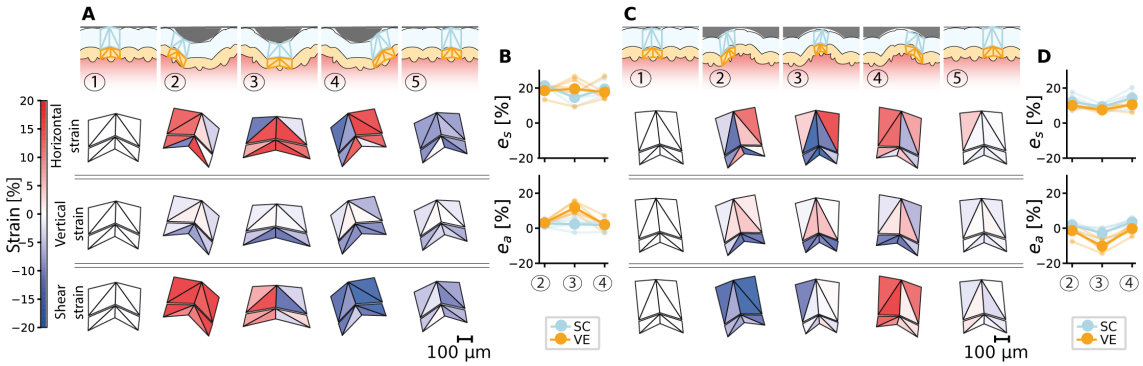

Fig. 16: Ridge deformations and skin strains during transit of small tactile features. A. Top row: Illustration of identified phases and associated skin deformations for an edge stimulus. Bottom rows: Average ridge deformation and associated horizontal (top), vertical (middle), and shear strains (bottom) for a single participant. Note that all strains are calculated with respect to the mesh shown in the left-most column, which represents the ridge during full slip before the interaction with the tactile feature. **B.** Maximum shear strain (top row) and area variation (bottom) in the stratum corneum (light blue) and viable epidermis (yellow) during the interaction with the tactile feature. Faded lines denote results from individual participants. **C, D.** Same as A and B, but for transit of tactile groove.

To summarise the effect and compare across different phase transitions and different participants, we computed the maximum shear strain e_s and the area variation e_a from the principal component of the strain, as detailed in Methods. We found that stick-to-slip transitions consistently led to larger deformations and, therefore, higher maximum shear strain than did plate reversals (see ridge deformations for different participants in Fig. 15B, their associated maximum shear strain in Fig. 15C top, and area variation in Fig. 15C bottom): maximum shear strains for stick-to-slip transitions were about twice as large as those for reversals, and this effect was of roughly similar magnitude in the stratum corneum and in the viable epidermis (on average 12.9% versus 7.4% in the stratum corneum, and 10.4% versus 6.5% in the viable epidermis). The variation in the area of every triangular element was overall small but still larger during the stick-to-slip transitions than reversals (on average, 3.3% in the stratum corneum and 3.5% in the viable epidermis for stick-to-slip transitions; 0.6% in the stratum corneum and 0.6% in the viable epidermis for reversals). This behavior was consistent across participants, though the magnitude of the effect varied considerably between them.

2.3 Large deformations in the viable epidermis during contact with tactile features

Next, we tracked ridge deformation and sub-surface strains during the transit of small tactile features that were close in size to that of a single fingerprint ridge itself. For this experiment, we

used the plates with the edge and groove, respectively, keeping all other parameters the same.

After discarding time windows where the ridges adhere to the plate (sticking), five distinct phases were identified and automatically classified (see Methods for details) for every ridge tracked, which depended on its position with respect to the edge or groove (see top rows in Fig. 16A and C for illustrations): before and after approaching the tactile feature, the flat part of the plate slides over the fingertip (analogous to the slip phase identified using the flat plate above); additionally, each ridge might be approaching the feature and affected by its geometry, be located directly under the feature, or moving away from the feature while still being affected by it. Each of these phases occurs consecutively for all the ridges visible in the frame as the feature moves across them. When aligned according to their movement phase, individually tracked ridges showed similar deformation patterns (across phases, on average, the standard deviation of the distance of every tracked point from the overall averaged ones was 14μm in the stratum corneum and 15μm in the viable epidermis for the edge plate, and 12μm in the stratum corneum and 12μm in the viable epidermis for the groove plate. Without distinction of movement phase, the standard deviation was 61μm in the stratum corneum and 62μm in the viable epidermis for the edge plate, and 39μm in the stratum corneum and 42μm in the viable epidermis for the groove plate, analogous to the results for the flat plat), and, therefore, we again calculated a stereotypical ridge mesh for each participant by averaging across all the individual meshes in that phase. We quantified the deformation of the stereotypical ridge during the plate transit by computing the horizontal, vertical, and shear strains between the ridge in the initial slipping phase and its deformed mesh in each other phase.

Both the horizontal and shear deformation profiles were mirrored between the plate with the edge and that with the groove, as the ridges conformed to the shape of the feature. Thus, ridges bent down, stretched horizontally, and then bent up during the transit of the edge, while ridges bent up, compressed horizontally, and then bent down during the transit of the groove (see ridge deformations and strains for a single participant in Fig. 16 A and C). The vertical strain, on the other hand, was comparable for both plates and larger in the viable epidermis than the stratum corneum. For both plates, we measured different horizontal strain profiles on the left and right sides of the meshed ridge. When approaching or moving away from the feature (phases 2 and 4), one side of the ridge gets horizontally compressed while the other gets stretched. In the same

phases, the shear deformation was uniform across the whole ridge area and had an opposite profile in the approach and moving-out phases. In all cases, the ridge, after interacting with the plate features, reverts to a shape closely resembling the initial one, and this is reflected in the small magnitude of the strain changes between the initial and final sliding phases. For this reason, phase 5 was not included in the subsequent analysis.

To compare the overall magnitude of deformation across phase and plates, we computed the maximum shear strain e_s averaged across all the mesh facets (see Figure 16 B and D, top row) and the average variation of the area of each triangular element e_a (see Figure 16 B and D, bottom), both in the stratum corneum and the viable epidermis in the three central phases of the feature transition against the initial sliding. For the edge plate, the maximum shear strain e_s was nearly constant in the three phases analyzed (20.3%, 16.6%, 19.4%) in the stratum corneum, and in the viable epidermis (18.4%, 19.5%, 17.6%). The area variation e_a followed the same pattern, with almost constant variation in the stratum corneum (2.6%, 2.3%, 1.8%), and a positive peak in the viable epidermis when the ridge was completely under the feature (3.1%, 11.8%, 2.1%). This result indicates that the viable epidermis gets expanded more than the stratum corneum during the transit of the small engraved feature over the skin surface.

For the groove plate, the maximum shear strain e_s was mostly constant in the three phases analyzed, both in the stratum corneum (12.1%, 9.4%, 14.2%), and in the viable epidermis (10.0%, 7.5%, 10.5%). The area variation e_a had a negative peak when the ridge was in full contact with the groove (phase 3) both in the stratum corneum (1.8%, -2.8%, 3.5%), and in the viable epidermis (-1.3%, -10.2%, –0.2%). Thus, the ridge was contracted during the interaction with the engraved tactile feature. Again, the area deformation in the viable epidermis was greater than in the stratum corneum.

Overall, the maximum shear strain was higher for the edge plate. On the contrary, the area variation had comparable values for the two different features but with opposite signs: skin expanded for the edge and contracted for the groove. Interestingly, in both cases, the area variation was considerably higher in the viable epidermis than in the stratum corneum.

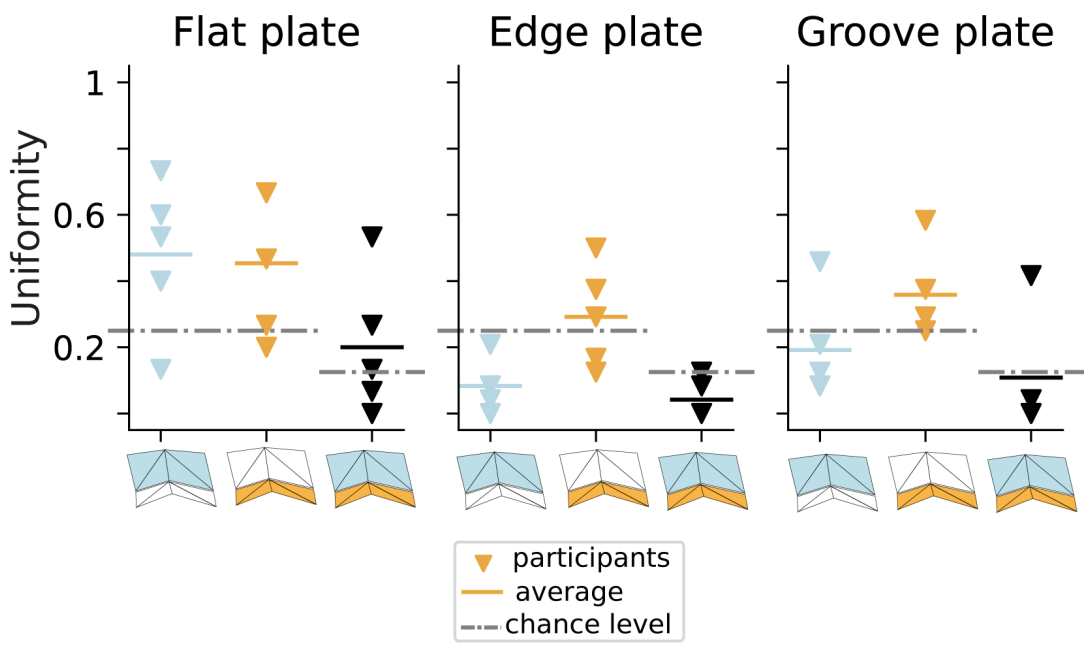

Fig. 17: Uniformity of ridge deformation across ridge flanks and skin layers. Triangular markers denote results from individual participants. The full line represents the average uniformity across participants in the stratum corneum (blue), in the viable epidermis (yellow), and across the whole tracked ridge (black). The dotted gray line represents the chance level above which the area deformation is considered uniform across the ridge portions considered. stratum corneum (blue) and viable epidermis (yellow).

2.4 Deformations of ridge sub-units

After quantifying the deformation profiles for the flat and feature plates, we asked whether the ridge geometry plays a role in the propagation of the deformation, both horizontally within a ridge and vertically across different layers. In particular, we were interested in assessing whether the ridge deforms as a single unit. If this was the case, a force acting at any point on the surface of the ridge would lead to consistent strain patterns (whether tensile or compressive) across the ridge as a whole. Conversely, the distal flank of a ridge might deform differently than the proximal flank. This question is important because it determines the spatial resolution at which small features are discriminable. To answer this question, we used a simple metric assessing the uniformity of the deformation profile across different ridge sub-units, defined as the ratio between the phases where all ridge sub-units had the same area variation profile (expansive or contractile) over the total number of phases (see Methods for details). We computed this measure over the 4 sub-units composing the stratum corneum, over the 4 sub-units composing the viable epidermis, and over the 8 sub-units composing the whole stereotypical ridge (see Figure 17).

For the flat plate, the uniformity metric was above chance level in the three cases examined: within the stratum corneum, within the viable epidermis, and to a lesser extent across the whole ridge. These results suggest that the deformation induced by sliding the flat surface typically generated uniform profiles of area variation across the stratum corneum, the viable epidermis, and even, though to a weaker extent, across the 8 meshed triangles composing the stereotypical ridge. In contrast, for both of the feature plates, the area variation profile was clearly not uniform across different sub-units of the stratum corneum, though slightly above chance level in the viable epidermis. At the same time, there was no uniformity across the eight meshed triangles in the two layers. This result indicates that, within the stratum corneum, the ridge can experience simultaneously expansive or contractile area variation, and thus subunits of a single ridge deformed differently. However, the area variations measured in the deeper layer, the viable epidermis, have a higher uniformity coefficient, suggesting that the deformation experienced in the outer layer of the epidermis is not identically mirrored in the layer immediately beneath.

3 Discussion

This study examined subsurface deformation of the fingertip skin in vivo during dynamic tactile stimulation. We employed OCT, a technique that is commonly used in research and clinical studies to investigate the skin. However, in most cases, its application has been limited to static characterization of the skin morphology, such as measuring tissues' thickness and roughness [214–218]. Here we built an experimental set-up to acquire images of the skin subsurface, to the level of the dermis-epidermis junction, during dynamic stimulation of the fingertip with different surfaces. We used the resulting data to measure the skin deformation in the stratum corneum and viable epidermis during dynamic stimulation at high spatial resolution, allowing us to characterize deformations smaller than the scale of a single fingertip ridge. When scanning the skin with a flat surface, we found that the whole ridge deformed uniformly and was subject to higher deformation in the transition from partial to full slip than when the movement direction of the plate was changed. When scanning the skin with small features on the scale of a single ridge, different ridge sub-units experienced different deformations, and those were higher in the deeper viable epidermis than in the stratum corneum surface layer of the skin.

3.1 Large deformation during stick-to-slip transitions matches strong neural activity discharge

In trials with the flat surface, we measured larger deformations during stick-to-slip transitions than during reversals of the plate's movement direction. If mechanoreceptors are directly responsive to strains, these findings would suggest that they should be more active during stick-to-slip transitions. Indeed, a previous study recorded neural responses from different afferent classes during similar sliding stimulation of the fingertip and reported that these are sensitive to slip events and generally more active during the partial slip phase [223]. Rapidly adapting type I afferents (RA-I), which innervate Meissner corpuscles located at the dermis-epidermis border on either side of ridge flanks, in particular showed little to no response during the onset and offset of the tangential load but faithfully encoded the stick-to-slip transition. That study also measured the skin surface strain and observed that the discharge of RA-I units was strongly coupled to compressive strain changes taking place within their receptive fields on the skin surface during the partial slip phase. Our findings extend these results by demonstrating that the large surface strains measured during the transition from adherence to slipping are mirrored in the subcutaneous tissues and specifically at the depth at which type-1 mechanoreceptors are located. Altogether these results provide a physiological explanation for the widely observed human capacity of fine-tuned grasping with quick adjustments of the grip force to friction changes [224, 225].

3.2 Surface skin deformations are amplified in the viable epidermis

We measured larger deformation in the viable epidermis compared to the stratum corneum when small tactile features interacted with a ridge. Interestingly, this effect was not found in the stimulation with the flat surface, where the strain values and the variation of area were comparable for both layers. This difference is likely explained by the stimulus geometry, which is the only factor that differs in the two experiments. For the flat surface, the stimulation can be defined as global, as all the ridges tracked were simultaneously stimulated in the same way. The stimulation applied to the skin during the image acquisition was purely tangential since the normal load was applied before the tangential movement started and kept constant across the whole trial. As a result, the entire portion of skin in contact with the plate was subject to a

pre-compression state whose effect we did not measure. When the plate presented an embossed or engraved feature, likewise, there was a state of pre-compression due to the initial normal loading on the finger. In addition, small portions of the skin were subject to high compressive or stretching deformation due to the interaction with the feature. The plate transit generated a localized normal load over the skin region in the proximity of the feature. Consequently, we measured the effect of purely tangential load for the flat plate, while for the feature plates, the measured strains and deformations were due to tangential and localized normal load. Due to different structural characteristics, tissue composition, and orientation of the Langer lines and of the tissue fibers, the stratum corneum and viable epidermis have distinct anisotropic properties as shown by several studies [219, 226]. Consequently, different types of stimulation (purely tangential, purely normal, or mixed) spread differently in the different skin layers. Our results give a hint of this anisotropy as the magnification effect in the viable epidermis is measured only when a punctual normal load is applied to the skin, while it is not present when the skin is stimulated only with a tangential load.

The reason for the strain magnification in the deep layers of the skin is to be found in the skin's particular topography and microstructure (i.e., geometry and mechanical properties of its layers), as demonstrated through computational models in [205]. In particular, they showed that morphological characteristics of the skin tissues, such as ridges, can efficiently deflect, convert, and redistribute strain within the stratum corneum, viable epidermis, and dermis. Thus, the geometrical structure of ridged skin combined with varying mechanical properties of different layers -the stratum corneum is stiffer compared to the lower layers- results in an amplification of the strain values in the viable epidermis. Under a compressive deformation, they predicted strain in viable epidermis up to one order of magnitude higher than in the stratum corneum, with the level of amplification depending on the specific combination of some elasticity parameters, namely the Poisson's ratio and Young's module. We measured an area variation up to three times larger and a maximum shear strain in the viable epidermis twice the ones measured in the stratum corneum. In our study, we don't provide any measure of the Poisson's ratio and Young's module, the stimulation was not purely compressive, and we use different metrics to quantify the effect. Consequently, a direct comparison of the magnitude of the magnification effect is impossible. At the same time, the arguments proposed by Leyva-Mendivil et al. (2015) [205] for magnification

in the viable epidermis can serve as a starting point for investigating, in future analyses, the phenomenon that they observed through computational simulation, and we experimentally measured.

Further analysis would be needed for a complete understanding of the measured effect. However, this result is particularly valuable because it shows that the deformations occurring at the surface of the skin are not equivalent to those measured at deeper levels.

3.3 Sub-ridge resolution of skin deformation

We studied the uniformity of the deformation profile within a single ridge unit. During the transit of the flat surface, we found that the area variation for the four sub-ridge facets we used to characterize the ridge deformation was mostly uniform, as if the ridge acted as a single unit. On the contrary, when small features interacted with the ridge, the area of different ridge sub-units got expanded and contracted differently.

A previous study from Johansson and laMotte (1983) [227] observed that the human ability to resolve small features over a smooth surface is higher when the feature is scanned across than when the feature is just indented into the skin. They speculate that the vertical component of the skin displacement alone may not account for the detection thresholds, but a quite localized displacement resulting from the ridge catching with the features might produce a local deformation large enough to the detection of small asperities on a smooth surface. Thus, the ability to resolve small features emerges from the large lateral displacement of single ridges in the skin.

The perception of small features depends mainly on the stimulation of Merkel cells and the signals arising in the SA1 afferents [228]. However, the detection of very fine spatial structures, too small to appreciably deform the skin, must be perceived in some nonspatial way. Indeed, the finest features scanned across the skin produce vibratory waves that propagate through the skin rather than produce significant deformations. Their perception is thus mediated by the activation of the Pacinian corpuscles, which sit in deeper layers of the skin and are tuned to detect vibrations. Accordingly, a series of experiments [229, 230] predicted that the transition between the PC-mediated and SA1-mediated perception of small asperity occurs around a spatial resolution of 200 μm in dynamic conditions, thus approximately half the width of a single ridge of the fingerprint.

A more recent study investigated the spatial acuity of the receptive subfields of RA1 and SA1 afferents, which was reported to be in the submillimeter range, roughly matching the width of a single ridge [231]. The study argued that a combination of the ridge structural compartmentalization of the skin and the ridge-governed contact mechanics of the fingertip might account for such spatial selectivity.

Even though in our study the scale of the feature was larger than those tested in these previous studies, our result provides mechanical evidence for the hypotheses proposed. The skin deformation we measured clearly propagated to the Merkel cells' location, thus resulting in SA1-mediated spatial perception. We experimentally demonstrated that when scanning the skin with small features, high and localized strains emerged when the asperity affected the ridge. We additionally showed that different deformation could involve each sub-unit of the ridge, possibly revealing a spatial resolution higher than the dimension of the single ridge, as already suggested by previous findings. Further experiments and analysis coupling psychophysical tests and skin imaging acquisition would be required to test this hypothesis.

3.4 Limitations and future work

This study pioneered the possibility of measuring skin deformation in vivo and dynamically. Although we explored a rather limited class of stimulations, we demonstrated the feasibility of this technique and paved the way for a huge variety of case studies that might eventually ensure an accurate and complete characterization of the skin properties.

A major step forward for future studies of this kind would require improving the imaging resolution and clarity to visualize more morphological and functional structures below the skin surface. For example, the primary ridges, to the tip of which Merkel cells are anchored, can be detected in some images of our dataset but with an insufficient resolution to ensure stable tracking over frames. Indeed, we employed a state-of-the-art, standard clinical OCT scanner, routinely used in the dermatology department of the local hospital for diagnostic purposes. This kind of machine is susceptible to coherent noise (speckle noise) [232], imposing significant limitations on the resolution and clarity of images acquired. A previous study revealed the possibility of resolving even small structures in the tissues, such as sweat ducts and Meissner's

corpuscle in the human fingertip skin, by applying a light manipulation method that eliminates speckle noise originating from a sample, namely speckle-modulating OCT [233]. Coupling this advanced imaging technique with our unique experimental set-up and analysis pipeline might further advance the understanding of subsurface skin properties and deformation mechanisms.

In our study, we included a rather small group of participants, balanced in terms of sex but uniform in the age range. However, the skin is a biological structure with multiple layers, each of which has a unique set of characteristics such as geometry, elasticity, thickness, friction, etc. Several studies proved how morphological and mechanical skin properties could greatly vary in relation to physiological and physical factors as, for example, age [234, 235], sex [236, 237], level of moisturization [238], room temperature and humidity [239]. In order to consolidate and generalize the results obtained in this study, we will, at the minimum, include a wider range of participants in terms of age in future acquisitions. Still, we are providing a set of in-vivo data representing a novel and valuable contribution to the field. Our dataset and results can inform and validate complex computational models that simulate skin behavior with different physiological and physical parameters.

4 Material and Methods

4.1 Participants

Five healthy participants (3 females, age mean: 19.6, std: 1.0) participated in the experiment after providing informed consent in accordance with the Declaration of Helsinki. The experiment was performed on the subjects' left middle finger. Before any trial, the finger was thoroughly cleaned with water and dried carefully, and a thin layer of petroleum jelly was applied. Environmental conditions during the test were controlled with 20 °C room temperature and 50% relative humidity. The study's protocol was approved by The University of Sheffield (Ethics Number 039144).

4.2 Experimental set-up

The experimental set-up for the present study was adapted from the design of an earlier study [220]. Transparent plates were held in place by a support rig fixed on a linear stage that could move distally and proximally with respect to the fingertip, sliding the plate against the fingertip,

which was glued on a finger holder to maintain its position during acquisitions. The support rig was mounted on a force plate (HE6X6-10, Advanced Mechanical Technology, Inc.) to measure the load along the axes parallel and perpendicular to the direction of the movement and along the axis normal to the plate surface. The plates were made from polymethyl methacrylate (PMMA) and were 30x40x0.5 mm in size (produced by Shape Technology S.r.l., Casale Monferrato, Italy). One plate was flat, while the two others had an embossed oriented half-circular edge (1 mm base diameter and 0.4 mm height) or an engraved oriented groove (1 mm based diameter and 0.3 mm depth) traversing the middle of the surface (see Figure 13B).

Prior to each trial, the plate specimens were cleaned with deionized water and dried thoroughly with paper towels. Before starting the imaging acquisitions in every trial, the plate was manually lowered onto the participant's fingertip until reaching a 0.2N normal load. For every trial, the plate was displaced by 4 mm for 4 times in each direction (distal to proximal and vice versa) at a constant speed of 0.8 mm/s.

4.3 Image acquisition and pre-processing

For image acquisition, we used the clinically approved Vivosight® OCT system (Michelson Diagnostics, Kent). It has a Fourier domain with a 20 kHz swept-source laser at 1300 nm centre wavelength, $< 7.5\mu m$ lateral, and $< 5\mu m$ axial resolution. The image capturing rate was 20 frames per second, and the dimension of each image was 895 × 483 pixels with 256 gray levels.

After the acquisition, images were preprocessed using the cv2 library in Python. The first step of the processing was the histogram equalization to normalize the brightness and increase the images' contrast. A gamma transformation ($\gamma = 5$) was then used to enhance the contrast further and adjust the saturation of the images. Finally, to remove noise while keeping the edges sharp, a bilateral filter was applied (parameters: diameter of each pixel neighborhood = 5, sigmaColor = 110, sigmaSpace = 190).

4.4 Tracking of individual ridge deformation

The top and the valley of each ridge in the field of view were semi-automatically tracked at the surface, at the border between the stratum corneum and the viable epidermis, and at the dermis-

epidermis junction, in each frame. For every set of 700 frames acquired (i.e., frames acquired during a single trial), a subset of frames uniformly distributed over the whole acquisition period was manually labeled using the Python polygonal annotation library Labelme [240]. Depending on the trial, the size of the manually labeled set of frames varied between 1/4 and 1/3 of the total number of frames. The set of manually annotated frames was then employed as a training set to build a DeepLabCut model [241] to automatically estimate the position of each tracked point in the remaining frames. A model was trained for every set of frames with an average accuracy of 2.96 pixels on the training set and 14.64 pixels on the test set. The automatic annotations were manually checked and corrected to ensure high precision and avoid artifacts coming from inaccurate tracking in the strain computation. To allow fine-grained measurements of individual sub-surface ridge deformation, the tracked features were used to draw a triangular mesh for every ridge in the field of view. Each mesh included 8 facets per ridge, split between the stratum corneum and viable epidermis and between the central ridge and adjacent groove, respectively.

4.5 Movement phase classification

The movement of the skin during the transits of the plate was studied by looking at the displacement of the tracked points from frame to frame. In particular, we considered the displacement along the x-axis for computing the horizontal component of the skin velocity v_x, while the displacement along the y-axis for the vertical component v_y. We computed the two components of the velocity of every ridge, v_x^{ridge} and v_y^{ridge}, by averaging across the velocity components of the nine tracked points belonging to the ridge.

For the flat plate trials, four phases were identified by analyzing the horizontal component of the velocity v_x^{ridge}:

1. Sticking proximally ($v_x^{plate} < 0$, $v_x^{ridge} < 0$): the plate is moving in distal to proximal direction, and the skin is sticking to the plate.
2. Slipping proximally ($v_x^{plate} < 0$, $v_x^{ridge} = 0$): the plate is moving in distal to proximal direction, slipping over the stationary skin.
3. Sticking distally ($v_x^{plate} > 0$, $v_x^{ridge} > 0$): the plate is moving in proximal to distal direction, and the skin is sticking to the plate.

4. Slipping distally ($v_x^{plate} > 0$, $v_x^{ridge} = 0$): the plate is moving in proximal to distal direction, slipping over the stationary skin.

The positive and negative extrema of the first derivative of v_x^{ridge} were taken as markers for the transition from the stick to the slip phase and vice versa. In each trial, which consisted of 4 plate transits in each direction, there were a total of 16 successive phases, as each of the 4 phases identified occurred 4 times. To consider for the subsequent mesh averaging an equal number of frames in each occurrence of a single phase, the central n_{phase} frames were selected for each phase. n_{phase} was chosen as the minimum duration of each phase among its 4 repetitions.

For trials with the feature plates, all frames where $v_x^{ridge} \neq 0$ were discarded to retain only data where the plate was fully slipping. Then, by examining the vertical component of the skin velocity v_y^{ridge}, four phases were classified for every ridge mesh separately:

1. full slipping ($v_y^{ridge} = 0$): before and after approaching the feature
2. approaching the feature ($v_y^{ridge} > 0$ for the groove plate and $v_y^{ridge} < 0$ for the edge plate)
3. moving away from the feature ($v_y^{ridge} < 0$ for the groove plate and $v_y^{ridge} > 0$ for the edge plate)
4. under the plate feature (frames in between the two previous phases, $v_y^{ridge} = 0$)

In each trial, there were a total of 40 successive phases, as each of the 5 phases identified occurred in each of the 8 transits of the plate. Again, the central n_{phase} frames were selected for each phase in order to consider the subsequent mesh averaging an equal number of frames in each occurrence of a single phase.

4.6 Strain computation

The mesh coordinates of each ridge in each frame were centered around the origin by subtracting from the coordinates of any tracked point in a ridge, the average of the coordinates across all the points in that ridge. Then, to obtain a single stereotypical ridge shape for every phase, the mesh coordinates of each ridge were averaged across all the ridges in a frame and all the frames in the same phase. Displacement field gradients were calculated for each triangle in the mesh,

- between two consecutive phases for the flat plate trials
- between the initial slipping phase and every other phase for the feature plates.

Green-Lagrange strains were estimated from the displacement gradient by the equations:

$$\varepsilon_{xx} = \frac{\partial u}{\partial x} + 0.5 \left[\left(\frac{\partial u}{\partial x} \right)^2 + \left(\frac{\partial v}{\partial x} \right)^2 \right] \tag{7}$$

$$\varepsilon_{yy} = \frac{\partial v}{\partial y} + 0.5 \left[\left(\frac{\partial u}{\partial y} \right)^2 + \left(\frac{\partial v}{\partial y} \right)^2 \right] \tag{8}$$

$$\varepsilon_{xy} = 0.5 \left(\frac{\partial u}{\partial y} + \frac{\partial v}{\partial x} \right) + 0.5 \left(\frac{\partial u}{\partial x} \frac{\partial u}{\partial y} + \frac{\partial v}{\partial x} \frac{\partial v}{\partial y} \right) \tag{9}$$

where ε_{xx} and ε_{yy} are the horizontal and vertical strain, ε_{xy} is the shear strain, and u and v are the displacements along x and y axes, respectively.

The principal component of the strain, e_1 and e_2, were obtained by eigenvalue decomposition of the strain matrix ε, as reported in [210]. The principal strain decomposition consists of a rotation of the reference coordinates so that the shear strain is canceled and the axial strains take their maximal and minimal value. Thus, the principal components e_1 and e_2 represent the maximum tensile and compressive deformation along perpendicular axes.

From the principal strain components, we computed the variation in area of every triangle composing the mesh as:

$$e_a = \frac{e_1 + e_2}{2} \tag{10}$$

To compare the deformation across different phases, the maximum shear strain was calculated as:

$$e_s = \frac{e_1 - e_2}{2} \tag{11}$$

4.7 Measure of the uniformity of the deformation profile

The uniformity metric was defined as follows:

$$uniformity = \frac{P_{uniform}}{P_{total}} \tag{12}$$

$P_{uniform}$ is the number of phases where all considered triangular subunits of the stereotypical ridge have uniform deformation profiles, i.e. the area variation e_a is uniformly positive or negative across subunits.

P_{total} is the total number of phase transitions considered. For the flat plate experiments, $P_{total} = 16$ (8 transits, 2 phases in each), while for the features plates experiments, $P_{total} = 24$ as we neglected the sliding phases of every transit and we considered only the deformation between the initial sliding and the 3 central phases of every transit when the features interact with the ridge.

Uniformity can range between 0 (the ridge subunits have uniform deformation profiles in none of the phases) and 1 (the ridge subunits have uniform deformation profiles in all the phases).

The uniformity in the stratum corneum and in the viable epidermis was computed across the 4 triangular subunits composing the mesh of each of these layers. Consequently, the chance level above which to consider the strain profile uniforms was set at 0.25. The uniformity across the whole ridge area was computed across the 8 triangular subunits composing the mesh of the whole stereotypical ridge. In this case, the chance level above which to consider the strain profile uniforms was set at 0.125.

References

[195] G. Corniani and H. P. Saal, "Tactile innervation densities across the whole body," *J. Neurophysiol.*, vol. 124, no. 4, pp. 1229–1240, Oct. 2020.

[196] V. E. Abraira and D. D. Ginty, "The sensory neurons of touch," *Neuron*, vol. 79, no. 4, pp. 618–639, Aug. 2013.

[197] J. D. Lieber and S. J. Bensmaia, "The neural basis of tactile texture perception," *Curr. Opin. Neurobiol.*, vol. 76, p. 102621, Aug. 2022.

[198] R. S. Johansson and J. R. Flanagan, "Coding and use of tactile signals from the fingertips in object manipulation tasks," *Nat. Rev. Neurosci.*, vol. 10, no. 5, pp. 345–359, Apr. 2009.

[199] H. Fruhstorfer, U. Abel, C. D. Garthe, and A. Knüttel, "Thickness of the stratum corneum of the volar fingertips," *Clin. Anat.*, vol. 13, no. 6, pp. 429–433, 2000.

[200] E. J. Kelly, G. Terenghi, A. Hazari, and M. Wiberg, "Nerve fibre and sensory end organ density in the epidermis and papillary dermis of the human hand," *Br. J. Plast. Surg.*, vol. 58, no. 6, pp. 774–779, Sep. 2005.

[201] N. Cauna, "Nature and functions of the papillary ridges of the digital skin," *Anat. Rec.*, vol. 119, no. 4, pp. 449–468, 1954.

[202] G. J. Gerling and G. W. Thomas, "The effect of fingertip microstructures on tactile edge perception," in *First Joint Eurohaptics Conference and Symposium on Haptic Interfaces for Virtual Environment and Teleoperator Systems. World Haptics Conference*, Mar. 2005, pp. 63–72.

[203] G. J. Gerling and G. W. Thomas, "Fingerprint lines may not directly affect SA-I mechanoreceptor response," *Somatosens. Mot. Res.*, vol. 25, no. 1, pp. 61–76, Mar. 2008.

[204] J. M. Pereira, J. M. Mansour, and B. R. Davis, "The effects of layer properties on shear disturbance propagation in skin," *J. Biomech. Eng.*, vol. 113, no. 1, pp. 30–35, Feb. 1991.

[205] M. F. Leyva-Mendivil, A. Page, N. W. Bressloff, and G. Limbert, "A mechanistic insight into the mechanical role of the stratum corneum during stretching and compression of the skin," *J. Mech. Behav. Biomed. Mater.*, vol. 49, pp. 197–219, Sep. 2015.

[206] M. F. Leyva-Mendivil, J. Lengiewicz, A. Page, N. W. Bressloff, and G. Limbert, "Implications of multi-asperity contact for shear stress distribution in the viable epidermis – an image-based finite element study," *Biotribology*, vol. 11, pp. 110–123, Sep. 2017.

[207] J. W. Y. Jor, M. D. Parker, A. J. Taberner, M. P. Nash, and P. M. F. Nielsen, "Computational and experimental characterization of skin mechanics: identifying current challenges and future directions," *Wiley Interdiscip. Rev. Syst. Biol. Med.*, vol. 5, no. 5, pp. 539–556, Sep. 2013.

[208] H. Joodaki and M. B. Panzer, "Skin mechanical properties and modeling: A review," *Proc. Inst. Mech. Eng. H*, vol. 232, no. 4, pp. 323–343, Apr. 2018.

[209] L. Willemet, K. Kanzari, J. Monnoyer, I. Birznieks, and M. Wiertlewski, "Initial contact shapes the perception of friction," *Proc. Natl. Acad. Sci. U. S. A.*, vol. 118, no. 49, Dec. 2021.

[210] B. Delhaye, A. Barrea, B. B. Edin, P. Lefèvre, and J.-L. Thonnard, "Surface strain measurements of fingertip skin under shearing," *J. R. Soc. Interface*, vol. 13, no. 115, p. 20150874, Feb. 2016.

[211] A. G. Podoleanu, "Optical coherence tomography," *J. Microsc.*, vol. 247, no. 3, pp. 209–219, Sep. 2012.

[212] X. Liang and S. A. Boppart, "Biomechanical properties of in vivo human skin from dynamic optical coherence elastography," *IEEE Trans. Biomed. Eng.*, vol. 57, no. 4, pp. 953–959, Apr. 2010.

[213] R. Maiti, L.-C. Gerhardt, Z. S. Lee, R. A. Byers, D. Woods, J. A. Sanz-Herrera, S. E. Franklin, R. Lewis, S. J. Matcher, and M. J. Carré, "In vivo measurement of skin surface strain and sub-surface layer deformation induced by natural tissue stretching," *J. Mech. Behav. Biomed. Mater.*, vol. 62, pp. 556–569, Sep. 2016.

[214] R. Maiti, M. Duan, S. G. Danby, R. Lewis, S. J. Matcher, and M. J. Carré, "Morphological parametric mapping of 21 skin sites throughout the body using optical coherence tomography," *J. Mech. Behav. Biomed. Mater.*, vol. 102, p. 103501, Feb. 2020.

[215] S. Adabi, M. Hosseinzadeh, S. Noei, S. Conforto, S. Daveluy, A. Clayton, D. Mehregan, and M. Nasiriavanaki, "Universal in vivo textural model for human skin based on optical coherence tomograms," *Sci. Rep.*, vol. 7, no. 1, p. 17912, Dec. 2017.

[216] C. Czekalla, K. H. Schönborn, J. Lademann, and M. C. Meinke, "Noninvasive determination of epidermal and stratum corneum thickness in vivo using Two-Photon microscopy and optical coherence tomography: Impact of body area, age, and gender," *Skin Pharmacol. Physiol.*, vol. 32, no. 3, pp. 142–150, Mar. 2019.

[217] B. Ding, H. Wang, P. Chen, Y. Zhang, Z. Guo, J. Feng, and R. Liang, "Surface and internal fingerprint reconstruction from optical coherence tomography through convolutional neural network," *IEEE Trans. Inf. Forensics Secur.*, vol. 16, pp. 685–700, 2021.

[218] Y. Lin, D. Li, W. Liu, Z. Zhong, Z. Li, Y. He, and S. Wu, "A measurement of epidermal thickness of fingertip skin from OCT images using convolutional neural network," *J. Innov. Opt. Health Sci.*, vol. 14, no. 1, p. 2140005, 2021.

[219] M. A. Kirby, P. Tang, H.-C. Liou, M. Kuriakose, J. J. Pitre, Jr, T. N. Pham, R. E. Ettinger, R. K. Wang, M. O'Donnell, and I. Pelivanov, "Probing elastic anisotropy of human skin in vivo with light using non-contact acoustic micro-tapping OCE and polarization sensitive OCT," *Sci. Rep.*, vol. 12, no. 1, p. 3963, Mar. 2022.

[220] Z. S. Lee, R. Maiti, M. J. Carré, and R. Lewis, "Morphology of a human finger pad during sliding against a grooved plate: A pilot study," *Biotribology*, p. 100114, Dec. 2019.

[221] R. T. Moore, "Analysis of ridge-to-ridge distance on fingerprints," *Journal of Forensic Identification*, vol. 39, no. 4, pp. 231–238, Jul. 1989.

[222] B. Delhaye, P. Lefèvre, and J.-L. Thonnard, "Dynamics of fingertip contact during the onset of tangential slip," *J. R. Soc. Interface*, vol. 11, no. 100, p. 20140698, Nov. 2014.

[223] B. P. Delhaye, E. Jarocka, A. Barrea, J.-L. Thonnard, B. Edin, and P. Lefèvre, "High-resolution imaging of skin deformation shows that afferents from human fingertips signal slip onset," *Elife*, vol. 10, Apr. 2021.

[224] R. S. Johansson and G. Westling, "Roles of glabrous skin receptors and sensorimotor memory in automatic control of precision grip when lifting rougher or more slippery objects," *Exp. Brain Res.*, vol. 56, no. 3, pp. 550–564, 1984.

[225] G. Cadoret and A. M. Smith, "Friction, not texture, dictates grip forces used during object manipulation," *J. Neurophysiol.*, vol. 75, no. 5, pp. 1963–1969, May 1996.

[226] A. Ní Annaidh, K. Bruyère, M. Destrade, M. D. Gilchrist, C. Maurini, M. Otténio, and G. Saccomandi, "Automated estimation of collagen fibre dispersion in the dermis and its contribution to the anisotropic behaviour of skin," *Ann. Biomed. Eng.*, vol. 40, no. 8, pp. 1666–1678, Aug. 2012.

[227] R. S. Johansson and R. H. LaMotte, "Tactile detection thresholds for a single asperity on an otherwise smooth surface," *Somatosens. Res.*, vol. 1, no. 1, pp. 21–31, 1983.

[228] K. O. Johnson and S. S. Hsiao, "Neural mechanisms of tactual form and texture perception," *Annu. Rev. Neurosci.*, vol. 15, pp. 227–250, 1992.

[229] M. Hollins and S. R. Risner, "Evidence for the duplex theory of tactile texture perception," *Percept. Psychophys.*, vol. 62, no. 4, pp. 695–705, May 2000.

[230] S. J. Bensmaia and M. Hollins, "The vibrations of texture," *Somatosens. Mot. Res.*, vol. 20, no. 1, pp. 33–43, 2003.

[231] E. Jarocka, J. A. Pruszynski, and R. S. Johansson, "Human touch receptors are sensitive to spatial details on the scale of single fingerprint ridges," *J. Neurosci.*, vol. 41, no. 16, pp. 3622–3634, Apr. 2021.

[232] J. M. Schmitt, S. H. Xiang, and K. M. Yung, "Speckle in optical coherence tomography," *J. Biomed. Opt.*, vol. 4, no. 1, pp. 95–105, Jan. 1999.

[233] O. Liba, M. D. Lew, E. D. SoRelle, R. Dutta, D. Sen, D. M. Moshfeghi, S. Chu, and A. de la Zerda, "Speckle-modulating optical coherence tomography in living mice and humans," *Nat. Commun.*, vol. 8, p. 15845, Jun. 2017.

[234] R. D. Jobanputra, C. J. Boyle, D. Dini, and M. A. Masen, "Modelling the effects of age-related morphological and mechanical skin changes on the stimulation of tactile mechanoreceptors," *J. Mech. Behav. Biomed. Mater.*, vol. 112, p. 104073, Dec. 2020.

[235] R. Püllen, J. Konrad, R. Merkel, and B. Hoffmann, "Skin under strain: From epithelial model tissues to adult epithelia," *Cells*, vol. 10, no. 7, Jul. 2021.

[236] S. Luebberding, N. Krueger, and M. Kerscher, "Mechanical properties of human skin in vivo: a comparative evaluation in 300 men and women," *Skin Res. Technol.*, vol. 20, no. 2, pp. 127–135, May 2014.

[237] S. Diridollou, D. Black, J. M. Lagarde, Y. Gall, M. Berson, V. Vabre, F. Patat, and L. Vaillant, "Sex- and site-dependent variations in the thickness and mechanical properties of human skinin vivo," *Int. J. Cosmet. Sci.*, vol. 22, no. 6, pp. 421–435, Dec. 2000.

[238] S. E. Tomlinson, R. Lewis, X. Liu, C. Texier, and M. J. Carré, "Understanding the friction mechanisms between the human finger and flat contacting surfaces in moist conditions," *Tribol. Lett.*, vol. 41, no. 1, pp. 283–294, Jan. 2011.

[239] M. Klaassen, D. J. Schipper, and M. A. Masen, "Influence of the relative humidity and the temperature on the in-vivo friction behaviour of human skin," *Biotribology*, vol. 6, pp. 21–28, Jun. 2016.

[240] K. Wada, "Labelme: Image Polygonal Annotation with Python." [Online]. Available: https://github.com/wkentaro/labelme

[241] T. Nath, A. Mathis, A. C. Chen, A. Patel, M. Bethge, and M. W. Mathis, "Using deeplabcut for 3d markerless pose estimation across species and behaviors," *Nature Protocols*, 2019. [Online]. Available: https://doi.org/10.1038/s41596-019-0176-0

Conclusion

This chapter recaps the main results of the thesis, reflects on the impact of our findings, and points out research directions to be addressed in the future.

1 Outline of the results

The research presented in this manuscript overall aimed to improve existing models of peripheral tactile responses. The implementation of such models is grounded on the characterization of the skin and afferents, as well as the understanding of mechanotransduction and stimuli encoding processes. Consequently, we identified two key unresolved issues in the literature related to the early stages of sensory tactile processing and designed three studies to contribute to addressing these open questions.

The first question involves identifying the critical features of the signal sent to the central nervous system by peripheral tactile afferents contributing to the tactile sensation. In this context, we developed two research studies to improve the characterization of the human peripheral tactile afferents on a population level. In particular, the first study offers a quantitative and qualitative description of the composition of the population of tactile afferents innervating the whole human body. We estimated the number of tactile afferents innervating the whole human body and their breakdown into different afferent types, and we studied the relationship between these numbers and other metrics representative of the human somatosensory system. The second study analyses the interplay strategies among afferents when encoding tactile stimuli showing how the information encoded into the population activity is affected by the population composition. We highlighted the interplay of afferents within each class and across classes. We found that

information is generally spread across different afferent classes, and combining information from multiple classes improves information transmission and is often more efficient than increasing the density of afferents from the same class.

The second open question in the literature on the early stages of sensory tactile processing regards the skin's mechanical properties and how they affect the mechanoreceptors' activation. To fill literature gaps and contribute to addressing this open issue, we designed an experimental study exploiting an imaging technique, Optical Coherence Tomography, suitable for capturing the skin tissue below the surface. On the one hand, the study offers a characterization of the strain propagation under the skin surface during sliding interactions of the fingerpad. In particular, we observed a stick-to-slip transition when scanning the skin with a flat surface, and we measured higher strain in the transition from the adherence to the full slipping phase compared to the reversal of the plate movement. When scanning the skin with small features on the scale of a single ridge, we measured higher strains in the deepest layer of the skin, closer to the mechanoreceptor location. On the other hand, we pioneered a methodology that paves the way to further investigate the skin's deformation at the receptors' location, in vivo, and during dynamic stimulation.

2 Impact

In this manuscript, we presented three studies that, as a whole, might advance the state of the art of spiking models of human tactile afferents. There is a great deal of interest in improving models of the human peripheral tactile system, as better models can lead to a number of different impacts. First, they can improve our understanding of how touch works by providing more accurate and detailed representations of how the peripheral tactile system responds to different stimuli. Second, they can guide the design of more effective haptic interfaces and technologies by providing a better understanding of how the human body interacts with these systems. Finally, they may enable the development of more effective neuroprosthetic devices. Accurate models of how afferents encode tactile information can indeed lead to more realistic simulations of touch, which can, in turn, lead to more naturalistic sensory feedback from neuroprosthetic devices.

In addition to the impact of the presented research as a whole, it should also be mentioned that the

three studies taken individually can have further important scientific implications.

The first study might have a significant impact because it offers quantification of the sense of touch in humans. This metric was missing, but it is crucial. Indeed, this characterization might be useful to anyone who deals with the sense of touch in any way because it provides a simple way to quantify this phenomenon in humans and compare it to other systems. A quick indicator of this is the fact that the citations received after the publication of this work come from a very broad range of research fields, including neuroscience, biology, robotics, electronic and neuromorphic engineering, virtual reality, haptics, etc.

The second study has a three-fold potential impact. First of all, it uses a methodology that has been proposed as promising for the study of neural coding over the last twenty years but which is still scarcely used and widespread. More importantly, we used this methodology to quantify crucial effects in neural coding, such as redundancy and complementarity, and to the best of our knowledge, no one had ever quantified these quantities in terms of information content. Overall, this study provides a valuable example of how to use information theoretic tools to study the activity of populations of neurons. As a second contribution, our study provides interesting insights into the functioning of the population of tactile afferents that can inspire experimental studies to confirm what we found based on simulated data. We also believe that our findings could provoke thoughts on how the information contained by afferents at the peripheral level converges toward the central nervous system. Finally, from a more practical point of view, this study provides a very important lesson for designers of artificial skin, neuromorphic tactile circuits, and, more generally, artificial tactile systems. Indeed, it shows that between density and heterogeneity of afferents, which in technology translates to sensors, heterogeneity is preferable in terms of efficiency in encoding tactile stimuli.

We foresee that the third study will pave the way for a wave of studies using the same technology. OCT is an imaging technique that has seen great growth in use in various clinical and research fields in recent years. Our study can be considered a pioneer in the use of OCT to characterize skin features in vivo and under dynamic conditions. This characterization of the skin, which we partially offer with our study, is critical in a wide range of research fields, including the development of haptic devices, artificial skin, medical and cosmetic products, the description and

modelization of the touch system, the definition of pathological conditions, and so on.

3 Future work

In this manuscript, we presented three complete and self-standing research studies, and each of them highlighted some further open questions in their specific research topic. At the same time, taking the research in this manuscript as a whole, it paves the way for some future work bringing together the results presented for improved modeling of the human peripheral tactile system.

In the first study, "Tactile innervation densities across the whole body", we provided an estimate of the number of human peripheral tactile afferents and the breakdown into different types. We were able to establish a plausible range for these afferents and their subtypes based on previous literature and evidence. However, there are still several important aspects of human tactile afferents that remain unclear. One key area of investigation that requires further attention is the nature of the corpuscles that act as mechanoreceptors, particularly in hairy skin. Another topic that needs more study is the relationship between the number of nerve endings and corpuscles. This relationship is likely complex and may depend on various factors, such as the type of afferent and the location of the corpuscles within the skin. A complete qualitative and quantitative characterization of peripheral tactile afferents is the basis for the advancement of the modeling of the human tactile system. For this reason, further studies in this context are necessary. These studies could include detailed histological and neuroanatomical analyses, electrophysiological measurements, and image acquisitions.

In the second study, "Population coding strategies in human tactile afferents" we examined the coding strategies of peripheral tactile afferents on a population level. This study was based on simulated data and investigated the activity of tactile afferents in response to a limited and simplistic set of stimuli, in contrast to the high variability and complexity of natural tactile interactions. As a result, there are two main areas where further research is needed to expand on the findings of this study. First, a follow-up to this study would include a broader and more complex simulation setup. To achieve this, a careful characterization of natural tactile interactions in terms of the statistical occurrence of different types of tactile stimuli is required. This would enable the simulation to reflect real-world tactile interactions' complexity better.

Second, this study highlights that the activity of tactile afferents cannot be limited to the study of a few units but must be extended to the entire population. With this in mind, future studies should develop new experimental protocols that can more accurately represent the whole population of afferents. This would provide a more comprehensive understanding of the coding strategies used by peripheral tactile afferents.

In the third study, "Sub-surface deformation of individual fingerprint ridges during dynamic contact", we developed an experimental setup using Optical Coherence Tomography and an analysis pipeline to measure the deformation of the skin in vivo and in dynamic conditions. Being the first of its kind, this work demonstrates the feasibility of such measurements using the methodology developed and opens up the possibility of answering numerous open questions in the literature. However, we limited ourselves to investigating the deformation caused by a very limited set of stimuli (sliding interaction of the fingertip with three surfaces at a fixed speed and normal load). To gain a more comprehensive understanding of the mechanical properties of the skin, additional studies using similar acquisition and analysis setups could be performed. These studies could vary the stimulus, for example, by investigating the role of speed, load, friction, and the geometrical properties of the surface. At the same time, the physiological condition of the skin (e.g., temperature, hydration, humidity, etc.) during the experiment could be measured and manipulated to infer how the skin deformation is affected by these factors. This would provide a more detailed understanding of the mechanical properties of the skin and how it responds to different stimuli. Overall, this study has provided critical new insights into the mechanics of skin deformation and has laid the foundation for future research in this area. By expanding on the findings of this study and investigating a more comprehensive range of stimuli and physiological conditions, we can gain a complete understanding of the mechanical properties of the skin and how it contributes to human tactile perception.

The global motivation behind this work was advancing the state-of-the-art spiking models of human peripheral tactile afferents, and, through the three studies presented in this thesis, we aimed to deepen our understanding of key aspects of human tactile afferents, such as the relationship between afferent firing patterns and sensory coding at a population level or the impact of skin deformation on afferent activity. Given the current limitations of existing spiking models of human tactile afferents, the natural next step is to bring together the knowledge

generated in this thesis and the numerous latest developments in the field to develop a new model. This new model should be capable of overcoming some of the limitations of existing models by incorporating the latest findings on the neural mechanisms underlying human tactile perception. This could include incorporating realistic models of the mechanical properties of the skin, as well as incorporating the interactions between different types of afferents. Furthermore, this new model should be tested on various stimuli and conditions that mimic real-life scenarios. This would be a meaningful step towards developing more accurate and realistic models of human tactile afferents, which would have far-reaching implications for the fields of neuroscience, robotics, and prosthetics.